Simulation of a 3-Fluid Membrane Liquid Desiccant Air-Conditioning System

A Thesis Submitted to the College of

Graduate and Postdoctoral Studies

In Partial Fulfillment of the Requirements

For the Degree of Master of Science

In the Department of Mechanical Engineering

University of Saskatchewan

Saskatoon

By

Devin Storle

PERMISSION TO USE

In presenting this thesis in partial fulfillment of the requirements for a Postgraduate degree from the University of Saskatchewan, I agree that the Libraries of this University may make it freely available for inspection. I further agree that permission for copying of this thesis in any manner, in whole or in part, for scholarly purposes may be granted by the professor or professors who supervised my thesis work or, in their absence, by the Head of the Department or the Dean of the College in which my thesis work was done. It is understood that any copying or publication or use of this thesis or parts thereof for financial gain shall not be allowed without my written permission. It is also understood that due recognition shall be given to me and to the University of Saskatchewan in any scholarly use which may be made of any material in my thesis.

Requests for permission to copy or to make other use of material in this thesis in whole or part should be addressed to:

Head of the Department of Mechanical Engineering
57 Campus Drive
University of Saskatchewan
Saskatoon, Saskatchewan S7N 5A9 Canada

OR

Dean
College of Graduate and Postdoctoral Studies
110 Science Place
University of Saskatchewan
Saskatoon, Saskatchewan S7N 5C9 Canada

ABSTRACT

A liquid-to-air membrane energy exchanger (LAMEE) is able to simultaneously cool and dehumidify air by transferring heat and moisture between the air stream and a liquid desiccant solution. The heat and moisture transfer rates in a LAMEE can be enhanced if a third fluid stream is used to control the desiccant solution temperature in the LAMEE. A LAMEE with a third fluid stream is known as a 3-fluid LAMEE. Published studies on 3-fluid LAMEEs are limited to experiments on the exchanger under limited test conditions.

This thesis focuses on simulating the performance of a 3-fluid LAMEE in a membrane liquid desiccant air-conditioning (M-LDAC) system. In the thesis, empirical correlations are developed based on experimental data to model the 3-fluid LAMEE and the limitations of the empirical model are evaluated. Subsequently, the 3-fluid and 2-fluid M-LDAC systems are simulated and compared at six different dehumidification load conditions. The simulation results show that, for most conditions, the 3-fluid M-LDAC system is able to meet the dehumidification load with a lower energy input than the 2-fluid M-LDAC system. The energy efficiency of the 2-fluid M-LDAC system is higher than the 3-fluid M-LDAC system at only the lowest dehumidification load.

The 3-fluid and 2-fluid M-LDAC systems are paired with a radiant cooling system to condition a small office building located in a hot-humid climate (Miami, Florida). Both the 2-fluid and 3-fluid systems provide acceptable thermal environment within the office building but the energy consumption of the 2-fluid system is 50% higher than the 3-fluid system. This thesis concludes that the 3-fluid M-LDAC system may be more suitable than the 2-fluid M-LDAC system for hot and humid climates and in buildings with high dehumidification loads.

ACKNOWLEDGEMENTS

I would like to thank my supervisor, Professor Carey Simonson, for this opportunity as well as his guidance, support, and leadership throughout this research. I am grateful to have worked under such a distinguished professor. This experience has taught me many professional and personal life lessons.

I also wish to extend my gratitude to Mohamed R.H. Abdel-Salam for his guidance and support throughout my research. I would also like to thank my fellow graduate students/post-doctoral fellows who have conducted their research during my studies as their thoughts and research have been of great help for me – Adesola Olufade, Ahmed Abdel-Salam, Amzad Hossain, Gaoming Ge, Pooya Navid, and Shirin Niroomand.

I would like to acknowledge the financial assistance from the University of Saskatchewan.

DEDICATION

I dedicate this thesis to my family and friends.

I would have never succeeded without your support and encouragement.

TABLE OF CONTENTS

LIST OF TABLES

Table **Page**

LIST OF FIGURES

Figure **Page**

NOMENCLATURE

Acronyms

AC	air-conditioning
ASHRAE	American Society of Heating, Refrigerating, and Air-Conditioning Engineers
CAC	conventional air-conditioning
DOE	Department of Energy
HVAC	heating, ventilation and air-conditioning
IAQ	indoor air quality
IEO	International Energy Outlook
IEA	International Energy Agency
LAMEE	liquid-to-air membrane energy exchanger
LCC	life cycle cost
LDAC	liquid desiccant air-conditioning
M-LDAC	membrane-liquid desiccant air-conditioning
RAMEE	run-around membrane energy exchanger
TRNSYS	transient system simulation

English Symbols

A	surface area of membrane, m^2
c_p	specific heat capacity, J/(kg·K)
C	thermal capacity rate, W/K
COP	coefficient of performance
Cr	thermal capacity rate ratio
ECR	energy consumption rate, kW
ETR	energy transfer rate, kW
h	convective heat transfer coefficient, W/(m^2·K); enthalpy, J/kg
h_g	specific enthalpy for saturated water vapor at 0°C, kJ/kg
h_m	mass transfer coefficient, (kg/(m^2·s))
h_r	radiative heat transfer coefficient, (W/(m^2·K))
k	thermal conductivity, J/(m·K)
k_m	membrane vapor permeability, (kg/(m·s))
$\dot{m}$	mass flow rate, kg/s
$\dot{m}_{rr}$	moisture removal rate, g_v/s
NTU	number of heat transfer units
NTU_m	number of mass transfer units
Q_c	cooling rate, W

Q_h	heating rate, W
Re	Reynolds number
RH	relative humidity, %
T	Temperature, °C
T_{mr}	mean radiant temperature of a building, °C
T_{op}	operative temperature, °C
U	overall heat transfer coefficient, $W/(m^2 \cdot K)$
U_m	overall mass transfer coefficient, $(kg/(m^2 \cdot s))$
W	humidity ratio, g_v/kg_{da}; power, kW
X	mass fraction for concentration, %

Greek Symbols

δ	Thickness, mm
ε	effectiveness
η	thermal efficiency, %

Subscript

air	air
c	cooling
chiller	chiller
da	dry air
ev	evaporator
fan	fan
h	heating
in	inlet conditions
lat	latent
mem	membrane
min	minimum
out	outlet conditions
pump	pump
ref	refrigerant
sen	sensible
SHX	sensible heat exchanger
sol	solution
w	water
v	water vapor

Chemical Symbols

$CaCl_2$	calcium chloride
LiBr	lithium bromide
LiCl	lithium chloride
LiI	lithium iodide
$MgCl_2$	magnesium chloride

CHAPTER 1

INTRODUCTION

1.1 Heating, ventilating, and air-conditioning (HVAC) systems

Heating, ventilating, and air-conditioning (HVAC) systems are used to maintain an acceptable thermal environment and indoor air quality (IAQ) within buildings. HVAC systems are important because people spend 90% of their time in buildings (Spengler and Sexton 1983). Unfortunately, HVAC systems are energy demanding and, as the population increases, this energy consumption will only increase. Buildings contribute 20% to 40% towards the total worldwide energy consumption (Kolokotsa et al. 2011; Wyon 2004; Navigant Research 2015) while HVAC systems account for approximately 40% to 50% of this building energy consumption (Navigant Research 2015; Pérez-Lombard et al. 2008). Furthermore, the International Energy Outlook 2016 projects worldwide energy demand to increase by 48% from 2012 to 2040 (U.S. Energy Information Administration 2016).

Heating and cooling systems are very energy intensive in extreme climates. In colder climates, such as Canada, space heating accounts for 55%-63% of the building energy consumption (Natural Resources Canada 2016), while in warmer climates, such as the Middle East, space cooling accounts for 70% of the building energy consumption (El-Dessouky, Ettouney, and Al-Zeefari 2004). Heating systems are efficient, with high-efficiency systems having an annual fuel utilization

efficiency (AFUE) of up to 98.5% (Energy Saver 2013), and cost effective. In contrast, the air cooling and dehumidifying process of conventional cooling systems is energy intensive.

1.1.1 Conventional air-conditioning (CAC) system

In this thesis, an air-conditioning system will defined as a system that cools and dehumidifies air. A conventional air-conditioning (CAC) system uses a vapor compression cycle to remove heat from a building. In a vapor compression cycle, refrigerant cycles through a compressor, condenser, expansion valve, and evaporator loop. Air is cooled and dehumidified by the evaporator heat exchanger before being supplied to a space. The heat from the air is then transferred to the condenser by the refrigerant and then to the environment as ambient air passes the condenser heat exchanger. CAC systems account for 6% of the electricity produced and costs $29 billion annually in the United States (Energy Saver 2014).

A CAC system is more efficient at cooling air than dehumidifying air. Figure 1.1 illustrates the air dehumidification process ($1 \rightarrow 2 \rightarrow 3$) of a CAC system on a psychrometric chart. This process is energy inefficient because the air must be cooled below its dew point temperature by the evaporator to condense water vapor from the air. Air at a temperature below the dew point temperature is often too cold and should be heated before being supplied to a space, thereby, further increasing the energy consumption. Moreover, condensate on the evaporator can lead to bacteria growth and increased maintenance costs.

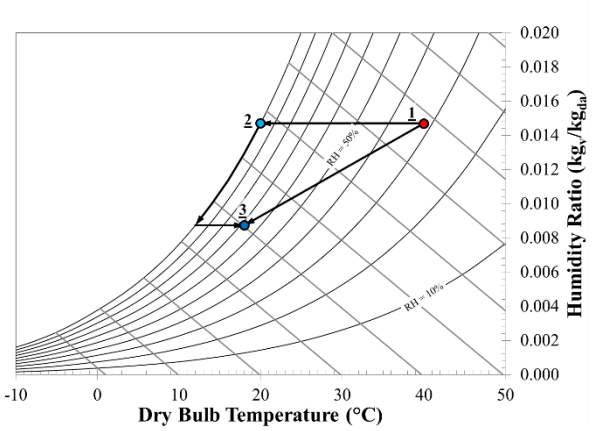

Figure 1.1: The dehumidification process of a CAC system (1 → 2 → 3) and a LDAC system (1 → 3) on a psychrometric chart.

1.1.2 Liquid desiccant air-conditioning (LDAC) system

An alternative to the CAC system is a liquid desiccant air-conditioning (LDAC) system. The LDAC system requires less energy to dehumidify air than the CAC system as shown by its dehumidification process (1 → 3) in Figure 1.1. When compared to the CAC systems, LDAC systems have been shown to reduce energy consumption by up to 26-80% in hot-humid climates (Mohammad et al. 2013). These systems implement a liquid desiccant solution which has a strong attraction towards water and will readily remove moisture from the air. A schematic of an LDAC system supplying air to building is presented in Figure 1.2.

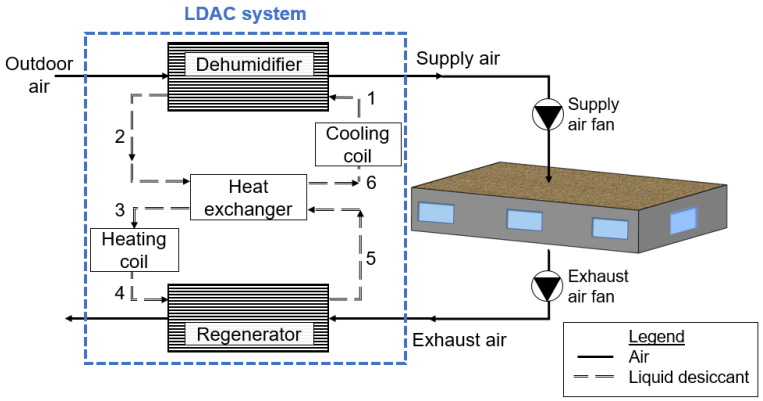

Figure 1.2: Schematic of an LDAC system supplying air to a building. The LDAC system in this example uses building exhaust air to regenerate the desiccant solution.

LDAC systems consist of two main components, a dehumidifier and regenerator, joined by a desiccant solution loop, which dehumidifies the air stream or regenerates the liquid desiccant. The dehumidifier and regenerator are heat and mass exchangers. In the dehumidifier, the desiccant solution removes heat and moisture from the air. After leaving the dehumidifier, the diluted desiccant solution must be restored to its initial concentration. Therefore, downstream of the dehumidifier, the diluted desiccant solution is first heated and then is restored to its initial concentration in the regenerator where moisture is transferred from the hot solution to an air stream (building exhaust air in Figure 1.2). Before returning to the dehumidifier, the desiccant must be cooled. A sensible heat exchanger can be used to transfer heat between solution streams from the dehumidifier and regenerator, thus, reducing the heating and cooling load required by the cooling and heating coils.

1.2 Liquid desiccant solutions

LDAC systems rely on desiccant solutions for air dehumidification. Aqueous liquid desiccant solutions are usually mixtures of ionic salts and water with the most common being calcium chloride ($CaCl_2$), lithium bromide (LiBr), lithium chloride (LiCl), and magnesium chloride ($MgCl_2$) (ASHRAE 2008). Different desiccants have different dehumidification capacities. For example, a saturated LiCl solution has a lower equilibrium relative humidity than a saturated LiI solution as it can reach an equilibrium relative humidity of 11.3% at 25°C while LiI produces an equilibrium relative humidity of 17.6% at the same conditions (Greenspan 1977). For further illustration, Figure 1.3 presents the equilibrium relative humidity lines of various saturated solution superimposed on a psychrometric chart.

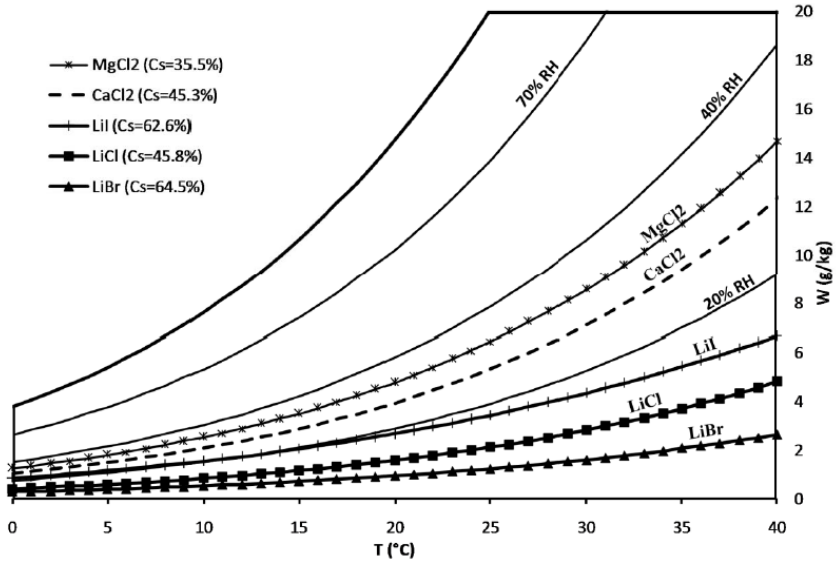

Figure 1.3: Equilibrium surface humidity ratio lines of various saturated desiccant solutions where Cs values indicate the saturation concentration of the solutions at 25°C (courtesy of Afshin 2010).

Ideal desiccants have low surface vapor pressure (low equilibrium humidity), minimal risk of crystallization, low corrosivity, low regeneration temperature, high density, low viscosity, and low cost (Mohammad et al. 2013). A major disadvantage of desiccants is their cost and, since ideal desiccants are usually the most expensive, mixtures or lower cost desiccants may be used to reduce cost. Furthermore, crystallization increases maintenance and operating costs. LiCl is used in the proposed LDAC system because it has low surface vapor pressure and a low risk of crystallization (Afshin 2010). In this thesis, these solutions are referred to as salt solutions, liquid desiccant solutions, liquid desiccants, and desiccant solutions.

Moisture transfer between a desiccant solution and air is driven by the difference between the vapor pressure associated with the desiccant solution and the partial pressure of water vapor in the air. Moisture is transferred from the fluid with a higher vapor pressure to the fluid with a lower vapor pressure. Partial vapor pressures of a desiccant solution are dependent on desiccant type, concentration and temperature. A desiccant solution with a higher desiccant concentration and/or

a lower temperature has a lower partial vapor pressure. A lower temperature reduces molecular energy thereby decreasing the amount of water vapor. In contrast, a liquid desiccant solution has a higher partial vapor pressure when its desiccant concentration is low and/or it has a higher temperature. Furthermore, as shown in Figure 1.3, desiccant solutions have varying dehumidifying capacities due to different strengths in ionic forces between chemical elements. That is, desiccant solutions with weaker ionic bonds between elements can remove more moisture from the air than desiccant solutions with stronger ionic bonds.

A disadvantage of using salt solutions is crystallization, where the desiccant precipitates out of the solution and can cause fouling. Fouling is the accumulation of the unwanted precipitate that can degrade equipment performance and increase the pressure drop across an exchanger. This can significantly increase operating and maintenance costs. Olufade and Simonson (2017) studied the effects of crystallization in an energy exchanger and found that fouling can reduce the moisture transfer rate by up to 60%.

1.3 Liquid desiccant exchangers

Liquid desiccant exchangers can be categorized as packed-bed exchangers, which allow direct contact between the liquid desiccant and air streams, and membrane exchangers, which use membranes to separate the liquid desiccant and air streams.

1.3.1 Packed-bed exchangers

A packed-bed dehumidifier sprays a cool desiccant solution onto a contact media which an air stream simultaneously passes over to cool and dehumidify the air. In a packed-bed regenerator, the diluted desiccant solution is heated before being sprayed onto a contact media to regenerate the desiccant solution. The main disadvantages of direct contact liquid desiccant systems are high

operating and maintenance costs, and desiccant carry-over. High operating costs are due to fans needing to overcome the high airside pressure drop caused by the packed-bed. Desiccant carryover is when some of the desiccant solution is entrained in the air stream and carried downstream, thereby, possibly corroding the ducts and contaminating the supply air stream leading to health concerns.

1.3.2 LAMEE

Another option for the dehumidifier and regenerator is an exchanger where the desiccant solution and air interact indirectly, such as a liquid-to-air membrane energy exchanger (LAMEE). A LAMEE separates the desiccant solution and air streams with a microporous membrane that allows for simultaneous heat and water vapor transfer while preventing liquids from penetrating through the membrane. LAMEEs eliminate the carry-over problem in the direct contact exchangers. Furthermore, the airside pressure drop is reduced since the packed-bed is replaced with a series of channels. An LDAC system that uses LAMEEs is referred to as a membrane liquid desiccant air-conditioning (M-LDAC) system.

The first study published on a LAMEE was in 1996 by Isetti et al. (1996) at the University of Genoa. Between 1996 and 2011, there has been an average of 1.5 papers per year on LAMEEs. Since 2011, research publications on LAMEEs increased significantly (at least eight publications per year) (Abdel-Salam et al. 2014). Of the research performed on the LAMEE, 58% of the publications were performed in Canada, 21% in China, 20% in Italy, and 1% in other countries (Abdel-Salam et al. 2014). These publications present different types of LAMEEs, experimental data, steady-state and transient performance, and numerical and analytical models to predict LAMEE performance.

1.3.3 Hollow-fiber LAMEE

A hollow-fiber LAMEE is like a shell-and-tube heat exchanger, except the metal tubing is replaced with a microporous membrane that permits heat and moisture transfer. Figure 1.4 presents a detailed schematic and cross-sectional view of a hollow-fiber LAMEE. The hollow-fiber LAMEE can be designed to accommodate cross and counter flow configurations.

(a)

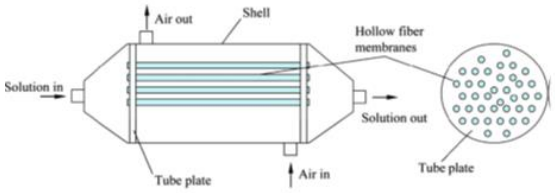

(b)

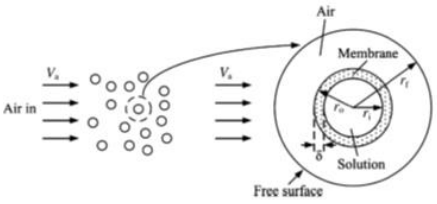

Figure 1.4: (a) Structure of a hollow-fiber LAMEE (Zhang 2010), and (b) a detailed schematic of a cross section of a single hollow fiber (Zhang et al. 2012)

Bergero and Chiari (2001) introduced the hollow-fiber LAMEE in 2001 at the University of Genoa where they experimentally and theoretically investigated a cross-flow hollow-fiber LAMEE during dehumidification and humidification conditions. The hollow-fiber membrane showed promise as experiments showed a high moisture transfer efficiency (Bergero and Chiari 2001). Subsequent research showed that the heat and moisture transfer effectiveness increases as the solution flow rate increases (Chiari 2000), air flow rate decreases (Bergero and Chiari 2001; Chiari 2000; Zhang and Huang 2011; Zhang 2011), and membrane surface area increases (Zhang and Huang 2011; Zhang 2011), where effectiveness of up to 90% has been observed under some conditions (Chiari 2000). In 2011, Zhang (2011) developed and verified an analytical model to compute the heat and moisture transfer in a counter flow hollow-fiber LAMEE.

1.3.4 Flat-plate LAMEE

A flat plate 2-fluid liquid-to-air membrane energy exchanger (LAMEE), pictured in a counter-cross flow configuration in Figure 1.5, can also be used as the dehumidifier and regenerator in the LDAC system. Like a parallel-plate heat exchanger, the LAMEE consists of alternating desiccant solution and air stream channels. However, in a flat-plate LAMEE, the impermeable metal sheets employed in the flat-plate heat exchanger are substituted for vapor permeable membranes that permit simultaneous heat and moisture transfer between the liquid desiccant and air. The 2-fluid LAMEE is most effective in the counter-flow configuration (ASHRAE 2004) but this configuration poses difficulty in manufacturing headers that permit adjacent air and solution flows. For this reason, Vali et al. (2009) proposed a counter-cross flow configuration, where 90% of the exchanger is in counter flow while the inlets and outlets are in cross flow configuration. The flat-plate LAMEE uses this configuration while still maintaining a high sensible and latent effectiveness.

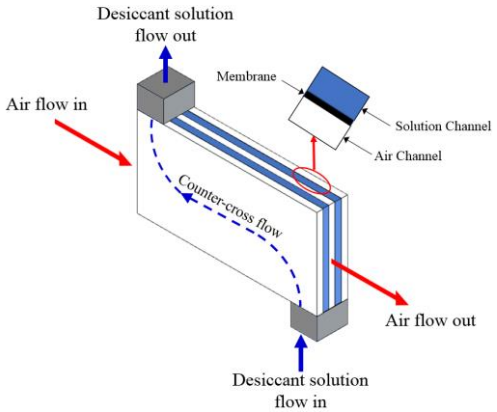

Figure 1.5: Diagram of a flat-plate 2-fluid liquid-to-air membrane energy exchanger

In 1996. Isetti et al. (1996) experimentally investigated the air dehumidification performance of a vapor-permeable flat-plate LAMEE used to control the humidity inside of a museum showcase. The following year, Isetti et al. (1997) performed a theoretical analysis on vapor mass flux across

a membrane and concluded that the vapor mass flux across the membrane is proportional to the temperature difference across the membrane and inversely proportional to the membrane thickness (Isetti et al. 1997). In his 2006 thesis, Vestrelli (2006) developed a Simulink model and investigated the effects of desiccant concentration and solution temperature on dehumidification and regeneration. To enhance dehumidification, a higher solution concentration and/or a low solution temperature is recommended whereas a lower solution concentration and/or high solution temperature improves solution regeneration (Vestrelli 2006).

At the University of Saskatchewan, a counter-cross flow 2-fluid LAMEE prototype was built and tested by Mahmud et al. (2009) in 2009 and by Beriault in 2011 (2011). Using Beriault's prototype, Namvar et al. (2012; 2013) experimentally and numerically studied the transient performance characteristics of a 2-fluid LAMEE. Moghaddam et al. (2013a; 2013b) performed various experimental and theoretical studies on the steady-state performance of a 2-fluid LAMEE. In 2013, Ge et al. (2013) modified and verified the analytical model developed by Zhang (2011) to account for counter-cross flow configuration in a flat plate 2-fluid LAMEE.

Most flat-plate LAMEE studies have been limited to exchanger-level (dehumidifier and regenerator) tests or implementation of LAMEEs in a run-around membrane energy exchanger (RAMEE) system, which is an LDAC system without the heating and cooling coils used for recovering energy from building exhaust air. In 2013, Abdel-Salam et al. (2013) used the analytical model developed by Ge et al. (2013) to simulate an M-LDAC system using the Transient System Simulation (TRNSYS) software and concluded that the system is effective at meeting the latent load for thermal comfort conditions. Following this study, Abdel-Salam and Simonson (2014)

showed that the energy consumption and life cycle cost (LCC) of the M-LDAC system are 19% and 12% lower than the CAC system.

1.3.5 The membrane

A key component of a LAMEE is the micro-porous membrane. These membranes can be made from various polymers, such as polypropylene (PP), polyethylene (PE), polytetrafluoroethylene (PTFE), and polyvinylidene fluoride (PVDF) (Khayet 2011). Larson (2006) and Beariault (2011) focused on membrane selection and testing in their theses. While selecting a membrane for the LAMEE, there are numerous desired characteristics to consider enhancing the heat and moisture transfer. It should have a high liquid penetration pressure, low vapor diffusion resistance, high modulus of elasticity, high porosity, low tortuosity factors, low thermal resistance, good thermal stability, resistant to various chemicals, cost-effective, durable, and resistant to fouling (Khayet 2011; Beriault 2011; Larson 2006).

Some disadvantages associated with LAMEEs include flow maldistribution and crystallization. Membranes are subject to bulge and deform due to their flexibility and can result in uneven channel thickness leading to unequal flow in each channel. Previous research has shown that flow maldistribution can decrease thermal performance in a heat exchanger by up 25% (Mueller 1987; Lalota et al. 1999). Flow maldistribution also increases the pressure drop across the exchanger (Chin and Raghavan 2011; Thulukkanam 2000). An insert is often placed in the air channels to support the membranes and can enhance total effectiveness by up to 13% due to an increased mixing in the air stream (Moghaddam et al. 2013a).

1.3.6 Phase change energy

When a substance undergoes a phase change, it releases phase change energy. When water vapor condenses as it does in the dehumidifier, phase change energy is released to the solution because water changes from a state of higher energy (gas) to state of lower energy (liquid). Similarly, when liquid water evaporates, as seen in the regenerator, energy needs to be added for the water to reach this higher energy state (vapor). In LAMEEs, phase change energy decreases the potential for heat and moisture transfer since the phase change energy is released to or absorbed by the solution, therefore, decreasing the temperature differential between the solution and air. Figure 1.6 depicts the effects of phase change energy on the solution temperature by comparing the solution temperature along a LAMEE and a parallel plate heat exchanger where the solution temperature shifts towards that of the air due to the phase change energy.

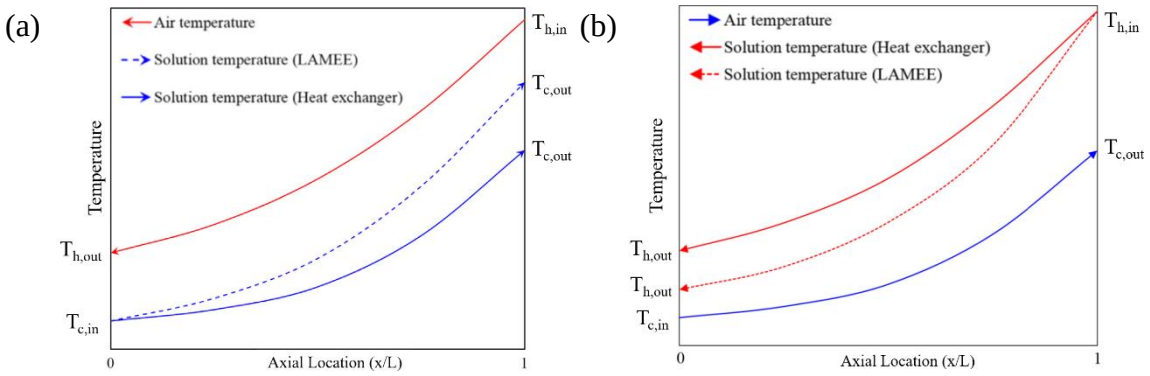

Figure 1.6: Schematic of the air and desiccant solution temperatures along a 2-fluid LAMEE and heat exchanger show that the phase change energy reduces the temperature difference between the air and desiccant solution streams under (a) dehumidification (Courtesy of Abdel-Salam et al. 2016a) and (b) regeneration operating conditions (Courtesy of Abdel-Salam et al. 2016b).

1.3.7 3-fluid LAMEE

To overcome the effects of phase change energy, Abdel-Salam et al. (2016a) introduced a third fluid (in addition to air and solution) to the LAMEE and called it a 3-fluid LAMEE, shown in Figure 1.7. The 3-fluid LAMEE has refrigerant piping within the solution channel to control the solution temperature across the entire length of the exchanger. The refrigerant reduces the change in the solution temperature, which enhances the heat and moisture transfer between the solution and air by keeping the temperature and vapor pressure differential between the air and solution more constant throughout the exchanger. In the design of Abdel-Salam et al. (2016a), the air and solution are in counter-cross flow configuration and the solution and refrigerant are in counter flow configuration.

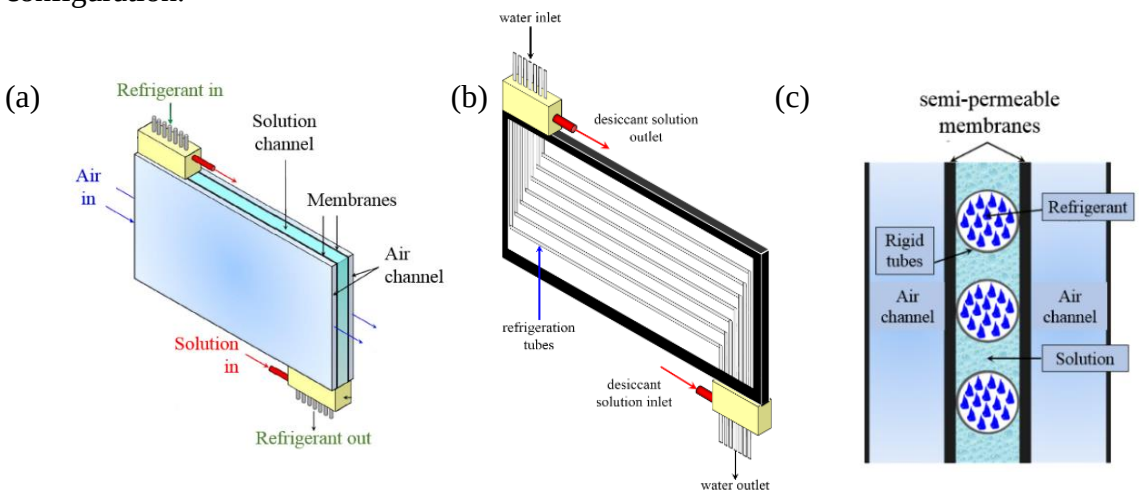

Figure 1.7: (a) A schematic of a small-scale prototype, (b) refrigerant piping, and (c) a vertical cross section of the 3-fluid LAMEE (Courtesy of Abdel-Salam et al 2016a).

Experiments were exclusive to the exchanger with water as the refrigerant where Abdel-Salam et al. (2016a; 2016b) evaluated the effectiveness of the 3-fluid LAMEE under dehumidifier and regenerator operating conditions and compared them with that of the 2-fluid LAMEE. Figure 1.8 shows the improvements in the sensible and latent effectiveness of the 3-fluid LAMEE compared to the 2-fluid LAMEE at different inlet water temperatures and mass flow rates (Cr) under air

cooling and dehumidifying conditions and solution regeneration conditions. Although sensible and latent effectivenesses were higher for the 3-fluid LAMEE than the 2-fluid LAMEE under all the tested conditions, the latent effectiveness notably increased under regeneration conditions.

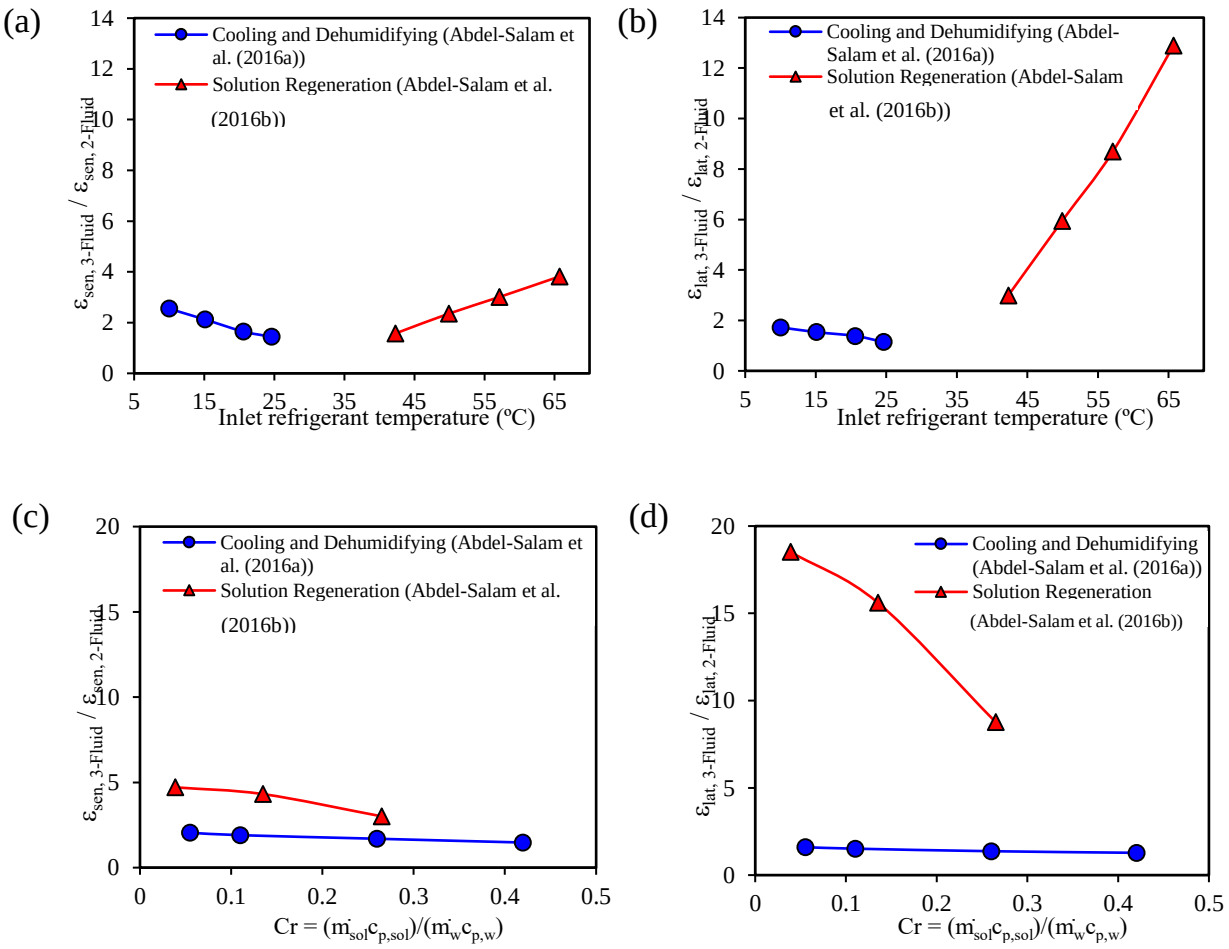

Figure 1.8: Ratio between the 3-fluid and 2-fluid LAMEEs (a) heat and (b) moisture transfer effectiveness (ε) at different inlet refrigerant temperatures, and (c) heat and (d) moisture transfer effectiveness at different refrigerant mass flow rates (Cr) (Abdel-Salam et al. 2016a; Abdel-Salam et al. 2016b)

1.4 Objectives

The main objective of this study is to simulate the 3-fluid LAMEE developed by Abdel-Salam et al. (2016a; 2016b; 2017) in a building. Specific objectives are to:

1. develop empirical models for the 3-fluid LAMEE as a dehumidifier and regenerator based on the experimental data of Abdel-Salam et al. (2016a; 2016b),
2. simulate 3-fluid and 2-fluid M-LDAC systems and compare their performance under six different design operating conditions,
3. simulate and compare the performance of 2-fluid and 3-fluid M-LDAC systems in a small office building during a week of warm weather in Miami, Florida, and
4. investigate the performance of the 2-fluid and 3-fluid M-LDAC systems under different dehumidification loads.

1.5 Thesis Structure

The thesis is a manuscript-style thesis consisting of four chapters where the middle two chapters are research papers that address the objectives of the thesis. In the second chapter, the first two objectives are addressed, which includes developing, presenting, and analyzing the limitations of the 3-fluid LAMEE models and then implementing these models in an M-LDAC system. Chapter 2 also includes a performance comparison between the 3-fluid and a 2-fluid M-LDAC system under multiple dehumidification load conditions.

Chapter 3 addresses objectives 3 and 4. An office building is modelled with a HVAC system that uses radiant cooling panels to cool the building (meet the sensible loads) and an M-LDAC system to dehumidify the building (meet the latent loads). Simulations are conducted over the warmest week of the year in Miami, Florida and the 3-fluid and 2-fluid M-LDAC systems are compared. Lastly, parametric studies are performed to determine if the systems can meet higher latent loads resulting from higher occupant densities or infiltration rates. Chapter 4 contains a summary of the thesis, conclusions, and recommendations for future work.

Appendix A presents the equations used to calculate the LiCl solution properties, Appendix B summarizes the experimental data used in the thesis, and Appendix C presents the model extrapolation analysis.

1.6 List of publications

The following papers are included as chapters in this thesis. At the time of thesis submission, both chapters had been submitted to journals and are currently under review.

Chapter 2: Storle D., Abdel-Salam M.R.H., Simonson C.J., 2017. Simulation of a 3-fluid membrane liquid desiccant air-conditioning system under different design loads. Energy and Buildings, Submitted.

Chapter 3: Storle D., Abdel-Salam M.R.H., Simonson C.J., 2017. Building energy simulation of a 3-fluid membrane LDAC system under hot and humid weather conditions. Energy and Buildings, Submitted.

The following conference paper was published as a part of this research but omitted from the thesis.

Storle, D., Abdel-Salam, M.R.H., Pourmahmoud N., Simonson, C.J., 2017. Performance of the Dehumidification Cycle of a 3-Fluid Liquid Desiccant Membrane Air-Conditioning System. Building Simulation 2017. San Francisco, August 7-9. 7 pages.

CHAPTER 2

THE 3-FLUID LAMEE MODEL

2.1 Overview of Chapter 2

The 3-fluid liquid-to-air membrane energy exchanger (LAMEE) is a novel energy exchanger and published studies on the 3-fluid LAMEE are limited to experimental studies under different operating conditions. This chapter focuses on developing an empirical 3-fluid LAMEE model and using this model to simulate system performance. The model is developed from and verified with experimental data, and a list of model limitations and constraints is established. Using the empirical 3-fluid LAMEE model, a 3-fluid membrane liquid desiccant air-conditioning (M-LDAC) system is modeled. A 2-fluid M-LDAC system is modeled using a previously developed analytical solution for the 2-fluid LAMEE. The 3-fluid and 2-fluid M-LDAC systems are then simulated at multiple different design conditions with different latent loads and their performances are evaluated and compared.

The manuscript presented in this chapter has been submitted to the Applied Energy journal. The three authors are Devin Storle (MSc student who performed the study and wrote the manuscript), Mohamed R.H. Abdel-Salam (post-doctoral fellow who reviewed the manuscript), and Carey J. Simonson (MSc supervisor who reviewed the manuscript and supervised the study).

Simulation of a 3-fluid membrane liquid desiccant air-conditioning system under different design loads

Devin Storle, Mohamed R.H. Abdel-Salam, Carey J. Simonson

2.2 Abstract

Liquid-to-air membrane energy exchangers (LAMEEs) permit heat and moisture transfer between a liquid desiccant solution and air streams through vapor permeable membranes. Liquid desiccant membrane air-conditioning (M-LDAC) systems implement LAMEEs to meet the latent or dehumidification loads in buildings. M-LDAC systems are better suited to dehumidify air than conventional air-conditioning (CAC) systems. One way to enhance the performance of LAMEEs is to install refrigeration tubes inside the solution channels to control the solution temperature inside the LAMEE, such an exchanger is called a 3-fluid LAMEE. The main objectives of this chapter are to develop a Transient System Simulation (TRNSYS) model of the 3-fluid LAMEE, and use it to simulate the performance of a 3-fluid M-LDAC system under a low, medium, and high latent load conditions. The results show that the 3-fluid M-LDAC system outperforms the 2-fluid M-LDAC system under the high and medium latent load conditions; whereas, the 2-fluid M-LDAC system outperforms the 3-fluid M-LDAC system under the lowest latent load condition.

2.3 Introduction

The rise in energy demand has led to concerns regarding limited resources and potential environmental and economic impacts. World energy consumption has increased over the past few decades and will continue to rise with population growth and infrastructure development. According to the International Energy Agency (IEA), world energy consumption from 1973 to 2014 increased by 102% (4661 Mtoe to 9425 Mtoe) (International Energy Agency 2016). Furthermore, the International Energy Outlook 2016 (U.S. Energy Information Administration

2016) projects a 48% increase in total world energy consumption from 2012 to 2040. Consequently, the U.S. Energy Information Administration (EIA) projects CO_2 emissions to increase annually by 1 % from 2012 to 2040 (U.S. Energy Information Administration 2016). The need to reduce energy use intensity is evident as rising CO_2 levels advance climate change and threaten the environment and the quality of life of humans.

The commercial and residential building sector represents a large portion of the global energy consumption. The IEO2016 states that the building sector accounted for 20% of the global energy consumption in 2016 (U.S. Energy Information Administration 2016), whereas, building energy consumption in developed countries reached between 20% and 40% of the total energy consumption (Pérez-Lombard et al. 2008). In addition, the IEO2016 forecasts a 42% increase in building energy consumption from 2012-2040 (U.S. Energy Information Administration 2016) due to new building construction, improved indoor air quality (IAQ), and more time spent inside buildings (Pérez-Lombard et al. 2008).

Within the building sector, heating, ventilation and air-conditioning (HVAC) systems are responsible for a large amount of energy consumption. HVAC systems condition (heating, cooling, dehumidifying and humidifying) air to maintain thermal comfort within a space. In 2012, U.S. Energy Information Administration (EIA) reported space heating, ventilation, and cooling contributed 25%, 10%, and 9%, respectively, towards the commercial building energy consumption in the United States (U.S. Energy Information Administration 2013). In colder climates, such as Canada, space heating and cooling account for 55% and 4%, respectively, of the commercial energy use (Natural Resources Canada 2016). Conversely, space cooling accounts for

70% of the total building energy consumption in hot and humid climates such as the Middle East (El-Dessouky et al. 2004).

Conventional air-conditioning (CAC) systems are used in over 80% of American homes (U.S. Energy Information Administration 2011) and consume a lot of energy to dehumidify and cool air. Figure 2.1 shows the air dehumidifying process for CAC systems ($1 \rightarrow 2 \rightarrow 3$) on a psychrometric chart. To dehumidify air, the CAC system cools the air to a temperature below its dew point temperature to remove moisture through condensation. If the air is too cold to be supplied to the space, it may need to be reheated before being supplied to the conditioned space. Although the CAC system can provide desirable thermal comfort, dehumidifying air by cooling it along its dew point temperature is energy intensive and inefficient. Furthermore, condensate on the evaporator coil can cause bacteria and mold to form, which can contaminate the supply air and lead to negative health effects.

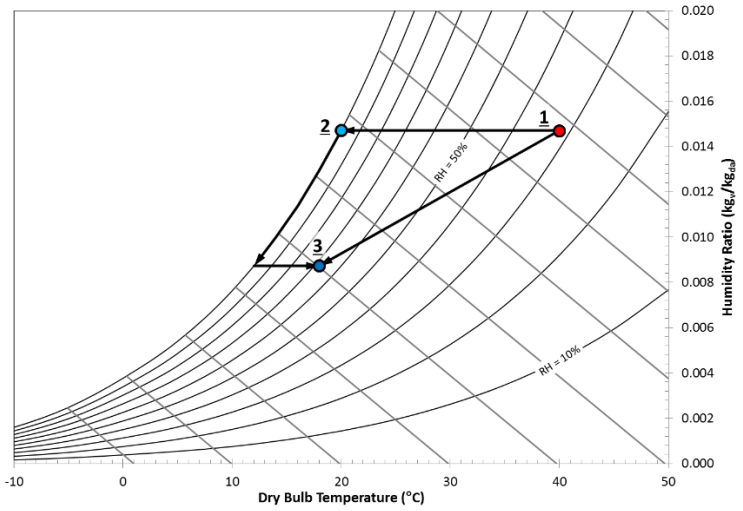

Figure 2.1: Cooling and dehumidifying processes on a psychrometric chart ($1 \rightarrow 2 \rightarrow 3$: air cooling and dehumidifying (CAC system), and $1 \rightarrow 3$: air cooling and dehumidifying (LDAC) system).

2.4 The LDAC System

An alternative to the CAC system is a liquid desiccant air-conditioning (LDAC) system. Over the past decade, several studies have shown that liquid desiccant air-conditioning (LDAC) systems can achieve significant energy savings compared to CAC systems (Abdel-Salam et al. 2014). LDAC systems use liquid desiccants to cool and dehumidify the outdoor air. Liquid desiccants readily absorb moisture from the air, and also kill germs and bacteria (Abdel-Salam et al. 2014), and can be regenerated using solar energy. Process 1 → 3 in Figure 2.1 represents the air cooling and dehumidifying process in a dehumidifier of an LDAC system shown in Figure 2.2.

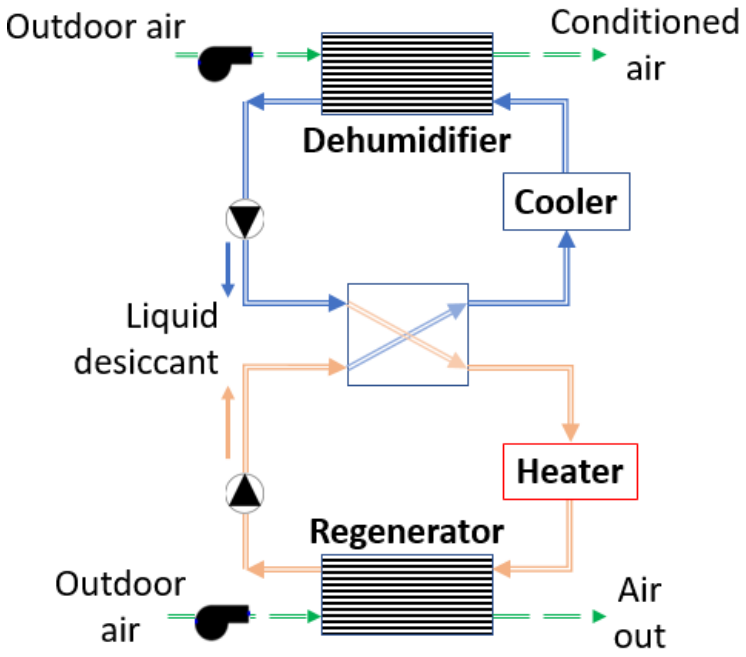

Figure 2.2: A schematic of a liquid desiccant air-conditioning system

The LDAC system uses a dehumidification-regeneration cycle where a concentrated desiccant solution (e.g. LiCl, LiBr, $MgCl_2$, $CaCl_2$) is used to cool and dehumidify the supply air in the dehumidifier and the desiccant solution is regenerated (dried) in the regenerator. Other components of the LDAC system include a heater, cooler, pumps, and a solution-to-solution heat exchanger.

The cooler cools the liquid desiccant solution before entering the dehumidifier to enhance air cooling and dehumidification. The heater heats the diluted desiccant solution prior to entering the regenerator to improve desiccant solution regeneration. A sensible heat exchanger is used to transfer heat between the heated and cooled liquid desiccant in counter flow configuration to reduce the heating and cooling loads of the heater and cooler.

In direct contact exchangers, the desiccant solution and air streams come into direct contact, exchange heat and moisture, and then are separated. Direct contact exchangers, such as packed-bed exchangers, are commonly used as the dehumidifier and regenerator in LDAC systems. However, direct contact exchangers can lead to desiccant entrainment in the air stream which can cause duct corrosion, increased maintenance costs, and reduction in indoor air quality.

2.5 Liquid-to-air membrane energy exchanger (LAMEE)

A liquid-to-air membrane energy exchanger (LAMEE) is an exchanger that resolves the issue of desiccant carryover. Figure 2.3 presents a schematic of a liquid-to-air membrane energy exchanger (LAMEE). The LAMEE allows for heat and moisture transfer between two fluids, commonly, air and a liquid desiccant solution. Analogous to a multi-channel flat plate heat exchanger, this exchanger consists of alternating fluid channels. However, the LAMEE uses a semipermeable membrane to separate the two fluids instead of impermeable plates. The pores in the vapor permeable membrane permit vapor transfer while preventing liquid penetration (Abdel-Salam et al. 2014; Huang and Zhang 2013). Furthermore, the thin membrane conducts heat between the two fluids.

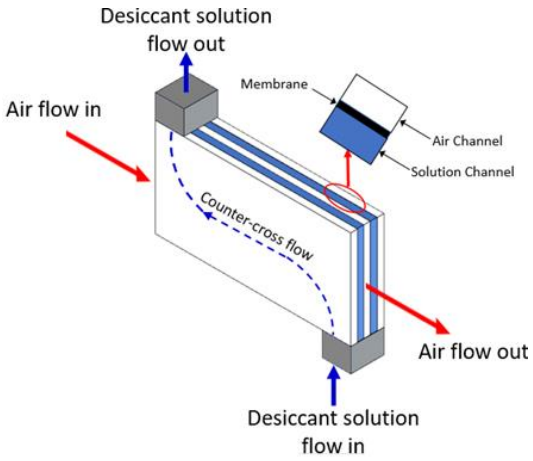

Figure 2.3: Schematic of a counter-cross flat-plate liquid-to-air membrane energy exchanger (LAMEE)

A membrane-liquid desiccant air-conditioning (M-LDAC) system uses LAMEEs as the dehumidifier and regenerator to transfer heat and moisture between the air and desiccant solution streams. Bergero and Chiari (Bergero and Chiari 2011; Bergero and Chiari 2010) studied the M-LDAC system and proposed potential energy savings exceeding 60% compared to the CAC system. Furthermore, the LDAC system is suitable for hot and humid climates and its thermal coefficient of performance (COP) value lies between 0.5 and 0.9 (Abdel-Salam et al. 2013). Abdel-Salam et al. (2013) simulated a M-LDAC system and recommended inlet desiccant solution temperatures to the dehumidifier and regenerator in the range of 15-20°C and 45-55°C, respectively, to improve performance (Abdel-Salam et al. 2013). Abdel-Salem et al. (2014) studied the payback period and life cycle cost of M-LDAC systems equipped with a solar thermal system and an electrical heat pump. A heat pump can be used to provide thermal energy for the regeneration of the diluted desiccant solution, thereby, decreasing annual operating cost and life cycle cost when compared to a M-LDAC system without a heat pump. Research has shown an immense potential for energy savings for M-LDAC systems.

2.6 3-fluid LAMEE

The potential for heat and moisture transfer between the desiccant solution and air streams depends significantly on the temperature and vapor pressure difference between the two fluids. Phase change energy accompanies the moisture transfer between the desiccant solution and air streams. This additional energy draws the desiccant solution temperature, up to 3°C (Abdel-Salam et al. 2016), towards the air temperature. Thus, phase change energy reduces the temperature and vapor pressure differential between the air and desiccant solution and limits heat and moisture transfer.

Abdel-Salam et al. (2016a) proposed, designed, and tested a prototype of a 3-fluid flat-plate LAMEE to mitigate the phase change energy effects. Figure 2.4 presents multiple views of this exchanger including (a) an overall view, (b) an inside view of the desiccant solution channel and (c) a vertical cross-section. The design of a 3-fluid LAMEE is similar to the 2-fluid LAMEE. However, the 3-fluid exchanger introduces internal cooling (or heating) to the desiccant solution channel by circulating a refrigerant in the piping inserted in the desiccant solution channel. This internal temperature control reduces the effects of phase change energy by absorbing or providing the phase change energy.

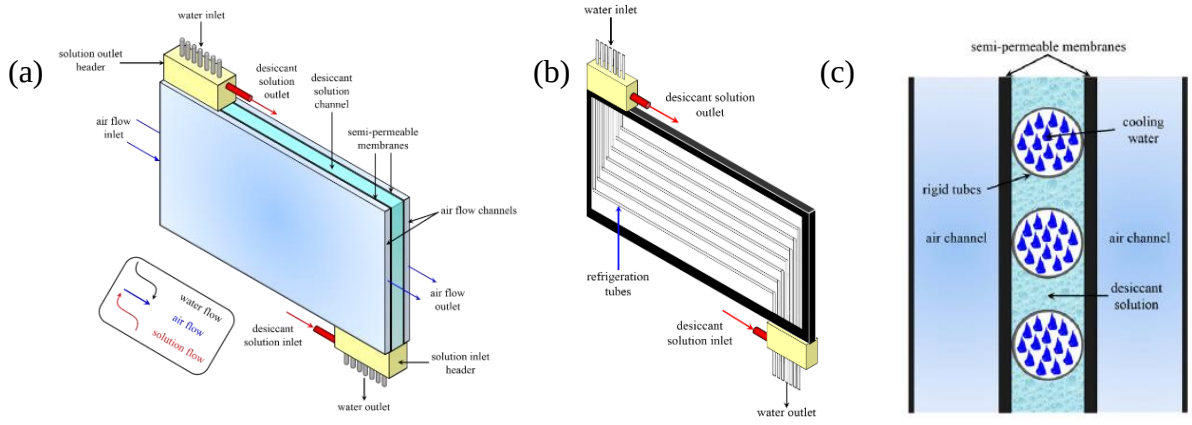

Figure 2.4: Schematic of a 3-fluid LAMEE showing (a) the entire exchanger, (b) the refrigerant tubing, and (c) a cross-sectional view (Courtesy of Abdel-Salam et al. 2016a)

Abdel-Salam et al. (2016a; 2016b; 2017) investigated the effects of the inlet refrigerant temperature and mass flow rate on the effectiveness of the 3-fluid LAMEE under different operating conditions (i.e., air cooling and dehumidifying, air heating and humidifying, and desiccant solution regeneration). Table 2.1 summarizes the design parameters of the studied 3-fluid LAMEE. There is one desiccant solution channel, two air channels and seven refrigerant tubes in the desiccant solution channel. Titanium tubing is used to circulate the refrigerant through the LAMEE. The studies used water as the refrigerant since it is inexpensive and has a large thermal capacity to serve as a good heat sink or source. The exchanger was set as a dehumidifier or regenerator and studied at various operating and design conditions. In the dehumidifier, the water acts as an internal coolant. Conversely, water provides internal heating in the regenerator.

Table 2.1: The 3-fluid LAMEE specifications and membrane properties (Abdel-Salam et al. 2016a).

	Parameter	Value	Unit
Exchanger	flow configuration (solution-air)	counter-cross	-
	flow configuration (solution-refrigerant)	counter	-
	length	470	mm
	height	100	mm
	exchanger solution entrance ratio*	0.11	-
	nominal air channel width	5	mm
	nominal solution channel width	4.2	mm
	number of air channels	2	-
	number of solution channels	1	-
	mass (empty)	1.7	kg
	desiccant solution	LiCl	-
Membrane	thickness	0.3	mm
	mass resistance	38	s/m
	liquid penetration pressure	124	kPa
Refrigeration tubes	refrigerant	water	-
	tube material	titanium	-
	number of tubes	7	-
	tube length	660	mm
	inner diameter	2.362	mm
	outer diameter	3.175	mm
	thickness	0.4	mm
	minimum spacing between tubes	9.7	mm
	thermal conductivity	21 (efunda 2017)	(W/(m·K))

**entrance ratio is defined as the ratio between the length of the inlet/outlet desiccant solution header and the length of the exchanger* (Vali 2009).

In the previous works by Abdel-Salam et al. (2016a; 2016b), the 3-fluid and 2-fluid LAMEEs were tested under the same operating parameters. The 3-fluid LAMEE prototype was tested as a 2-fluid LAMEE by turning the water flow off. Internal cooling and heating in the 3-fluid LAMEE improves the heat and moisture transfer effectiveness. Internal temperature control enhances the heat transfer effectiveness of the dehumidifier and regenerator by up to 66% (Abdel-Salam et al. 2016a) and 79% (Abdel-Salam et al. 2016b), respectively. Likewise, moisture transfer effectiveness increases from 8% to 48% (Abdel-Salam et al. 2016a) and 38% to 59% (Abdel-Salam et al. 2016b) when maintaining a constant desiccant solution temperature along the dehumidifier and regenerator, respectively.

2.7 Objectives

Previous studies on the 3-fluid LAMEE experimentally evaluated the performance of the 3-fluid LAMEE when operated as a dehumidifier or regenerator. There are no published studies on the performance of a M-LDAC system that includes 3-fluid LAMEEs. Therefore, the main objective of this chapter is to develop a TRNSYS model for the 3-fluid LAMEE, and use the model to simulate and compare the performance of the 2-fluid and 3-fluid M-LDAC systems under different operating conditions.

2.8 Methods

This section presents the models developed to simulate the 3-fluid LAMEE, the 2-fluid LAMEE, and the M-LDAC system. The range of application of the models will also be presented.

2.8.1 3-fluid LAMEE model

This section presents the models of the 3-fluid LAMEE which is used to predict the output conditions of the dehumidifier and regenerator using the input conditions. The model will be based on traditional heat and moisture exchanger parameters such as effectiveness (ε).

2.8.2 Effectiveness

The performance of an exchanger can be defined by its effectiveness which is the ratio of the actual energy transfer rate to the maximum possible energy transfer rate in the exchanger. Effectiveness can be divided into sensible and latent (or moisture transfer) effectivenesses. Equations (2.1) and (2.2) present the sensible and latent effectiveness, respectively, for a 3-fluid LAMEE in a counter flow configuration (Abdel-Salam et al. 2017) for the case where the air stream has the minimum heat capacity rate (which is the case for all the data in this thesis and most practical LAMEE applications).

$$\varepsilon_{\text{sen}} = \frac{(T_{\text{air,in}} - T_{\text{air,out}})}{(T_{\text{air,in}} - T_{w,\text{in}})} \tag{2.1}$$

$$\varepsilon_{\text{lat}} = \frac{(W_{\text{air,in}} - W_{\text{air,out}})}{(W_{\text{air,in}} - W_{\text{sol@T}_{\text{w,in}},\text{X}_{\text{sol,in}}})} \tag{2.2}$$

where ε corresponds to effectiveness, W is air humidity ratio (g_v/kg_{da}), T is temperature (°C), X_{sol} is the mass fraction of desiccant in the desiccant solution, and $W_{sol@T_{w,in}X_{sol,in}}$ is the humidity ratio of air that would be in equilibrium with a desiccant solution that is at the temperature of the inlet refrigerant and concentration of the inlet desiccant solution. Subscripts in and out refer to the inlet and outlet, sen and lat are sensible and latent, sol and w denote the desiccant solution and refrigerant (water), respectively.

2.8.3 Dimensionless parameters

The most important dimensionless parameter is the number of heat transfer units, NTU. This design parameter relates the overall heat transfer coefficient between the desiccant solution and air to the minimum thermal capacity rate of the two fluids (air, in this case). Equation (2.3) is used to calculate the number of heat transfer units.

$$NTU = \frac{UA}{C_{\text{air}}} \tag{2.3}$$

where U is the overall heat transfer coefficient (W/(m^2·K)) and A is the membrane surface area (m^2). The overall heat transfer coefficient is determined from Equation (2.4).

$$U = \left[\frac{1}{h_{\text{air}}} + \frac{\delta_{\text{mem}}}{k_{\text{mem}}} + \frac{1}{h_{\text{sol}}}\right]^{-1} \tag{2.4}$$

where h_{air} is the airside convective heat transfer coefficient (W/(m^2·K)), h_{sol} is the desiccant solution side convective heat transfer coefficient (W/(m^2·K)), δ_{mem} is the membrane thickness (m), and k_{mem} is the thermal conductivity of the membrane (W/(m·K)).

Another important dimensionless parameter is the number of mass transfer units, NTU_m, which relates the mass transfer potential between the liquid desiccant and air to the minimum mass flow rate of the two fluids. It is calculated using Equations (2.5) and (2.6).

$$NTU_m = \frac{U_m A}{\dot{m}_{min}} \tag{2.5}$$

$$U_m = \left[\frac{1}{h_{m,air}} + \frac{\delta}{k_m}\right]^{-1} \tag{2.6}$$

where $\dot{m}_{min}$ refers to minimum mass flow rate (kg/s) between the fluids, U_m is the overall mass transfer coefficient (kg/(m^2·s)), h_m is the mass transfer coefficient (kg/(m^2·s)) and k_m is the membrane water vapor permeability (kg/(m·s)).

The thermal capacity rate ratio is a dimensionless operating parameter used to relate the mass flow rates of the air and refrigerant with that of the desiccant solution. The thermal capacity rate ratio between the desiccant solution and air (*Cr**) can be calculated using Equation (2.7).

$$Cr^* = \frac{C_{sol}}{C_{air}} = \frac{\dot{m}_{\text{sol}}\, c_{\text{p,sol}}}{\dot{m}_{\text{air}}\, c_{\text{p,air}}} \tag{2.7}$$

where C denotes the thermal capacity rate (W/K) and c_p is the specific heat capacity (J/(kg·K)).

The thermal capacity rate ratio (*Cr*) between the refrigerant (water) and desiccant solution is the ratio between the minimum and maximum thermal capacity rates of the refrigerant and desiccant solution. The refrigerant has the largest heat capacity rate under the considered operating conditions. Therefore, Cr is calculated using Equation (2.8).

$$Cr = \frac{C_{\text{sol}}}{C_w} = \frac{\dot{m}_{\text{sol}}\, c_{\text{p,sol}}}{\dot{m}_{\text{w}}\, c_{p,w}} \tag{2.8}$$

The temperature ratio (T^*) is a dimensionless parameter that relates all three inlet fluid temperatures. Equation (2.9) defines the temperature ratio (Abdel-Salam et al. 2016a).

$$T^* = \frac{T_{air,in} - T_{w,in}}{T_{air,in} - T_{sol,in}} \tag{2.9}$$

When:

- $T^* > 1$: Internal cooling is active in the dehumidifier or internal heating is active in the regenerator
- $T^* = 1$: The water and desiccant solution inlet temperatures are equal
- $T^* < 1$: The inlet refrigerant temperature is warmer than the inlet desiccant solution temperature of the dehumidifier or cooler than the inlet desiccant solution temperature of the regenerator.

2.8.4 Empirical correlations

The aim of the 3-fluid LAMEE model is to predict the four unknown outlet conditions (that is, the humidity ratio of the outlet air stream ($W_{air,out}$) and the temperatures of the outlet desiccant solution ($T_{sol,out}$), air ($T_{air,out}$), and water ($T_{w,out}$) using the known inlet fluid temperatures, air humidity ratio and mass flow rates. Therefore, four equations are required for both the dehumidifier and regnerator. Furthermore, NTU and NTU_m are omitted from the correlations because they were fixed in the experiments and, therefore, a relationship between effectiveness and NTU and NTU_m could not be developed from the experimental data. The empirical correlations were developed by observing the trends of sensible effectiveness, latent effectiveness and outlet solution temperature as a function of T^*, Cr, and Cr^* and perform linear and non-linear regression by using the "least squares" method to match the correlations and the experimental data of Abdel-Salam et al. (2016a; 2016b; 2017). The equations are presented below and section 2.10 will show how well the equations match the measured data.

Dehumidifier:

$$\varepsilon_{sen} = 0.52 - 0.0797 \cdot T^* - 0.204 \cdot \log(Cr) \tag{2.10}$$

$$\varepsilon_{lat} = 0.37 + 0.0189 \cdot T^* - 0.124 \cdot \log(Cr) \tag{2.11}$$

$$T_{sol,out} = 37.22 - 3.81 \cdot T^* + 7.32 \cdot \log(Cr) \tag{2.12}$$

Regenerator:

$$\varepsilon_{sen} = 0.36 - 0.026 \cdot T^* - 0.83 \cdot Cr + 0.13 \cdot Cr^* \tag{2.13}$$

$$\varepsilon_{lat} = 0.16 - 0.023 \cdot T^* - 0.74 \cdot Cr + 0.12 \cdot Cr^* \tag{2.14}$$

$$T_{sol,out} = 27.4 + 6.26 \cdot T^* - 32.4 \cdot Cr + 4.66 \cdot Cr^* \tag{2.15}$$

The effectiveness equations provide the outlet air temperature and humidity ratio, and equations (2.12) and (2.15) provide the outlet desiccant solution temperatures. The fourth unknown, that is, the outlet refrigerant (water) temperature, is calculated from an energy balance over the 3-fluid LAMEE as shown in Equation (2.16).

$$\dot{m}_{air}\left(h_{air,out} - h_{air,in}\right) + \dot{m}_{sol}\left(h_{sol,out} - h_{sol,in}\right) + \dot{m}_w c_{p,w}\left(T_{w,out} - T_{w,in}\right) = 0 \tag{2.16}$$

where h denotes enthalpy (J/kg).

The enthalpy of humid air is defined by Equation (2.17).

$$h_{air} = c_{p,air} T_{air} + W_{air}(h_g + c_{p,v} T_{air}) \tag{2.17}$$

where h_g corresponds to the specific enthalpy for saturated water vapor at 0°C (kJ/kg). The specific heat capacity of the desiccant solution remains relatively constant and, therefore, the energy loss of the desiccant solution is simplified into Equation (2.18).

$$\dot{m}_{sol}\left(h_{sol,out} - h_{sol,in}\right) = \dot{m}_{sol} c_{p,sol}\left(T_{sol,out} - T_{sol,in}\right) \quad (2.18)$$

In addition, Appendix A presents equations used to calculate LiCl solution properties (such as enthalpy, vapor pressure, equilibrium humidity ratio, and specific heat capacity).

2.9 2-fluid LAMEE model

An analytical model of a counter-cross-flow 2-fluid LAMEE is used in this thesis. The analytical model was developed by Ge et al. (2013) by modifying an analytical solution of a hollow-fiber LAMEE created by Zhang (Zhang 2011). The analytical model assumes the airside flow is laminar when the air flow is not always in the laminar flow region under experimental conditions and could be in the laminar-turbulent transition region (Ge et al. 2013). As a result, the actual NTU may be higher than the NTU used in the analytical model. Ge et al. (2013) found that the analytical model showed good agreement with experimental data where the maximum percent difference between experimental and analytical results was generally within 10% for the range of operating conditions investigated.

2.10 Verification of the 3-fluid and 2-fluid LAMEE models

In this section, the 3-fluid and 2-fluid LAMEE models are compared with the experimental data of Abdel-Salam et al. (2016a; 2016b; 2017). The model verification in this thesis is limited to the experimental dataset which is summarized in Table 2.2 and presented in Appendix B. Graphs are used to compare the dehumidifier model results with the experimental data in section 2.10.1 and the regenerator model results with the experimental data in section 2.10.2. The standard error of estimate and average differences between the 3-fluid LAMEE model results and the experimental data are provided in section 2.10.3. In section 2.10.4, the range of operating conditions that can be

used with the 3-fluid LAMEE model are presented. Appendix C presents the extrapolation analysis used to obtain the range of operating conditions.

Table 2.2. The input conditions used to verify the 3-fluid and 2-fluid LAMEE models.

		Input Parameter	Value		Unit
			2-fluid LAMEE	3-fluid LAMEE	
Dehumidifier	Air	Temperature, $T_{air,in}$	35.4	34.9-35.3	°C
		Humidity Ratio, $W_{air,in}$	18	17.0-18.1	(g_v/kg_{da})
	Solution	Temperature, $T_{sol,in}$	24.7	24.2-25.2	°C
		Concentration, X_{sol}	32.5	32.5	%
	Water	Temperature, $T_{w,in}$	-	10.1, 15.1, 20.6, 24.6	°C
	Design & Operating Parameters	NTU	1.8	1.8	
		Cr*	1.8	1.8	
		Cr	-	0.05, 0.11, 0.26, 0.42	
Regenerator	Air	Temperature, $T_{air,in}$	29.41	29.6-30.2	°C
		Humidity Ratio, $W_{air,in}$	13.0	12.4-13.2	(g_v/kg_{da})
	Solution	Temperature, $T_{sol,in}$	40.1	39.6-40.5	°C
		Concentration, X_{sol}	30	30	%
	Water	Temperature, $T_{w,in}$	-	42.3, 48.0, 57.1, 65.7	°C
	Design & Operating Parameters	NTU	2	2	
		Cr*	2	2	
		Cr	-	0.04, 0.14, 0.26	

2.10.1 Dehumidifier

Figures 2.5 and 2.6 present the measured and calculated outlet conditions from the 3-fluid and 2-fluid dehumidifiers. It should be noted that the exact measured inlet conditions (T, W, X, Cr, Cr^*) vary slightly in the different tests (ranges specified in Table 2.2) and the exact inlet conditions are used in the models to calculate the outlet conditions. Furthermore, Appendix B includes the experimental data, the 3-fluid LAMEE model results, and the percent differences between the experimental and model results.

The outlet air temperature, air humidity ratio and desiccant solution temperature of the 3-fluid LAMEE model are within 5% of the experimental data, and their trends and values coincide as shown in Figures 2.5(a-c) and Figures 2.6(a-c). This shows the correlations presented in equations

(2.10) to (2.15) accurately represent the experimental data. The outlet water temperatures are calculated using an energy balance (Equation (2.16)) and Figures 2.5(d) and 2.6(d) show that the largest discrepancy (within 8%) is between the simulated and experimental outlet water temperatures. The discrepancy is likely due to heat transfer with the environment in the experiment. Figure 2.5(d) shows that the difference between the model and experiment grows as the inlet water temperature decreases because the heat transfer rate from the environment increases as the temperature difference between the water and ambient air increases. Similarly, there is less agreement between the experimental and simulated outlet water temperatures at lower water mass flow rates (higher Cr), as shown in Figure 2.6(d), since at lower water flow rates, the heat transfer from the environment has a greater effect on the water temperature.

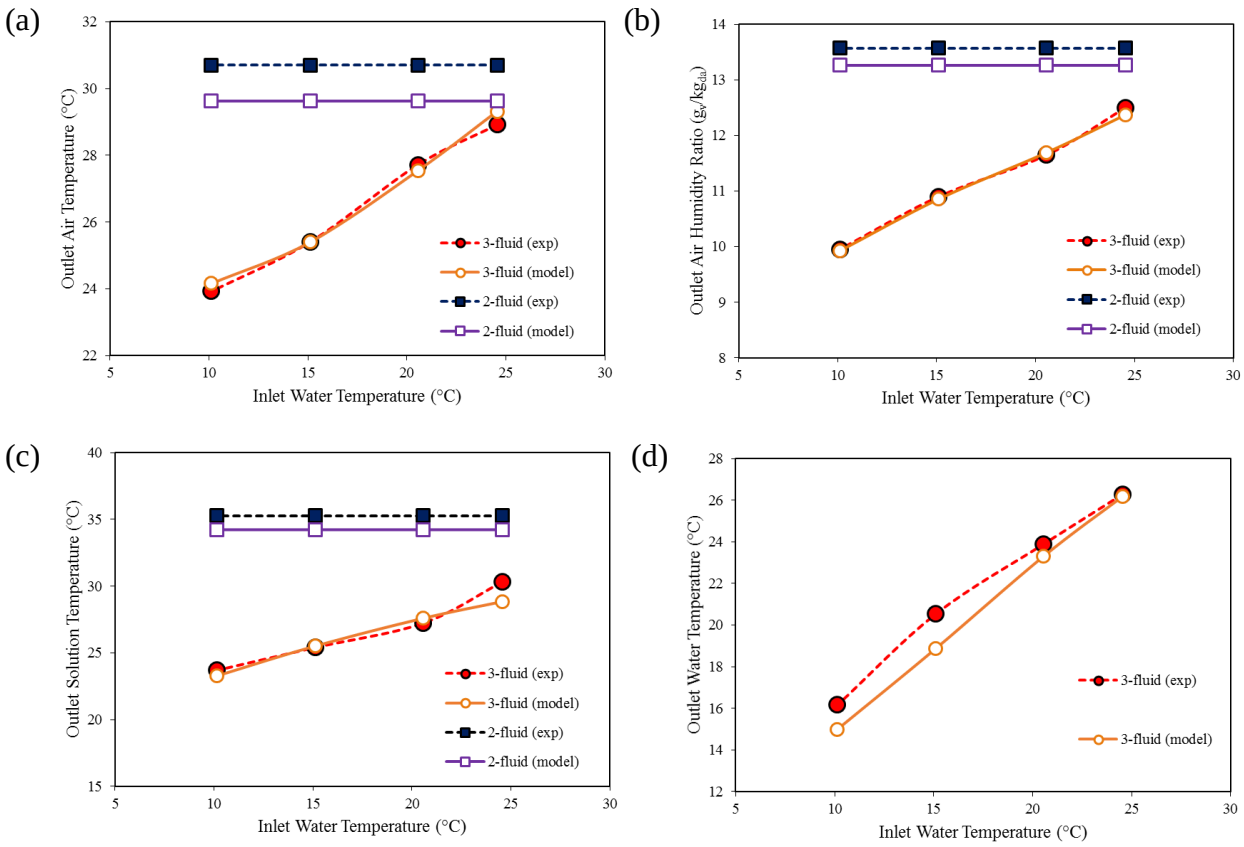

Figure 2.5: Comparison of the 2-fluid and 3-fluid LAMEE dehumidifier models with experimental data as a function of the inlet water temperature for: (a) outlet air temperature, (b) outlet air humidity ratio, (c) outlet solution temperature, and (d) outlet water temperature. The lines are drawn for information only as the experimental and model data are only determined at the locations of the symbols.

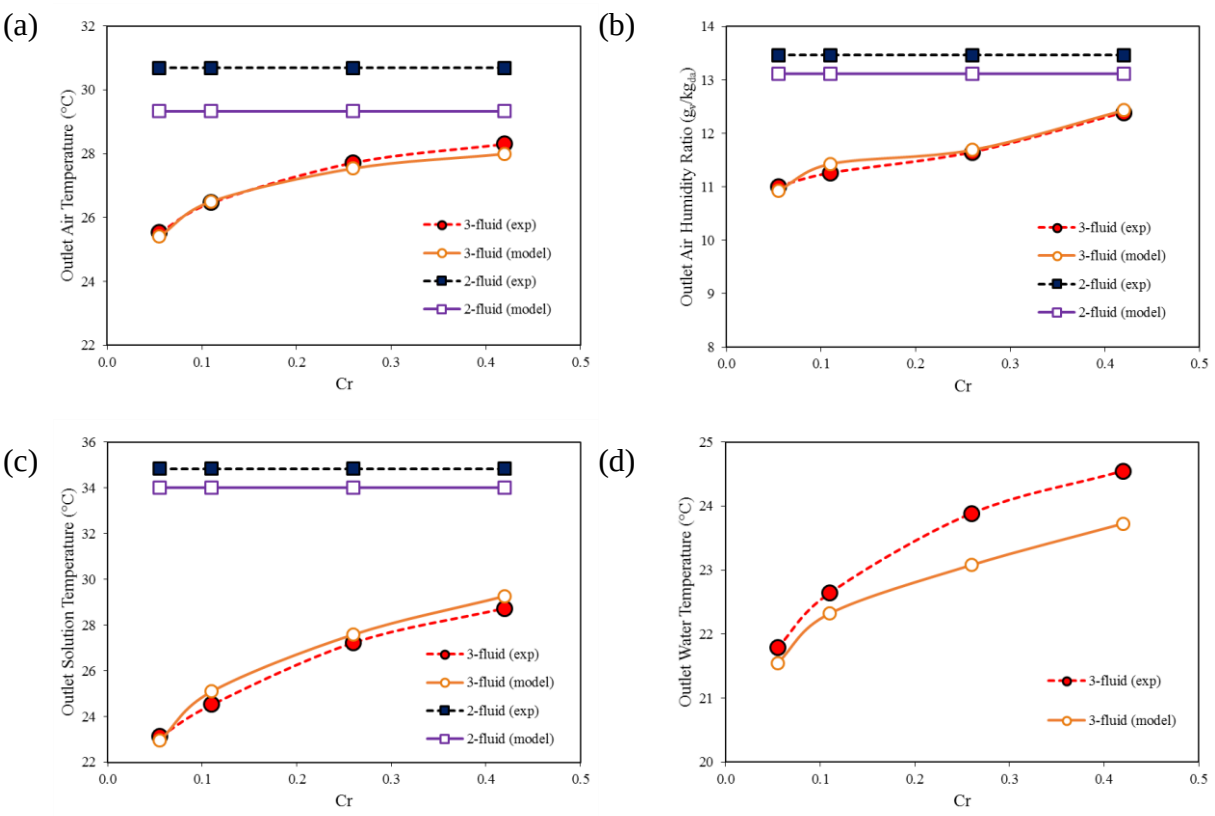

Figure 2.6: Comparison of the 2-fluid and 3-fluid LAMEE dehumidifier models with experimental data as a function of water flow rate (Cr): (a) outlet air temperature, (b) outlet air humidity ratio, (c) outlet desiccant solution temperature, and (d) outlet water temperature. The lines are drawn for information only as the experimental and model data are only determined at the locations of the symbols.

In Figures 2.5 and 2.6, the 2-fluid LAMEE outlet conditions are constant because the 2-fluid LAMEE does not have internal cooling or heating. The analytical model of the 2-fluid LAMEE estimates more air cooling and dehumidifying than the experimental data, whereas, the simulated and experimental outlet desiccant solution temperatures are in good agreement. However, the simulated outlet desiccant solution temperature is always lower than the experimental values. The discrepancy between the analytical model and experiments could be due to flow maldistribution and desiccant solution crystallization that occurs in practice but is unaccounted for in the analytical model (Ge et al. 2013; Afshin et al. 2010). Nevertheless, it is important to note that the analytical model for 2-fluid LAMEE over predicts exchanger performance.

The 3-fluid LAMEE model shows better agreement with the experimental data than the 2-fluid LAMEE model, which is expected since the 3-fluid LAMEE model was developed from this experimental dataset. Therefore, the exchanger performance predicted by the 3-fluid LAMEE model agrees with experimental results.

2.10.2 Regenerator

Figures 2.7, 2.8, and 2.9 present the comparison between the regenerator models and experimental data for the 2-fluid and 3-fluid LAMEEs at different inlet water temperatures, desiccant solution flow rates (Cr*), and water flow rates (Cr) values, respectively. As with the 3-fluid LAMEE dehumidifier model, there is good agreement between simulated and experimental outlet air and desiccant solution conditions for the 3-fluid LAMEE regenerator model (within 4%). Again, the largest discrepancy, 7%, is observed in the simulated outlet water temperature because the model calculates the outlet water temperature based on an ideal energy balance while there is some heat exchange with the environment in the experiments.

The results of the 2-fluid LAMEE regenerator model show a larger deviation from the experimental data when compared to the 2-fluid LAMEE dehumidifier model, which could be due to crystallization in the regenerator (Olufade and Simonson 2017) which is not considered in the model. The analytical model predicts more desiccant solution regeneration than observed in the experiment which appears as higher outlet air temperatures and humidity ratios in the simulated results than in the experimental results as shown in Figures 2.7(a) and (b), Figures 2.8(a) and (b), and Figures 2.9(a) and (b). The experimental and simulated outlet desiccant solution temperatures coincide well with the simulated temperature being slightly higher than the experimental temperature.

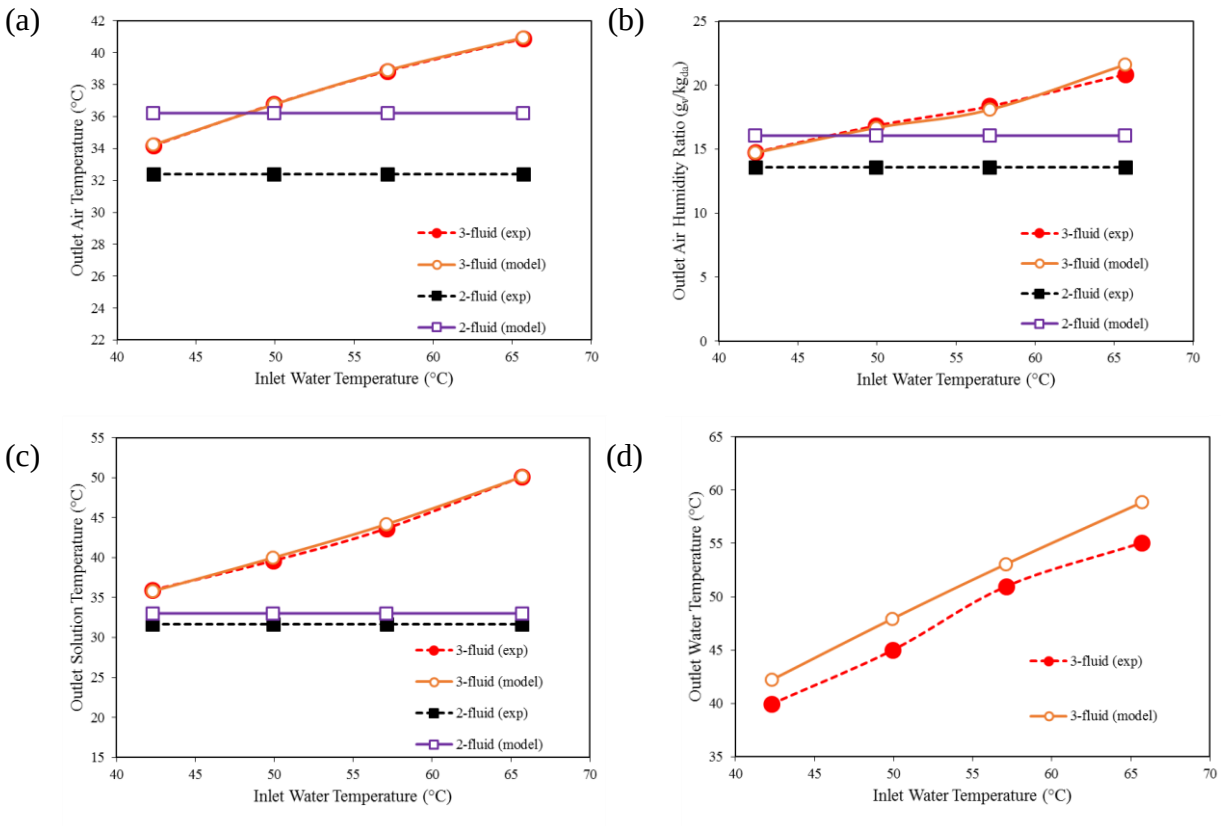

Figure 2.7: Comparison of the 2-fluid and 3-fluid LAMEE regenerator models with experimental data as a function of inlet water temperature for: (a) outlet air temperature, (b) outlet air humidity ratio, (c) outlet desiccant solution temperature, and (d) outlet water temperature. The lines are drawn for information only as the experimental and model data are only determined at the locations of the symbols

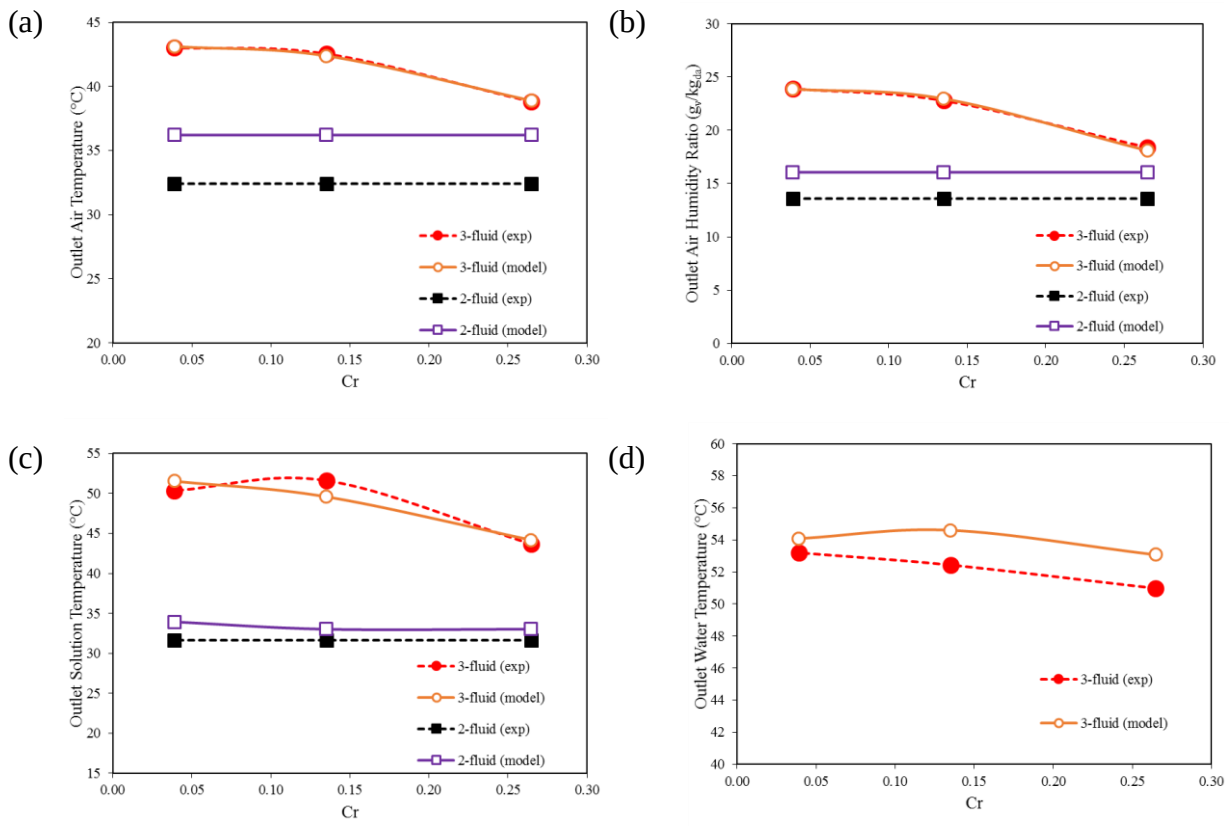

Figure 2.8: Comparison of the 2-fluid and 3-fluid LAMEE regenerator models with experimental data as a function of Cr: (a) outlet air temperature, (b) outlet air humidity ratio, (c) outlet desiccant solution temperature, and (d) outlet water temperature. The lines are drawn for information only as the experimental and model data are only determined at the locations of the symbols

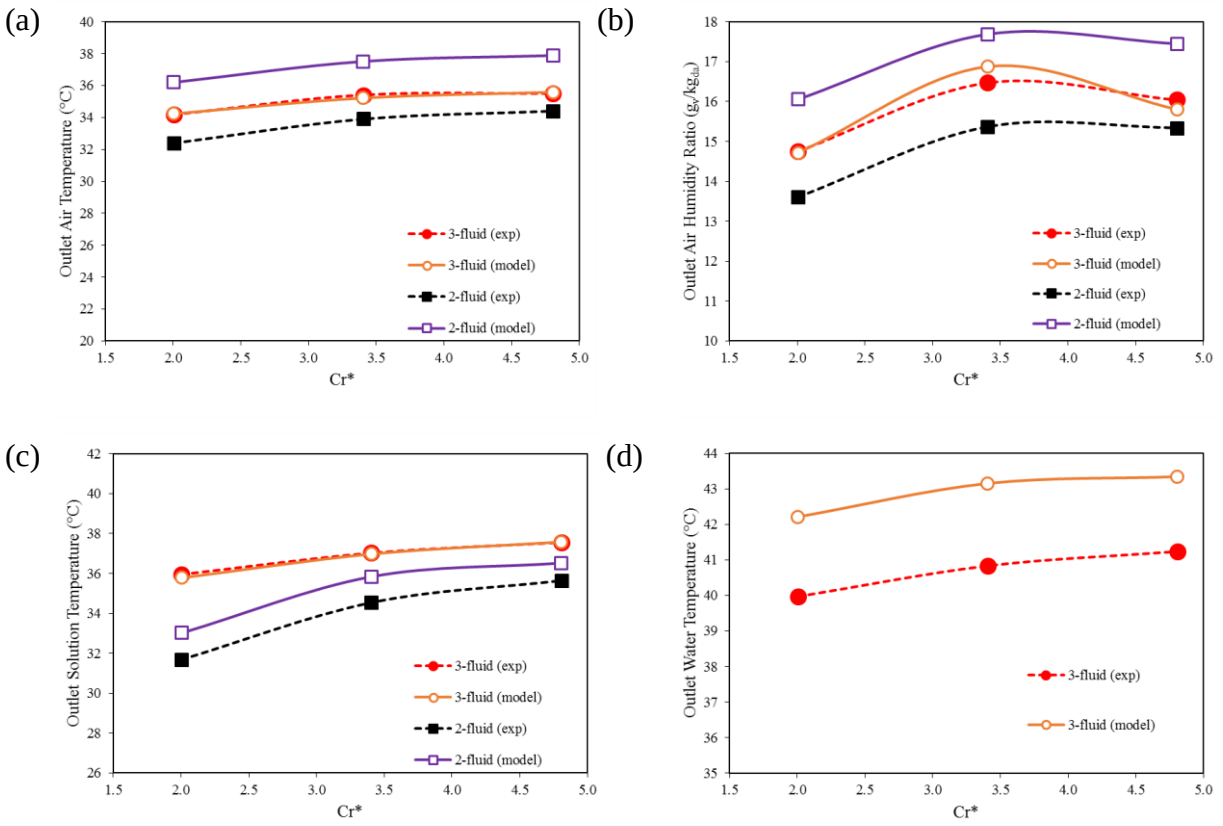

Figure 2.9: Comparison of the 2-fluid and 3-fluid LAMEE regenerator models with experimental data as a function of Cr* for: (a) outlet air temperature, (b) outlet air humidity ratio, (c) outlet solution temperature, and (d) outlet water temperature. The lines are drawn for information only as the experimental and model data are only determined at the locations of the symbols

2.10.3 Uncertainty

Table 2.3 presents the standard error of the estimate (SEE) and the average difference (AD) of the outlet parameters for the 2-fluid and 3-fluid LAMEEs where SEE is calculated using Equation (2.19) and AD is calculated using Equation (2.20).

$$SEE = \sqrt{\sum \frac{(Y - Y')^2}{N - 2}} \tag{2.19}$$

$$AD = \frac{\sum (Y - Y')}{N} \tag{2.20}$$

where Y is the experimental value, Y' is the estimated value, and N is the sample size.

Table 2.3: Standard error of the estimate between simulated results and experimental data of the 2-fluid and 3-fluid LAMEE models. N=8 for the dehumidifier and N=10 for the regenerator.

Outlet	Standard Error of Estimation (SEE)				Average Difference (AD)			
	3-fluid		2-fluid		3-fluid		2-fluid	
	Deh.	Reg.	Deh.	Reg.	Deh.	Reg.	Deh.	Reg.
Air Temperature (°C)	0.3	0.1	1.7	4.2	0.2	0.1	1.2	4.5
Solution Temperature (°C)	0.7	0.9	1.3	1.6	0.4	0.5	0.9	2.4
Water Temperature (°C)	0.9	2.7	-	-	0.7	2.3	-	-
Air Humidity Ratio (g_v/kg_{da})	0.1	0.4	0.5	2.7	0.1	0.2	0.3	4.1

As mentioned previously, Table 2.3 shows that the 3-fluid LAMEE model represents the 3-fluid LAMEE performance well where the 2-fluid LAMEE tends to overestimate the 2-fluid LAMEE performance. This should be kept in mind when the 2-fluid and 3-fluid M-LDAC systems are compared later in this chapter.

2.10.4 Model extrapolation

Due to the limited experimental dataset used to develop and verify the 3-fluid LAMEE model, it is necessary to extrapolate the model to other inlet conditions in order to simulate the M-LDAC system under real design conditions and actual weather data. A larger range of inlet air temperatures and humidity ratios are needed to represent real weather data. In addition, a larger range of inlet water temperatures and mass flow rates are needed to control the 3-fluid LAMEE performance to meet the building latent loads under a range of design weather conditions.

The model was tested under a range of $T_{air,in}$, $W_{air,in}$, $T_{w,in}$, and $\dot{m}_w$ to determine an acceptable range of extrapolation and the results are presented in Figures in Appendix C. The model performs well for all the tested inlet and calculated outlet conditions (see Appendix C) except for the calculated outlet air and solution temperatures of the dehumidifier at different inlet water and air temperatures (see Figure 2.10). Figure 2.10 presents the outlet air and solution temperatures as a function of inlet air and water temperatures for the 3-fluid LAMEE dehumidifier model. The

measured data are included to highlight the extrapolation. Figure 2.10 shows that as the inlet air temperature initially decreases from 40°C, the outlet air temperature decreases as expected. However, at some point the outlet air temperature begins to increase as the inlet air temperature decreases, which may be possible due to an increase in the operating condition factor (H*), which increases the moisture transfer and the release of phase change energy (Abdel-Salam et al. 2016; Simonson and Besant 1999; Hemingson et al. 2011) but is unlikely. Therefore, the point at which $T_{air,out}$ begins to increase as $T_{air,in}$ decreases is labelled in Figure 2.10 and is defined as the extrapolation limit for the model.

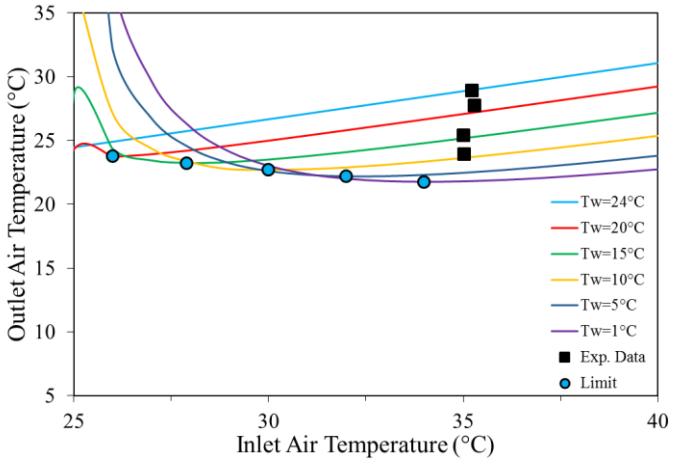

Figure 2.10: 3-fluid LAMEE dehumidifier model behavior for outlet air temperature at different inlet water and air temperatures ($T_{sol,in} = 24.2°C$, $W_{air,in} = 17.6 \frac{g_v}{kg_{da}}$, $Cr^* = 1.8$, $Cr = 0.26$)

The validity of the 3-fluid LAMEE dehumidifier model is determined from the point at which the outlet air temperature deviates from the expected trend as a function of inlet water and air temperatures (Figure 2.10). The extrapolation limit for inlet air temperature depends on the inlet water temperature and Cr. These limits are presented in Table 2.4 which shows the minimum allowable inlet water temperatures at different air temperatures. The inlet water temperature cannot go below 1.0°C and, is therefore, constrained to this value at inlet air temperatures above 38°C.

Table 2.5 summarizes the dimensionless operating and design conditions that can be used with the 3-fluid LAMEE model.

Table 2.4: Minimum inlet water temperatures for different inlet air temperatures

$T_{air,in}$ (°C)	40	38	36	34	32	30	28	26
T*	2.74	2.82	2.90	2.97	3.05	3.12	3.20	3.27
$T_{w,in}$ (°C)	1.0	1.0	2.7	5.8	9.2	12.8	16.8	21.1

Table 2.5: Dimensionless parameter limitations of the 3-fluid dehumidifier and regenerator models

	Dimensionless Parameter	Value
Dehumidifier	Cr	0.01-0.42
	Cr*	1.8
	NTU	1.8
Regenerator	Cr	0.04 - 0.63
	Cr*	2.0-4.8
	NTU	2

The air flow rates used in the experiment are much smaller than ventilation flow rates used in physical systems. The model must be able to accommodate for larger flow rates to replicate a realistic system. In order to apply the empirical correlation to different air flow rates, the dimensionless design (NTU) and operating (Cr and Cr*) parameters are maintained within their applicable ranges. Since the NTU is fixed, the model assumes that the area of the membrane increases proportionally to the thermal capacity rate of air to maintain the fixed NTU value. The area of the membrane is not calculated in this research. Furthermore, the Cr and Cr^* values are used to define the mass flow rates of the solution and water.

2.11 TRNSYS model of the M-LDAC system

Figure 2.11 presents a schematic of the 3-fluid M-LDAC system. The 3-fluid system is similar to the 2-fluid system (Figure 2.2) except the 3-fluid system has additional cooling and heating refrigerant loops. The 3-fluid LAMEE models are used to predict the outputs of the dehumidifier and regenerator. The simulation of a 2-fluid and 3-fluid M-LDAC system is achieved by linking the LAMEE models with components for the solution pumps, refrigerant pumps, fans, chillers, and heaters in TRNSYS. These components receive inputs, such as temperatures and flow rates, and calculate the required power to heat and cool the fluids to the desired temperatures and distribute the fluids (pumps and fans) throughout the system. The component equations are presented in subsequent sections.

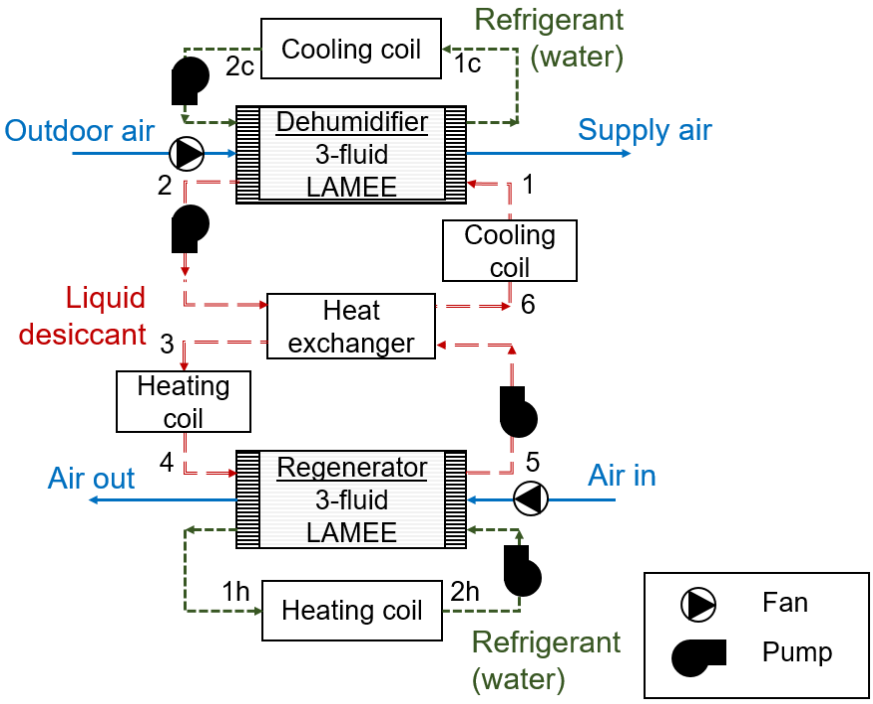

Figure 2.11: Schematic of a 3-fluid M-LDAC system

The 2-fluid and 3-fluid M-LDAC systems are responsible for air cooling and dehumidifying air. Air cooling and dehumidifying can be improved by decreasing the temperatures and increasing the mass flow rates of the desiccant solution and water entering the dehumidifier. In the 3-fluid M-LDAC system model, air cooling and dehumidifying is adjusted by changing the water flow rate and the temperature of the water entering the dehumidifier. In the 2-fluid M-LDAC system model, the solution temperature entering the dehumidifier and desiccant concentration are adjusted to provide air at different temperatures and humidity ratios. The temperature of the desiccant solution entering the dehumidifier in the 3-fluid M-LDAC system model cannot be adjusted because the 3-fluid LAMEE model is limited to a single inlet solution temperature.

Another important aspect of the M-LDAC systems is to ensure the desiccant solution concentration is maintained. If the desiccant solution is not regenerated to (or above) its initial concentration, then air dehumidifying will decrease. Therefore, the modeled 2-fluid and 3-fluid M-LDAC systems maintain desiccant solution concentration by setting the moisture released from the solution to the air in the regenerator within 5% of the moisture removed from the air in the dehumidifier. For the 3-fluid M-LDAC system, the water temperature entering the regenerator is adjusted to control the moisture released from the solution to the air, whereas, the solution temperature entering the regenerator is adjusted in the 2-fluid M-LDAC system. Therefore, the solution concentration does not change with time.

2.11.1 Performance

The coefficient of performance (COP) of the M-LDAC system is the ratio of the useful energy transfer rate (ETR) to cool and dehumidify the outdoor air to the total energy transfer rate (energy consumption rate) supplied to the system, and is calculated using Equation (2.21).

$$COP = \frac{Useful\ Energy\ Transfer\ Rate\ (ETR)}{Energy\ Consumption\ Rate\ (ECR)} \tag{2.21}$$

$$ETR = \dot{m}_{air}(h_{air,in} - h_{air,out}) \tag{2.22}$$

The COP of the 2-fluid and 3-fluid M-LDAC system are electricity-based COPs and determined using Equations (2.23) and (2.24), respectively.

$$COP_{2-fluid} = \frac{\dot{m}_{air}\left(h_{air,in} - h_{air,out}\right)}{E_{c,sol} + W_{p,sol} + W_{fan} + E_{h,sol} \cdot 0.3} \tag{2.23}$$

$$COP_{3-fluid} = \frac{\dot{m}_{air}\left(h_{air,in} - h_{air,out}\right)}{E_{c,w} + E_{c,sol} + W_{p,sol} + W_{p,w} + W_{fan} + (E_{h,w} + E_{h,sol}) \cdot 0.3} \tag{2.24}$$

where, W_{fan} and W_{pump} correspond to the electric power (W) consumed by the fan and pump, respectively, E_c denotes the electric power (W) consumed by the chillers, E_h is the thermal power (W) consumed by the heaters, and 0.3 is the assumed equivalent conversion coefficient from thermal power to electrical power.

The moisture removal rate ($\dot{m}_{rr}$) is the rate at which moisture is removed from air and is calculated using Equation (2.25).

$$\dot{m}_{rr} = \dot{m}_{air}\left(W_{air,in} - W_{air,out}\right) \tag{2.25}$$

2.11.2 Fan and pump power

Equation (2.26) is used to calculate the energy consumption rates of the air fans (W_{fan}) and solution and refrigerant pumps (W_p).

$$W = \frac{Q\Delta P}{\eta} \tag{2.26}$$

where Q denotes the volumetric flow rate of either the air, refrigerant or solution (m^3/s), ΔP is the pressure drop across the channel of interest (Pa), and η is the fan or pump efficiency. The efficiency of the fans and pumps are 0.6 and 0.85, respectively (Rasouli 2010).

The model assumes a pressure drop of at 250 Pa across each solution, air, and water channel in the LAMEE (Moghaddam et al. 2013c). Pressure drops in the solution piping and supply and exhaust air ducts are assumed negligible as they have the same effect on the 2-fluid and 3-fluid M-LDAC systems.

2.11.3 Hydronic heating and cooling systems

Heating and cooling of the liquid desiccant and water takes place in liquid-to-liquid heat exchangers coupled to heating and cooling coils. The coefficient of performance of the chiller system ($COP_{chiller}$) is calculated with Equation (2.27). $COP_{chiller}$ is strongly dependent on the evaporator set point temperature (T_{ev}) while the condenser temperature is assumed to be fixed at 45°C (Zhang et al. 2005). The water entering the heat exchanger is assumed to 3°C higher than T_{ev} and the cooling coil effectiveness is 0.85 (ASHRAE 2008).

$$COP_{chiller} = 0.0001T_{ev}^3 + 0.0016T_{ev}^2 + 0.0746T_{ev} + 2.637 \quad (2.27)$$

The heat transfer rate from the solution to the water ($Q_{c,sol}$) and from the water to the water ($Q_{c,w}$) are determined using Equation (2.28) and Equation (2.29), respectively.

$$Q_{c,sol} = \dot{m}_{sol} c_{p,sol} (T_6 - T_1) \quad (2.28)$$

$$Q_{c,w} = \dot{m}_w c_{p,w} (T_{1c} - T_{2c}) \quad (2.29)$$

where T_1, T_6, T_{1c}, and T_{2c} correspond to the labelled solution and water temperatures 1, 6, 1c, and 2c in Figure 2.7, respectively.

The electrical energy consumption rate of each of the cooling systems (E_c) can be calculated using Equation (2.30).

$$E_c = \frac{Q_c}{COP_{chiller}} \tag{2.30}$$

The heat transfer rate from the heating system to the solution and water is calculated using Equation (2.31) and Equation (2.32), respectively.

$$Q_{h,sol} = \dot{m}_{sol} c_{p,sol} (T_4 - T_3) \tag{2.31}$$

$$Q_{h,w} = \dot{m}_w c_{p,w} (T_{2h} - T_{1h}) \tag{2.32}$$

where T_4, T_3, T_{1h}, and T_{2h} denote the solution and water temperature at the labelled locations 4, 3, 1h, and 2h, respectively, in Figure 2.11. The energy consumption rate of the heaters is determined by using Equation (2.33).

$$E_h = \frac{Q_h}{\eta_{th}} \tag{2.33}$$

A thermal efficiency (η_{th}) of 95% is assumed for the heaters.

2.11.4 Solution-to-solution sensible heat exchanger

The effectiveness of the solution-to-solution sensible heat exchanger is set to a constant value of 0.75. The chilled diluted desiccant solution, from the dehumidifier, and the heated concentrated solution, from the regenerator, enter the exchanger in counter flow configuration. The outlet

temperatures of the diluted and concentrated solution are calculated using Equations (2.34) and (2.35), respectively.

$$\varepsilon_{SHX} = \frac{T_3 - T_2}{T_5 - T_2} \tag{2.34}$$

$$\varepsilon_{SHX} = \frac{T_5 - T_6}{T_5 - T_2} \tag{2.35}$$

where, T_2 and T_3 denote the solution temperature labelled at 2 and 3, respectively, in Figure 2.11.

Figure 2.12(a) presents a flow diagram illustrating the sequence of processes in the 3-fluid M-LDAC system model used to achieve set outlet air conditions. The inlet air temperature and humidity of the dehumidifier and regenerator fluctuate (can be set or inputted from a weather data file) whereas the inlet solution temperature of the dehumidifier and regenerator is fixed. The inlet water temperature and flow rate of the dehumidifier is adjusted to achieve the desired outlet air humidity and temperature. Similarly, the inlet water temperature and flow rate of the regenerator is adjusted until the moisture exchanged between the desiccant solution and air is equal to the moisture exchanged between the desiccant solution and air in the dehumidifier.

Figure 2.12(b) superimposes the presented parameters onto the 3-fluid M-LDAC system to illustrate how the system model functions and where each equation is applied. The dotted lines represent the equations. The figure shows that the desiccant solution flow rate is calculated using Cr^*_{deh} and the air flow rate into the dehumidifier. Likewise, the air flow rate into the regenerator is calculated from Cr^*_{reg} and the desiccant solution flow rate.

(a)

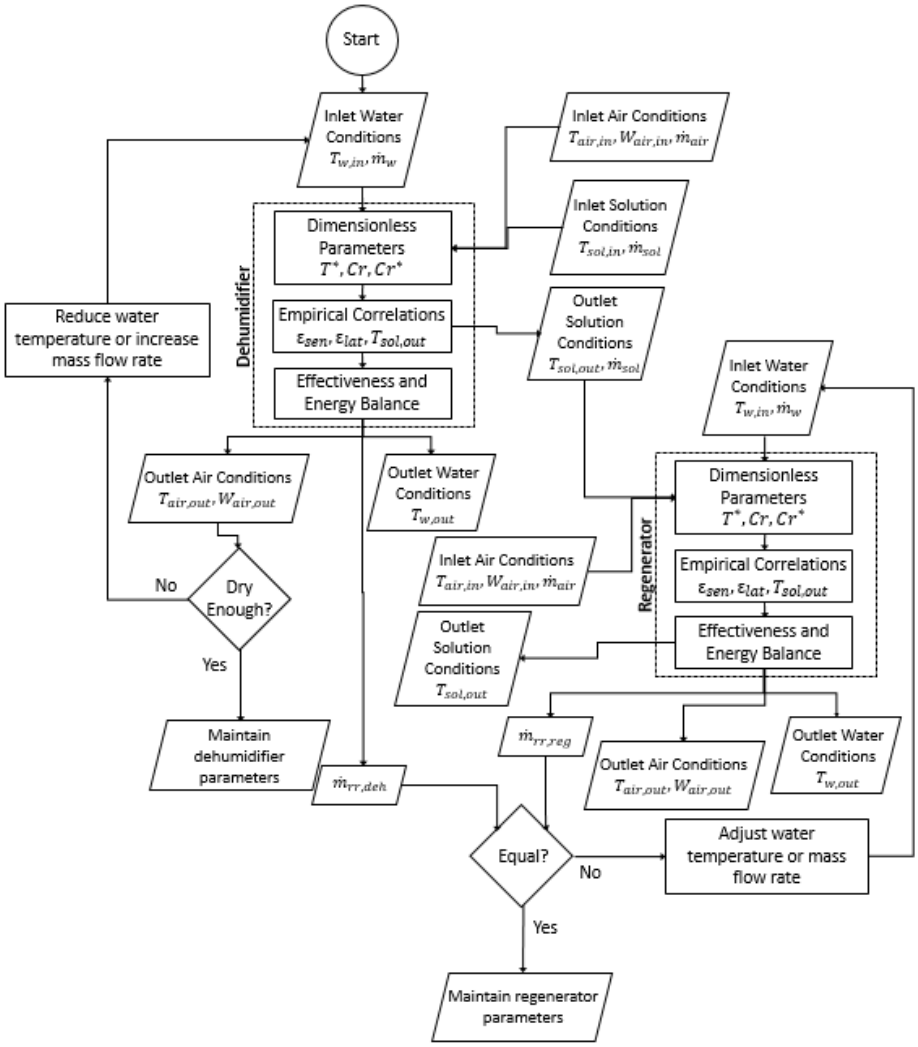

(b)

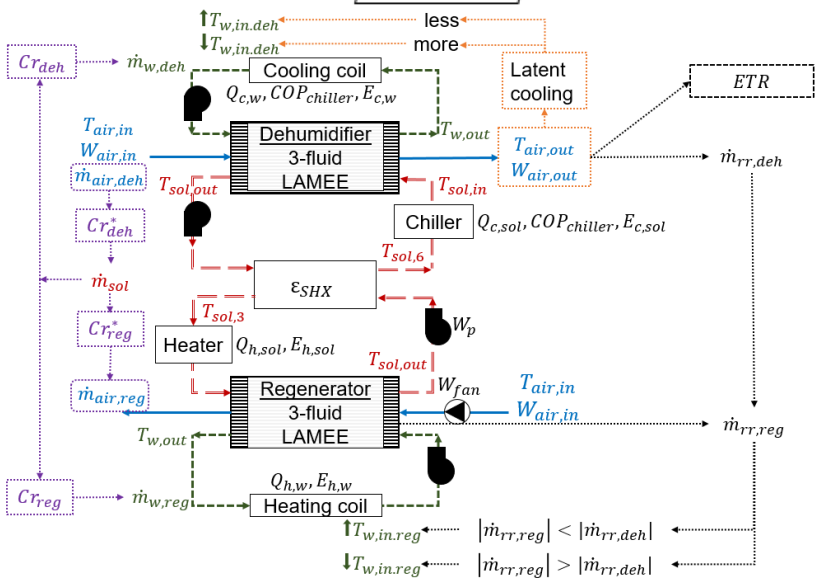

Figure 2.12: (a) Flow diagram of the 3-fluid M-LDAC system and (b) important parameters superimposed on a diagram of the 3-fluid M-LDAC system

2.11.5 Transient System Simulation (TRNSYS) tool

The Transient System Simulation (TRNSYS 2017) software is used to model and simulate the 3-fluid LAMEE. TRNSYS is a powerful software that can simulate multiple types of thermal systems under different climates. TRNSYS implements a flexible modular structure where components are connected to replicate a system. The software has a library of existing HVAC equipment to facilitate the simulation process. Furthermore, this software provides an interface for creating custom models consisting of user inputted equations that are entered in TRNSYS or within another program that TRNSYS can call (MATLAB, Excel, etc.).

2.12 Results and discussion

In this section, the performances of the 2-fluid and 3-fluid M-LDAC systems are simulated and compared under six different design conditions with different latent loads. In three of the latent load conditions, the M-LDAC systems take in outdoor air at a fixed temperature and humidity ratio and supply air at three different air humidity ratios. In the other three latent load conditions, the M-LDAC systems pull in outside air at a fixed temperature but different humidity ratios and supply air at a fixed humidity ratio. To reach the set outlet air conditions, the inlet water temperatures and mass flow rates are adjusted in the 3-fluid M-LDAC system while the inlet solution temperatures and concentration are adjusted in the 2-fluid M-LDAC system. The COP is the metric that is used to compare the performance of the 2-fluid and 3-fluid M-LDAC systems.

2.12.1 Variable supply air humidity ratio

The outdoor air conditions are constant and set at a temperature of $35.1°C$ and an air humidity ratio of 17.6 g_v/kg_{da} (49% RH) based on the experimental data which closely complies with the AHRI Standard 1060 summer conditions of $35°C$ and $16.8\frac{g_v}{kg_{da}}$ (47% RH) (AHRI 2005).

Likewise, the inlet air conditions of the regenerator are equal to those used in the experiment. The systems are compared based on their performance of meeting different latent loads. Therefore, the three output conditions are defined (low, medium, high) based on their air humidity ratio. The three sets of output (supply air) conditions are defined below and shown in Figure 2.13.

i) Low latent load

$$T_{air,out} = 22°\text{C}$$

$$W_{air,out} = 9.9 \frac{g_v}{kg_{da}} \ (60\%\ RH)$$

ii) Medium latent load

$$T_{air,out} = 20°\text{C}$$

$$W_{air,out} = 8.7 \frac{g_v}{kg_{da}} \ (60\%\ RH)$$

iii) High latent load

$$T_{air,out} = 18°\text{C}$$

$$W_{air,out} = 7.7 \frac{g_v}{kg_{da}} \ (60\%\ RH)$$

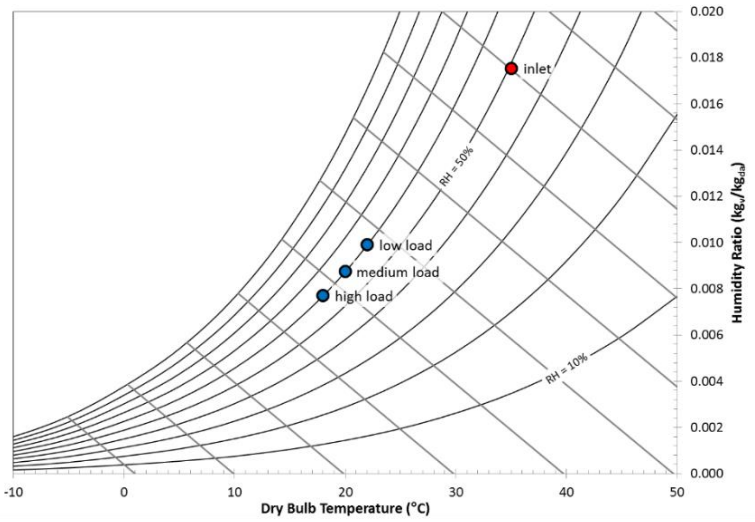

Figure 2.13: The inlet and outlet air conditions of the dehumidifier that represent high, medium and low latent loads and are used to compare the 2-fluid and 3-fluid M-LDAC systems.

The supply air temperature decreases at lower air humidity ratios due to model functionality, thus, the air temperature is chosen to be the temperature at which the humidity is 60% RH. The systems are set to supply air within ± 0.2°C and $\pm 2\%$ RH of these defined conditions.

Figure 2.14 presents the COP of the 2-fluid and 3-fluid M-LDAC systems at the low, medium, and high latent load conditions. Furthermore, Figure 2.14 includes the COP of the 3-fluid M-LDAC system at an increased effectiveness of 10% (1.1ε) and a decreased effectiveness of 10% (0.9ε). These COPs are included in case of a discrepancy between the effectiveness predicted by the 3-fluid LAMEE model and measured in experiment. A ±10% change in effectiveness typically leads to less than ±10% change in COP.

Figures 2.15, 2.16, and 2.17 present the effect that the inlet water temperature of the dehumidifier has on different parameters as it is adjusted in order to supply air at the high, medium, and low latent load conditions, respectively. Figures 2.15(a), 2.16(a), and 2.17(a) present the supply air temperature and COP of the 3-fluid M-LDAC system as a function of the inlet water temperature of the dehumidifier. These figures illustrate the COP and inlet water temperature at which the desired supply air temperatures are achieved. Figures 2.15(b), 2.16(b), and 2.17(b) present the supply air humidity ratio and the moisture release rate as a function of the inlet water temperature of the dehumidifier. These figures show the inlet water temperature at which the desired supply air humidity ratio is obtained. The inlet water temperature used to reach the supply air temperature and humidity ratio should be the same. Lastly, Figures 2.15(c), 2.16(c), and 2.17(c) present the regenerator inlet water or desiccant solution temperature and percent difference between the moisture exchanged in the dehumidifier and regenerator as a function of the dehumidifier inlet water temperature. These figures show the inlet desiccant solution temperature (2-fluid) or water

temperature (3-fluid) of the regenerator required to regenerate the desiccant solution. The percent difference between the moisture exchanged in the dehumidifier and regenerator illustrates how well the solution regeneration is performed. The 2-fluid system results are presented as constant because there is no cooling fluid and these results identify when the 3-fluid system reaches the required supply air conditions. Table 2.6 summarizes the parameters used to reach the output air conditions for the low, medium, and high latent load test cases.

Table 2.6: Input parameters used for the 2-fluid and 3-fluid M-LDAC systems to reach the low, medium, and high latent load conditions under constant inlet air conditions

Case		low load		medium load		high load	
Set	$T_{air,out}$ (ºC)	22 ± 0.2		20 ± 0.2		18 ± 0.2	
	$W_{air,out}$ (g_v/kg_{da})	9.6 - 10.2		8.4 - 9		7.4 - 8	
System		2-fluid	3-fluid	2-fluid	3-fluid	2-fluid	3-fluid
Dehumidifier	$T_{air,in}$ (ºC)	35.1		35.1		35.1	
	$W_{air,in}$ (g_v/kg_{da})	17.6		17.6		17.6	
	$T_{air,out}$ (ºC)	22	22.1	20	20.1	18	17.8
	$W_{air,out}$ (g_v/kg_{da})	9.9	9.7	8.8	8.9	8	8
	$T_{sol,in}$ (ºC)	13	24.5	11	24.5	11	24.5
	X_{sol} (%)	37	32.5	42	32.5	47	32.5
	$T_{w,in}$ (ºC)	-	10	-	10	-	12.2
	Cr	-	0.12	-	0.05	-	0.01
	Cr*	1.8	1.8	2.0	1.8	3.2	1.8
	NTU	1.8	1.8	1.8	1.8	1.8	1.8
Regenerator	$T_{air,in}$ (ºC)	29.9		29.9		29.9	
	$W_{air,in}$ (g_v/kg_{da})	13		13		13	
	$T_{sol,in}$ (ºC)	59.8	40.2	69	40.2	75.8	40.2
	$T_{w,in}$ (ºC)	-	66.6	-	68.6	-	71.2
	Cr	-	0.26	-	0.26	-	0.26
	Cr*	1.9	2	2	2	3.2	2
	NTU	2	2	2	2	2	2
COP		0.68	1.04	0.61	1.04	0.45	1.05
$\dot{m}_{rr}$ (g_v/h)		32.9	34.0	37.9	37.0	41.1	41.1

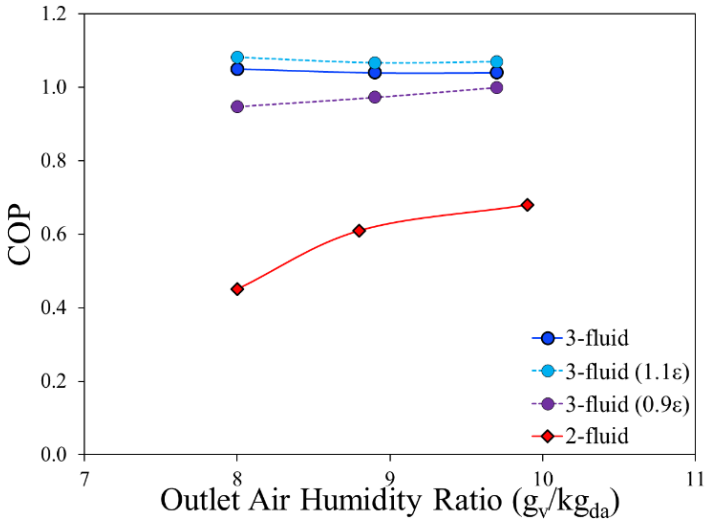

Figure 2.14: The COP for the 2-fluid and 3-fluid M-LDAC systems at the low, medium, and high latent load conditions.

The 3-fluid M-LDAC system outperforms the 2-fluid M-LDAC system in the high latent load test case (Figure 2.15). The 3-fluid M-LDAC system meets the latent load with a COP of 1.05 while the 2-fluid M-LDAC system meets the latent load with a COP of 0.45. To cover this load, both systems dehumidify the air at a rate of 41 g_v/h. Furthermore, the desiccant concentration in the 2-fluid system is 47% in order to meet the high latent load, which is impractical for a LiCl solution because it will likely cause crystallization and reduce system performance (Afshin et al. 2010). Similarly, the analytical model used for the 2-fluid LAMEE overestimates performance as shown in Section 2.10. Therefore, the actual performance of the 2-fluid M-LDAC system would be less than what the model predicts.

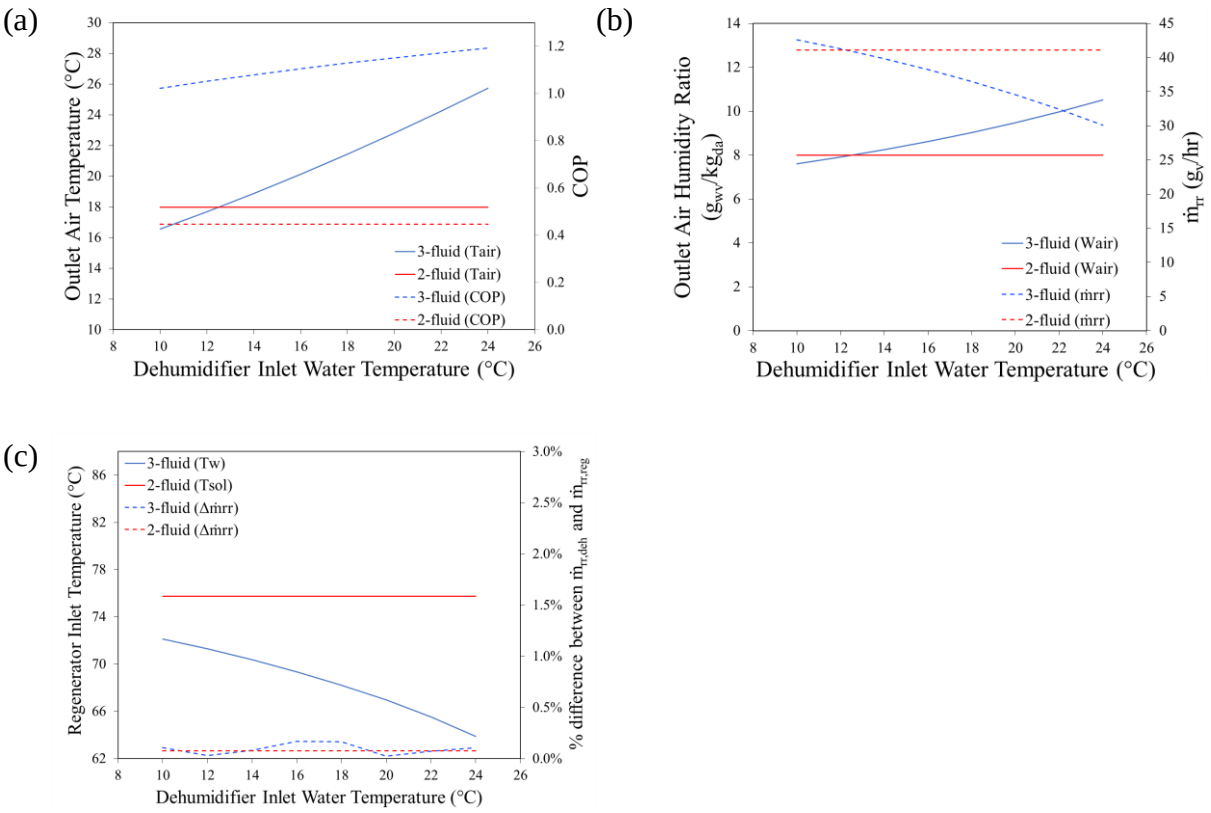

Figure 2.15: Comparison of the performance of the 2-fluid and 3-fluid systems under the high latent load test case conditions and constant inlet air conditions: a) outlet air temperature and COP, b) humidity ratio and moisture removal rate, and (c) regenerator inlet water or desiccant solution temperature and percent difference between moisture release rate between the dehumidifier and regenerator.

The 3-fluid M-LDAC system outperforms the 2-fluid M-LDAC system in both the medium (Figure 2.16) and low (Figure 2.17) latent load test conditions. The 3-fluid M-LDAC system supplies the air conditions of the medium latent load case (20°C and 60%RH) with a COP of 1.04. The 2-fluid system provides these air conditions with a COP of 0.61. Both systems are dehumidifying air at a rate of 37 g_v/h to meet the medium latent load. The 3-fluid system supplies the desired air conditions of the low latent load case (22°C and 60% RH) with a COP of 1.04. Conversely, the 2-fluid system supplies the desired air conditions with a COP of 0.68. Each system is dehumidifying the air at a rate of approximately 33 g_v/h.

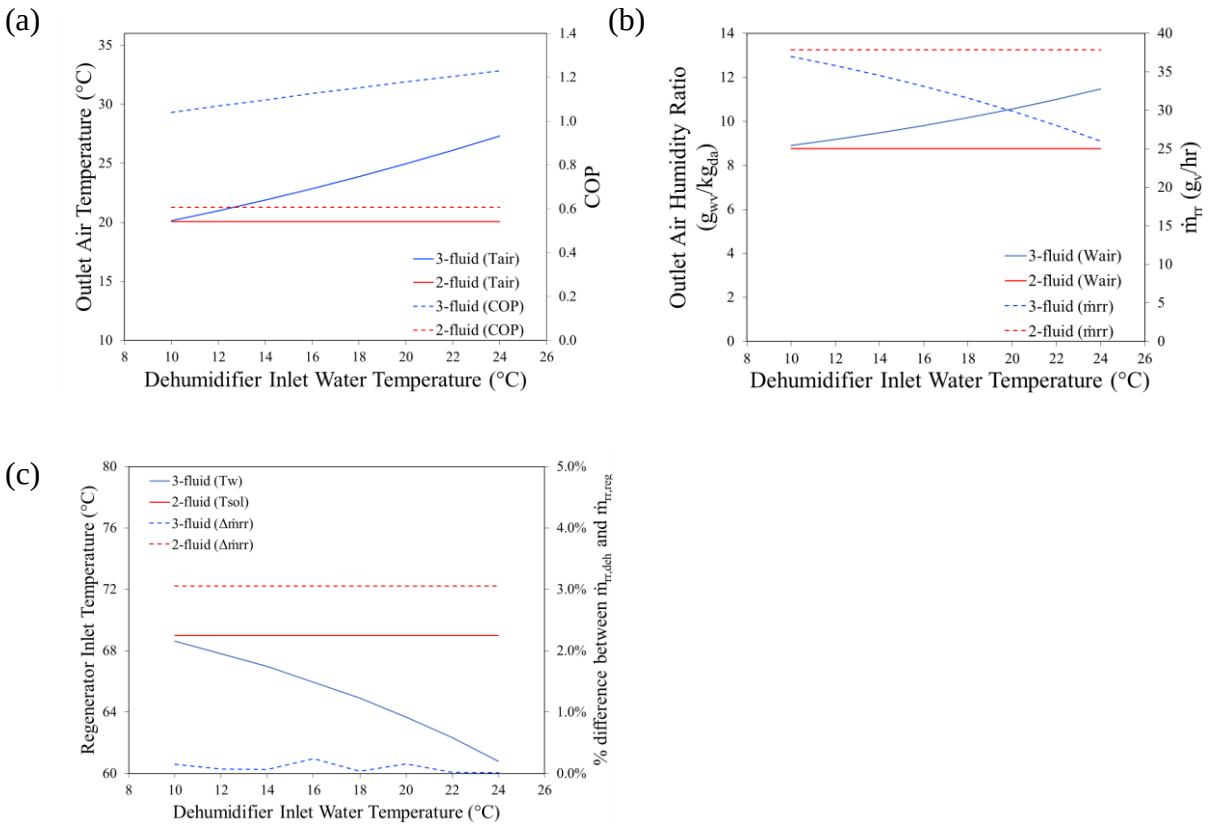

Figure 2.16: Comparison of the performance of the 2-fluid and 3-fluid systems under the medium latent load test case conditions and constant inlet air conditions: a) outlet air temperature and COP, b) humidity ratio and moisture removal rate, and (c) regenerator inlet water or solution temperature and percent difference between moisture release rate between the dehumidifier and regenerator.

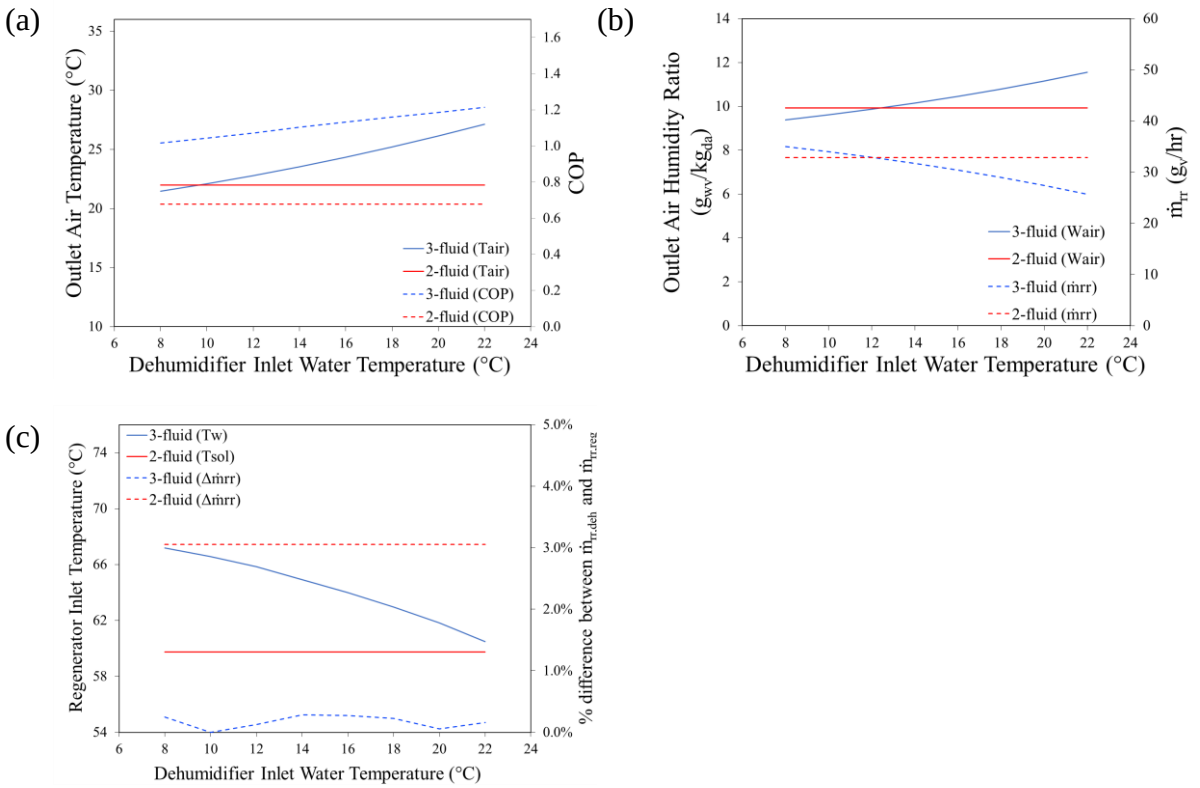

Figure 2.17: Comparison of the performance of the 2-fluid and 3-fluid systems under the low latent load test case conditions and constant inlet air conditions: a) outlet air temperature and COP, b) humidity ratio and moisture removal rate, and (c) regenerator inlet water or desiccant solution temperature and percent difference between moisture release rate between the dehumidifier and regenerator.

The COPs of the 3-fluid M-LDAC system are similar across the different load scenarios; being 1.04, 1.04, and 1.05 for the low, medium, and high load, respectively. For the low and medium load, the desired output conditions are met at the same inlet water temperature (10°C) but the Cr value is lower (0.05 versus 0.12) for the medium latent load test case. Thus, in the medium load scenario, the impact of the additional energy consumed by the pumps on the COP is negligible. The high load is met at a higher inlet water temperature (12°C) but at a low Cr value (0.01), and the additional cooling and dehumidifying performed is larger relative to the energy consumed. This equivalency between COPs across multiple loads suggests that the COP will be similar when delivering any air temperature at 60% RH

2.12.2 Variable outdoor air humidity ratio

In this comparison, the outdoor air conditions are different between cases. The outdoor air humidity ratio changes while the supply air humidity ratio is held constant. The supply air temperature is set to 35.1°C with an inlet relative humidity ranging from 30% RH to 70% RH and the outlet air humidity ratio is set to 9.9 g_v/kg_{da}. With this comparison, the performances of the 2-fluid and 3-fluid M-LDAC systems are again compared. The three design conditions are defined as high, medium, or low latent load conditions with a fixed supply air humidity ratio and are:

i) Low latent load with a fixed supply air humidity ratio

$$W_{air,in} = 10.6 \frac{g_v}{kg_{da}} \ (30\% \ RH)$$

ii) Medium latent load with a fixed supply air humidity ratio

$$W_{air,in} = 17.8 \frac{g_v}{kg_{da}} \ (50\% \ RH)$$

iii) High latent load with a fixed supply air humidity ratio

$$W_{air,in} = 25.3 \frac{g_v}{kg_{da}} \ (70\% \ RH)$$

Figure 2.18 presents the COP of the 2-fluid and 3-fluid M-LDAC systems at the low, medium, and high latent load conditions. Figure 2.18 also includes the COP of the 3-fluid M-LDAC system at an increased (1.1ε) and decreased (0.9ε) effectiveness. This is to show the effects of a potential discrepancy between the effectiveness predicted by the 3-fluid LAMEE model and measured in experiment. A ±10% change in effectiveness typically leads to less than ±10% change in COP. Figures 2.19, 2.20, and 2.21 present the same parameters as Figures 2.15, 2.16, and 2.17 for the high, medium and low latent load conditions with a fixed supply air humidity ratio, respectively. Table 2.7 summarizes the input parameters used to meet the high, medium, and low latent loads.

Table 2.7: Input parameters used for the 2-fluid and 3-fluid M-LDAC systems to reach the low, medium, and high latent load conditions under different inlet air humidity ratios.

	Case	low load		medium load		high load	
Set	$W_{air,out}$ (g_v/kg_{da})	9.7 - 10.1					
System		2-fluid	3-fluid	2-fluid	3-fluid	2-fluid	3-fluid
Dehumidifier	$T_{air,in}$ (°C)	35.1		35.1		35.1	
	$W_{air,in}$ (g_v/kg_{da})	10.6		17.9		25.3	
	$T_{air,out}$ (°C)	29.6	31.8	21.6	22.7	10.5	15.5
	$W_{air,out}$ (g_v/kg_{da})	9.9	9.9	9.9	9.9	10.7	9.9
	$T_{sol,in}$ (°C)	27.0	24.5	13	24.5	1	24.5
	X_{sol} (%)	32.5	32.5	37	32.5	50	32.5
	$T_{w,in}$ (°C)	-	29.1	-	15.8	-	8
	Cr	-	0.4	-	0.05	-	0.01
	Cr*	1.8	1.8	2.0	1.8	3.8	1.8
	NTU	1.8	1.8	1.8	1.8	1.8	1.8
Regenerator	$T_{air,in}$ (°C)	29.9		29.9		29.9	
	$W_{air,in}$ (g_v/kg_{da})	13		13		13	
	$T_{sol,in}$ (°C)	37.3	40.2	59.0	40.2	85	40.2
	$T_{w,in}$ (°C)	-	36.7	-	66.2	-	69.1
	Cr	-	0.26	-	0.26	-	0.15
	Cr*	1.9	2	1.9	2	3.5	2
	NTU	2	2	2	2	2	2
COP		0.68	0.5	0.66	1.10	-	1.0
$\dot{m}_{rr}$ (g_v/h)		3		34		63	66

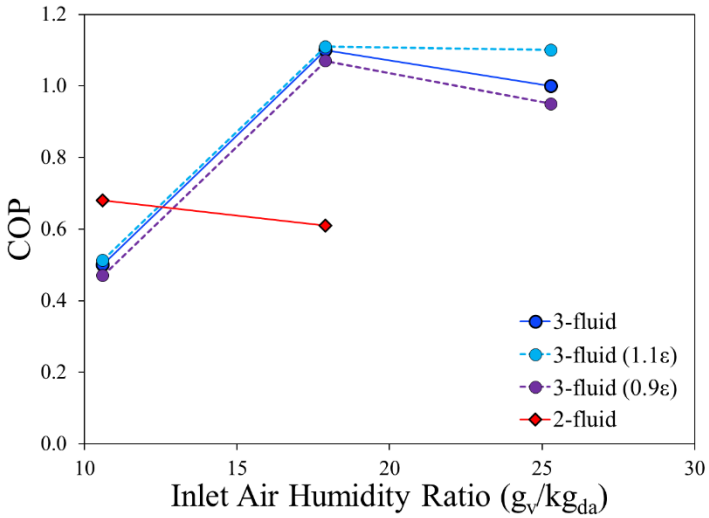

Figure 2.18: The COP for the 2-fluid and 3-fluid M-LDAC systems at the low, medium, and high latent load conditions.

The 3-fluid M-LDAC system outperforms the 2-fluid M-LDAC system under the high (Figure 2.19) and medium (Figure 2.20) latent load test conditions. For the high latent load test case, the 2-fluid M-LDAC system is incapable of reaching the outlet air humidity ratio of 9.9 g_v/kg_{da}. In contrast, the 3-fluid M-LDAC system is able to achieve this outlet air humidity with a COP of 1.0 and an air dehumidifying rate of 66 g_v/h. The 3-fluid M-LDAC system meets the medium latent load with a COP of 1.11 whereas the 2-fluid M-LDAC system meets the load at a COP of 0.66. Both systems are dehumidifying the air at a rate of 34 g_v/kg_{da}.

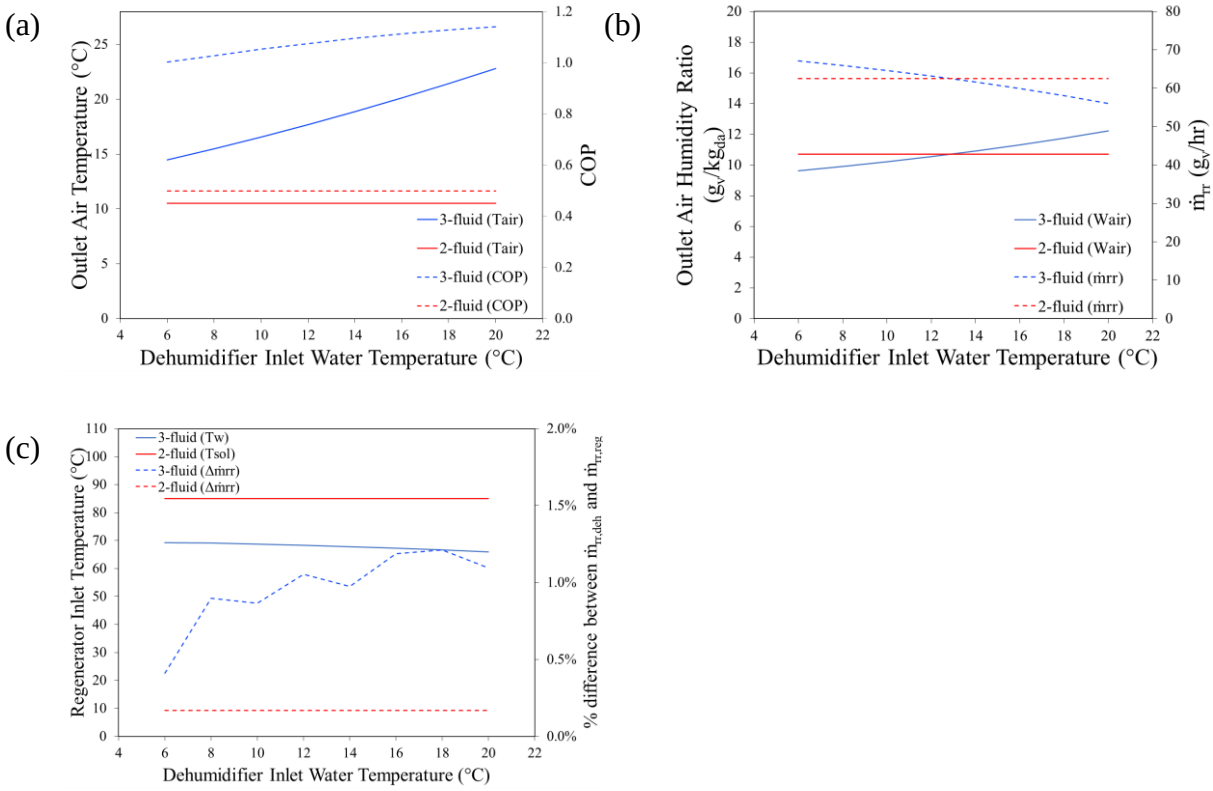

Figure 2.19: Comparison of the performance of the 2-fluid and 3-fluid systems under the high latent load test case conditions and variable inlet air humidity ratio: a) outlet air temperature and COP, b) humidity ratio and COP, and (c) regenerator inlet water or desiccant solution temperature and percent difference between moisture release rate between the dehumidifier and regenerator.

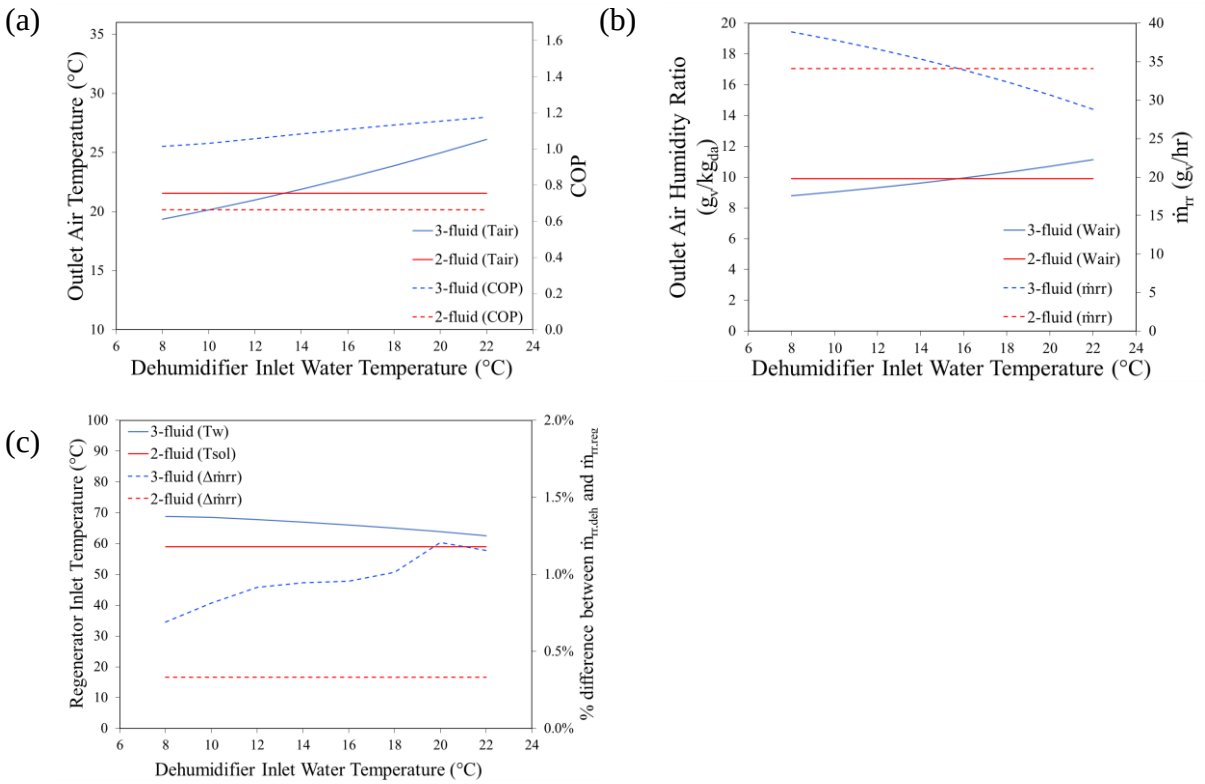

Figure 2.20: Comparison of the performance of the 2-fluid and 3-fluid systems under the medium latent load test case conditions and variable inlet air humidity ratio: a) outlet air temperature and COP, b) humidity ratio and COP, and (c) regenerator inlet water or desiccant solution temperature and percent difference between moisture release rate between the dehumidifier and regenerator.

The 2-fluid M-LDAC system outperforms the 3-fluid M-LDAC system in the low (Figure 2.21) latent load test case. The 2-fluid M-LDAC system covers the load with a COP of 0.68 whereas the 3-fluid M-LDAC system meets the load with a COP of 0.66. To supply air at these conditions, both systems are dehumidifying the air at a rate of 3 g_v/kg_{da}. The COP of the 3-fluid M-LDAC system decreases once the inlet water temperature exceeds the desiccant solution temperature because the water leaves the dehumidifier at a lower temperature than what it is set at, therefore, the water needs to be heated. The energy transfer rate decreases but the heating power increases, thus, COP decreases. This decrease in COP may also be a result of the model limitations.

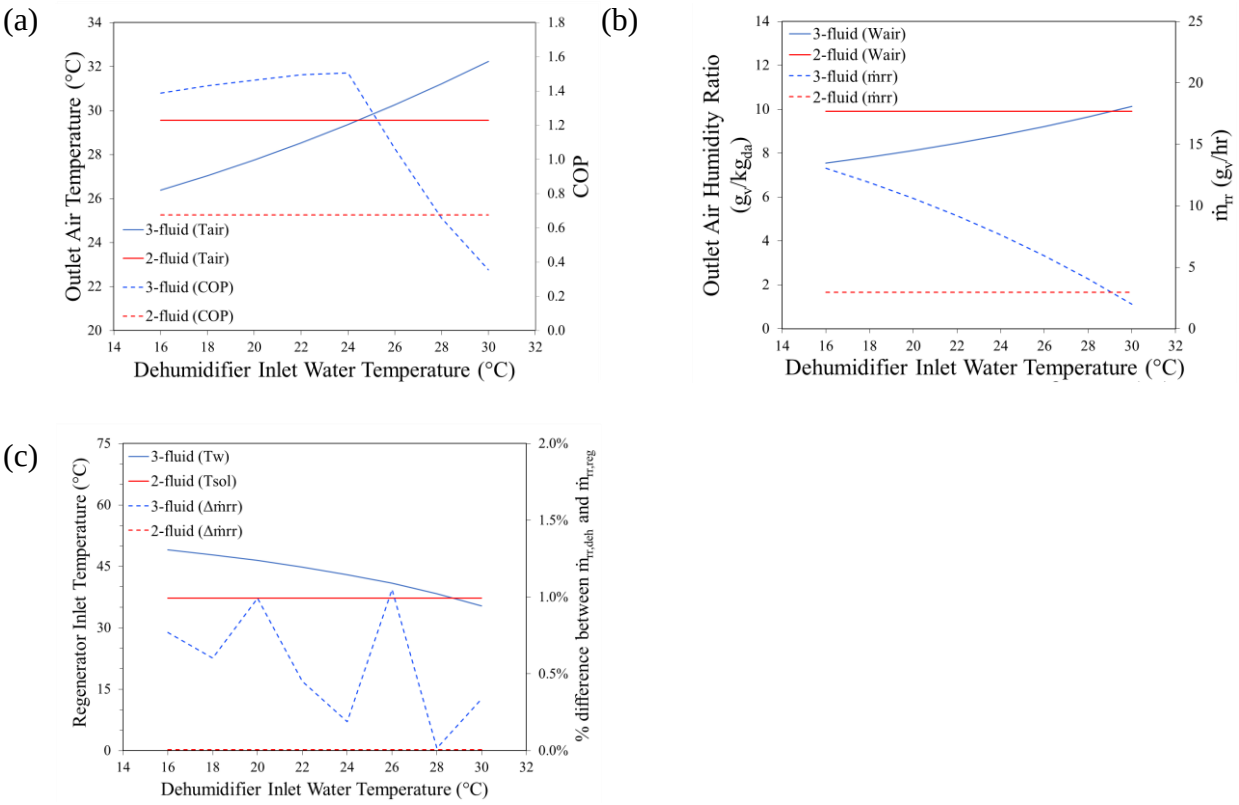

Figure 2.21: Comparison of the performance of the 2-fluid and 3-fluid M-LDAC systems under the low latent load test case conditions and variable inlet air humidity ratio: a) outlet air temperature and COP, b) humidity ratio and COP, and (c) regenerator inlet water or desiccant solution temperature and percent difference between moisture release rate between the dehumidifier and regenerator.

2.13 Conclusion

This chapter focuses on the development of an empirical model of a 3-fluid LAMEE and implementation of the model into a TRNSYS model of a membrane liquid desiccant air-conditioning (M-LDAC) system. The 3-fluid LAMEE dehumidifier model and experimental data agree within 8%, whereas the regenerator model and experimental data agree within 7%. The performance of the 3-fluid M-LDAC system is compared with a 2-fluid M-LDAC system. The 2-fluid and 3-fluid M-LDAC systems were compared under six different design conditions reflecting low, medium, and high latent load conditions. The 3-fluid M-LDAC system outperformed the 2-fluid M-LDAC system under most latent load conditions whereas the 2-fluid M-LDAC

outperformed the 3-fluid M-LDAC system under the condition with the lowest latent load. Moreover, in the high latent load conditions, the 2-fluid system required desiccant solution with a concentration that exceeds the saturation concentration of the liquid desiccant. Using desiccant solutions with concentration above the saturation concentration causes solution crystallization where salt crystals block some or all membrane pores, and, thus, significantly deteriorating the system performance. This suggests that the 3-fluid M-LDAC system may be more efficient in hot and humid climates where the dehumidification loads are generally higher and in specific applications that need low indoor air humidity ratios. While this chapter focused on simulating the 2-fluid and 3-fluid M-LDAC systems under design conditions, the following chapter focuses on system performance over hourly simulations.

CHAPTER 3

SIMULATION OF A 3-FLUID M-LDAC SYSTEM IN AN OFFICE BUILDING

3.1 Overview of Chapter 3

In this chapter, the 2-fluid and 3-fluid membrane liquid desiccant air-conditioning (M-LDAC) system models developed in Chapter 2 are used to condition the air inside an office building. A small office building is modeled and equipped with an HVAC system composed of either the 2-fluid or 3-fluid M-LDAC system and a radiant cooling panel system. The purpose of this chapter is to determine whether the HVAC systems can provide thermal comfort within the building. Each HVAC system is evaluated in terms of COP, and their ability to provide thermal comfort. Additionally, the impact of different latent loads due to different occupant densities and infiltration rates on thermal comfort and the HVAC systems are examined through sensitivity studies.

This chapter has been submitted to the Energy and Buildings journal. Of the three contributing authors, Devin Storle (MSc student) performed the study and wrote the manuscript. Mohamed R.H. Abdel-Salam (post-doctoral fellow) reviewed the manuscript and Carey J. Simonson (MSc supervisor) supervised the study and reviewed the manuscript.

Building energy simulation of a 3-fluid membrane LDAC system under hot and humid weather conditions

Devin Storle, Mohamed R.H. Abdel-Salam, Carey J. Simonson

3.2 Abstract

In this chapter, the cooling and dehumidifying capacities of two liquid desiccant membrane air-conditioning (M-LDAC) systems are investigated and compared when installed in an office building located in a hot-humid climate (Miami, Florida). The building HVAC system consists of a radiant cooling system to cover the sensible load and either a 2-fluid or 3-fluid M-LDAC system to meet the latent load. The systems are simulated over the warmest week of the year using TRNSYS simulation software and modelled using a previously developed analytical model for the 2-fluid M-LDAC system and empirical models for the 3-fluid M-LDAC systems. Sensitivity studies are performed where the systems are evaluated under different latent load conditions due to different occupant densities and infiltration rates. The 2-fluid and 3-fluid M-LDAC systems can meet the latent loads at lower occupant densities and infiltration rates but fail to provide thermal comfort conditions as occupancy and infiltration rates increase. It is concluded that the 3-fluid M-LDAC system uses less energy to meet the latent load than the 2-fluid M-LDAC system. The 2-fluid M-LDAC system consumes 50% more energy than the 3-fluid M-LDAC system in order to provide thermal comfort to the office building during the weekly simulation.

3.3 Introduction

Liquid desiccant technology has shown potential in air dehumidification when compared to conventional air-conditioning (CAC) systems. Liquid desiccant air-conditioning (LDAC) systems use liquid desiccants to remove moisture from an air stream whereas CAC systems dehumidify air by cooling the air below its dew point temperature. LDAC systems are less energy intensive and can reduce energy consumption by up to 26-80% in hot-humid climates (Mohammad et al. 2013). In addition, CAC related condensation can lead to mold, bacteria, and water related damages which reduces indoor air quality (IAQ) and can affect occupant health and productivity (Stetzenbach et al. 2004).

Industrial liquid desiccant systems commonly use a packed-bed liquid desiccant dehumidifier (Lowenstein 2008). These dehumidifiers spray a cooled liquid desiccant into a porous contact media through which air flows and is subsequently cooled and dehumidified. Although these devices have shown dehumidification effectiveness of up to 90% under some operating conditions (Longo and Gasparella 2005), direct contact dehumidification can lead to desiccant entrainment in the supply air, which can result in corroded ducts and a reduction in IAQ (Ge et al. 2016).

Membrane-based liquid desiccant dehumidification prevents desiccant entrainment in the air stream by separating the liquid desiccant and air streams with a membrane that is impermeable to liquid but permeable to water vapor. Such exchangers are called liquid-to-air membrane energy exchangers (LAMEEs) and are typically flat-plate or shell-and-tube exchangers (Isetti et al. 1996; Bergero and Chiari 2001; Vestrelli et al. 2006; Mahmud et al. 2009; Beriault et al. 2011).

The performance of the LAMEE may be improved by adding a third fluid to internally heat or cool the liquid desiccant solution. Abdel-Salam et al. (Abdel-Salam et al. 2016a) designed and tested

an internally cooled/heated 3-fluid LAMEE where a refrigerant is used to cool or heat the liquid desiccant. The ability to control the temperature of the desiccant solution increased the heat and mass transfer rates in the dehumidifier by 79% and 95% (Abdel-Salam et al. 2016a), respectively. In the regenerator, the heat and mass transfer rates increased by 104% and 141% (Abdel-Salam et al. 2016b), respectively.

In Chapter 2, empirical correlations were developed for the 3-fluid LAMEE dehumidifier and regenerator. The empirical correlations were used to simulate a 3-fluid M-LDAC system under different design conditions and to compare the results with that of a 2-fluid M-LDAC system. It was found that the 3-fluid M-LDAC system outperformed the 2-fluid M-LDAC system under high and medium latent load conditions.

3.4 Objectives

The objective of this chapter is to investigate the capability of the 2-fluid and 3-fluid M-LDAC systems to provide thermal comfort conditions within a small office building in a hot-humid climate using TRNSYS building energy simulation software (TRNSYS 2017). Additionally, the effects of occupant density and infiltration rates (the main latent loads) on the performance and energy consumption of the 2-fluid and 3-fluid M-LDAC systems are evaluated through sensitivity studies.

3.5 Building model and climate description

3.5.1 Building model

A small single-story office building is used in the simulations. The important building parameters are summarized in Table 3.1. The building is modelled based on the small office reference building

in the U.S. Department of Energy Commercial Reference Building Models of the National Building Stock (Deru et al. 2011). The building has a floor area of 511 m^2 (Deru et al. 2011), ceiling height of 3m, and width-to-length aspect ratio of 1.5 (Deru et al. 2011). The thermal properties of the building envelop satisfy the maximum U-values in ASHRAE Standard 90.1 (2013) for a hot-humid climate. The building construction consists of wood framed walls, concrete floors, and a roof with insulation entirely above the deck. The windows are selected to satisfy the solar heat gain coefficient (SHGC) provided in ASHRAE Standard 90.1 (2013). The occupant density is chosen to comply with the occupant density for an office space specified in ASHRAE Standard 62.1 (2016). The ventilation rate is calculated assuming the building is a single zone and using the minimum ventilation rates for an office space specified in ASHRAE Standard 62.1 (2016). The HVAC systems are 100% outdoor air systems. The ventilation effectiveness is 1.0 since cool air is supplied from the ceiling and the outdoor air intake is equal to ventilation rate required (ASHRAE 2016). The lighting is chosen in accordance with the lighting power density specified for an office space in ASHRAE Standard 90.1 (2013). Finally, the equipment (computers) load is the load factor recommended by Wilkins and Hosni (2011) for desktops with dual monitors, 1 printer per 10 computers, and medium-to-heavy use.

Table 3.1: Small single-story office building model specifications

Parameter	Value	Unit
Floor area[a]	511	m^2
Aspect Ratio[a]	1.5	-
Floor to ceiling height[a]	3.1	m
Window-to-wall ratio[a]	21	%
Wall U-value[b]	0.33	$W/(m^2 K)$
Roof U-value[b]	0.27	$W/(m^2 K)$
Floor U-value[b]	1.8	$W/(m^2 K)$
Window U-value[b]	1.04	$W/(m^2 K)$
Window SHGC[b]	0.23	-
Occupant density[c]	5	# of people/100 m^2
Occupancy	25	-
Ventilation airflow rate[c]	0.50	ACH
Infiltration[d]	0.2	ACH
Equipment heat gain[e]	10.8	W/m^2
Lighting heat gain[b]	11	W/m^2
Occupants sensible heat gain[b]	75	W/person
Occupants latent heat gain[b]	75	W/person

[a] Deru et al. (Deru et al. 2011)
[b]ASHRAE Standard 90.1-2013 (ASHRAE 2013)
[c]ASHRAE Standard 62.1-2016 (ASHRAE 2016)
[d]Gowri et al. (Gowri, Winiarski, and Jarnagin 2012)
[e]Wilkins and Hosni (Wilkins and Hosni 2011)

3.5.2 Thermal comfort

The aim of the HVAC system is to provide a thermal environment that is comfortable during occupancy. An acceptable thermal environment is dependent on the air temperature, air speed, air humidity, occupant clothing, occupant metabolic rate, and mean radiant temperature. Of which, the operative temperature (a combination of the air and mean radiant temperature), air humidity and air speed can be controlled by HVAC equipment. The operative temperature is calculated by using Equation (3.1).

$$T_{op} = \frac{h_r T_{mr} + h_c T_{air,blg}}{h_r + h_c} \tag{3.1}$$

where $T_{air,blg}$ is the internal air temperature of the space (°C), T_{mr} is the mean radiant temperature of the space (°C), h_r is the radiative heat transfer coefficient (W/(m^2·K)), and h_c is the convective heat transfer coefficient (W/(m^2·K)).

The range of operative temperatures and air humidity ratios that satisfy thermal comfort are indicated by the thermal comfort zone in Figure 3.1. Table 3.2 summarizes the thermal comfort parameters used in this simulation as well as their values. The air speed, occupant clothing factor and metabolic rate comply with the recommended values specified in ASHRAE Standard 55 (2013) for comfortable air flow, occupants wearing trousers, a long-sleeve shirt and suit jacket, and occupant activity limited to typing and filing while seated. The chosen clothing factor is high for hot and humid weather conditions, where the clothing factor is typically around 0.5 clo for outdoor air temperatures above 25°C (ASHRAE 2013). However, the office building is assumed to follow a professional dress code and, while the thermal comfort factors are chosen based on a clothing factor of 0.96 clo, the thermal comfort factors also satisfy the 0.5 clo zone in Figure 3.1.

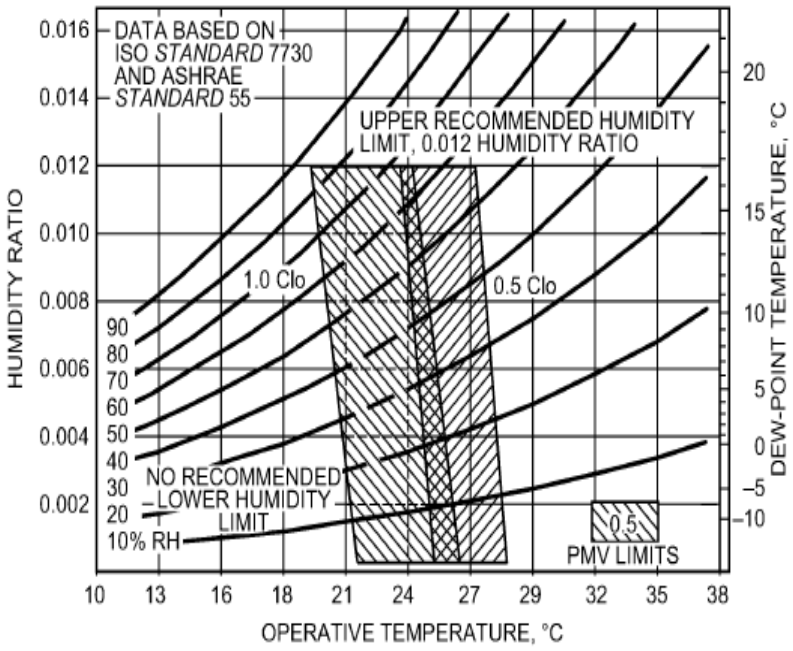

Figure 3.1: Thermal comfort zone (ASHRAE 2017)

Table 3.2: Factors defining thermal comfort

Parameter	Value	Unit
Operative temperature	24	°C
Air humidity ratio	12	g_v/kg_{da}
Metabolic rate	1.2	met
Clothing factor	0.96	clo
Air speed	0.2	m/s

3.5.3 Schedules

Schedules are defined in order to simulate a realistic office building. Occupancy, set point temperature, lighting, and equipment schedules are as shown in Figure 3.2. Full occupancy is assumed for weekdays and 40% occupancy is assumed on the weekends. During weekdays, occupancy decreases by 50% during the noon hour. The occupancy hours are set between 9 am and 6 pm. The other schedules are based on the occupancy schedule.

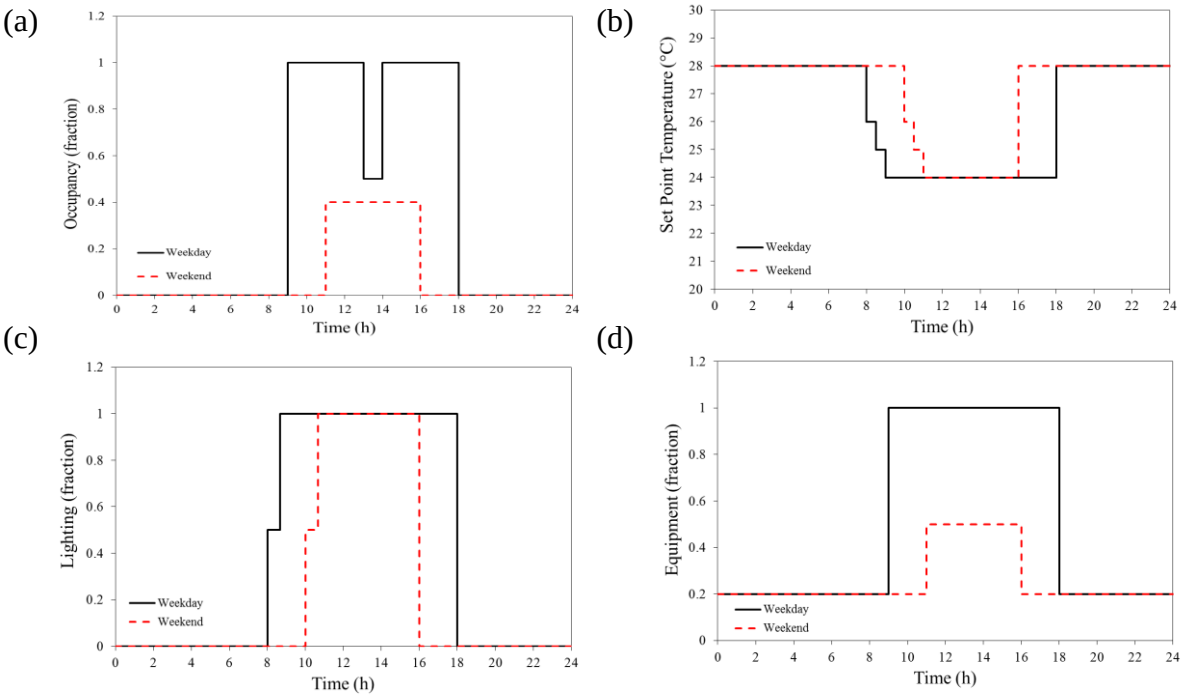

Figure 3.2: Schedules for (a) occupancy, (b) set point temperature, (c) lighting, and (d) equipment.

The operative temperature is controlled to provide adequate thermal comfort within the building. The operative set point temperature is maintained at 24°C during occupancy and is to never exceed 28°C. The operative temperature is decreased in three steps to balance energy consumption and peak energy demand in the morning (Hilliard 2012). An hour before occupancy, the operative temperature is decreased to 26°C and then to 25°C a half hour before occupancy, and, lastly, to

24°C at occupancy. Lighting is turned off during off hours except for an hour before occupancy where a fraction (50%) of the lights are turned on to comply with the automatic lighting requirements listed in ASHRAE Standard 90.1 (2013). The equipment mainly consists of computers that are assumed to be on during occupancy and in sleep mode during off hours.

3.5.4 Climate

The building is simulated in Miami, Florida which is a very hot and humid climate (Climate Zone 1A). Climate zone designations are provided by ASHRAE Standard 90.1 (2013) where a climate is given a number and letter to indicate typical air temperature and humidity. The numbers are ordered from 1 to 8 with low numbers defining warmer climates and higher number denoting cooler climates. Climate humidity is designated by the letters A, B, and C which correspond to moist, dry, and marine climates, respectively. A very hot and humid climate is chosen for this simulation because air cooling and dehumidification equipment is heavily used in these climates and this climate meets the 3-fluid LAMEE empirical model requirements (outlined in Chapter 2). Furthermore, to satisfy model limitations, the simulation is restricted to the hottest week of the year (July 27th to August 2nd) where the average air temperature is 29.3°C and the average air humidity ratio is 17.6 g_v/kg_{da}. An EnergyPlus weather file (Type TMY3) is used to provide the weather data for the simulation. The air temperatures and humidity ratios throughout this week are illustrated in Figure 3.3(a) and (b), respectively, where the horizontal line indicates the weekly average value. In the simulation, the second and third days (July 28-29) are weekend days, therefore, the weekend schedules are applied during these days.

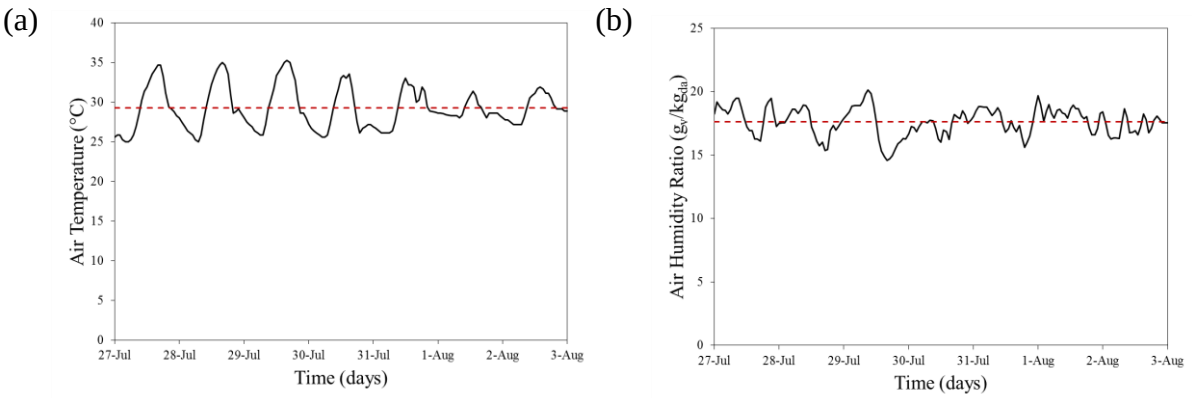

Figure 3.3: Weekly hourly ambient air (a) temperature and (b) humidity ratio in Miami, Florida (Wilcox and Marion 2008).

The hottest day of the year (July 29) and the most humid day of the week (July 31) are presented in Figure 3.4. On July 29, the average air temperature is 29.9°C and the average air humidity ratio on July 31 is 18.2 g_v/kg_{da}. July 29 falls on the weekend and follows the weekend schedules while July 31 falls on a weekday and follows the weekday schedules.

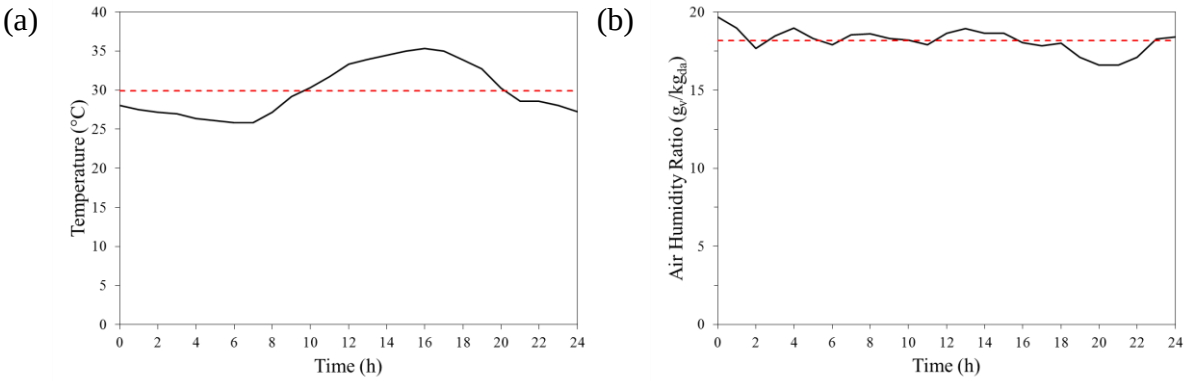

Figure 3.4: Hourly ambient (a) air temperatures on the hottest day and (b) air humidity ratios on the most humid day of the week in Miami, Florida (Wilcox and Marion 2008).

3.6 HVAC systems

The HVAC systems studied in this chapter consist of separate equipment to meet the sensible and latent requirements of the building. The HVAC systems are composed of a radiant cooling system and, either, a 2-fluid or 3-fluid M-LDAC system. Therefore, the two systems are referred to as

either a 2-fluid or 3-fluid M-LDAC HVAC system. The HVAC systems are 100% outdoor air systems.

3.6.1 Radiant cooling panels

Radiant ceiling panels are used to cover most of the sensible load in the office building. The radiant system is activated an hour before occupancy to reach a comfortable operative temperature for when the occupants arrive. Furthermore, the radiant panels continually cool throughout the day and are inactive during the evenings and mornings. The surface temperature of the aluminum radiant panels is controlled with chilled water and the panels remove heat from the space by convection and radiation. To meet the varying sensible load, the water mass flow rate into the radiant panel is adjusted by a controller. To avoid condensation on the surface of the panels, the supply water temperature is set to 17°C which is slightly above the dew point temperature of the building which corresponds to 16.9°C, an air temperature of 24.5°C and an air humidity ratio of 12 g_v/kg_{da}. Table 3.3 lists the design specifications of the radiant cooling panels used in this study.

Table 3.3: Radiant cooling panel system specifications

Parameter	Value	Unit
Pipe Spacing	0.2	m
Pipe inside diameter	0.02	m
Panel area	70	m^2
Number of panels	7	panels
Supply water temperature	17	℃
Heat transfer coefficient	40	$\frac{W}{m^2 \cdot K}$
Capacity	85	$\frac{W}{m^2}$

3.6.2 M-LDAC system

Figure 3.5 presents a schematic of the 3-fluid M-LDAC system supplying air to the office building. The 2-fluid and 3-fluid M-LDAC systems cool and dehumidify the outdoor air before supplying it to a building. They are also responsible for meeting the latent load of the building. The 2-fluid and 3-fluid M-LDAC systems supply 100% outdoor air to the building. The systems supply and exhaust air at the same rate to maintain a neutral air pressure within the building.

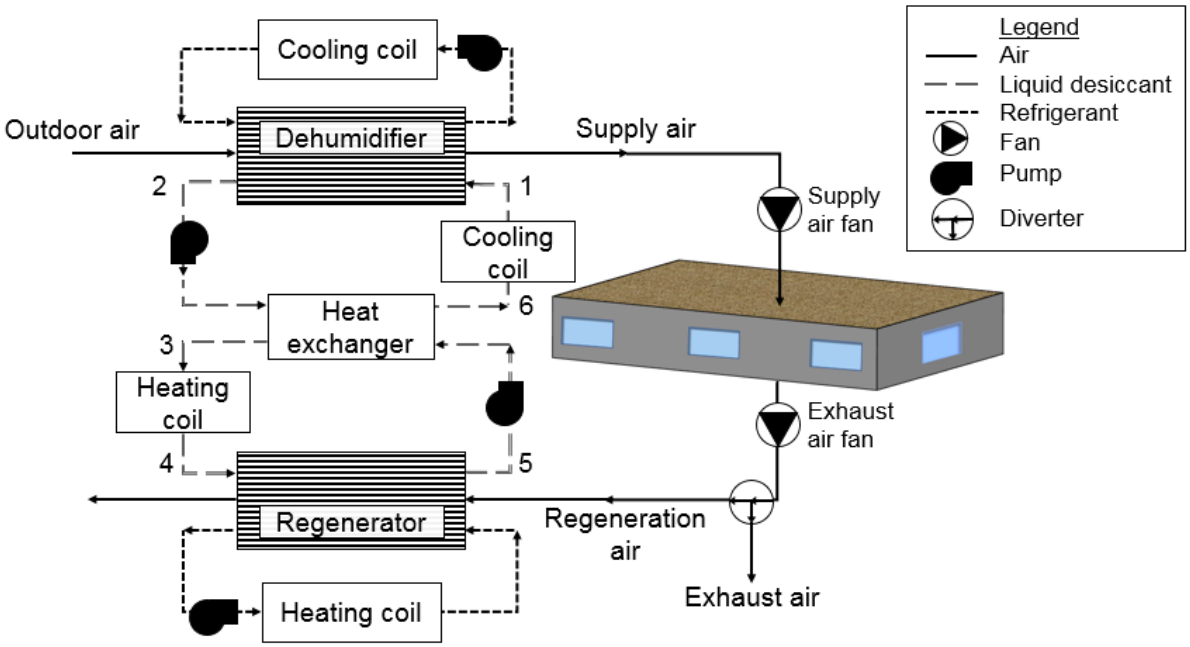

Figure 3.5: Schematic of the M-LDAC system

The majority of the exhaust air is used to regenerate the liquid desiccant solution in the regenerator in the M-LDAC systems whereas the remaining exhaust air is diverted to the environment. In the 3-fluid M-LDAC system, heating and cooling refrigerant loops are used to control the desiccant solution temperature within the dehumidifier and regenerator, respectively. The 2-fluid M-LDAC system does not have these loops. Pumps and fans are used to distribute the desiccant solution, refrigerant, and air around the system.

The analytical model derived by Ge et al. (2013) for the 2-fluid LAMEE and the empirical correlations developed in Chapter 2 for the 3-fluid LAMEE are used to simulate the M-LDAC systems. To meet the latent load, the desiccant solution temperature entering the 2-fluid LAMEE dehumidifier is controlled and the refrigerant (water) temperature entering the 3-fluid LAMEE dehumidifier is controlled. A lithium chloride (LiCl) aqueous solution is used in M-LDAC systems because of its high affinity for water and low risk of crystallization (Afshin et al. 2010; Afshin 2010).

3.6.2.1 Liquid-to-air membrane energy exchanger (LAMEE)

Figure 3.6(a) shows a schematic of a 2-fluid LAMEE, Figure 3.6(b) shows schematic of a 3-fluid LAMEE and Figure 3.6(c) presents a cross-sectional view of the 3-fluid LAMEE. LAMEEs consist of alternating desiccant solution and air channels separated by semi-permeable membranes that only permit heat and water vapor transfer between the desiccant solution and air. These semi-permeable membranes are chosen based on their moisture transfer properties to ensure a high moisture transfer and elastic properties to prevent membrane deflection and flow maldistribution. (Larson et al. 2007).

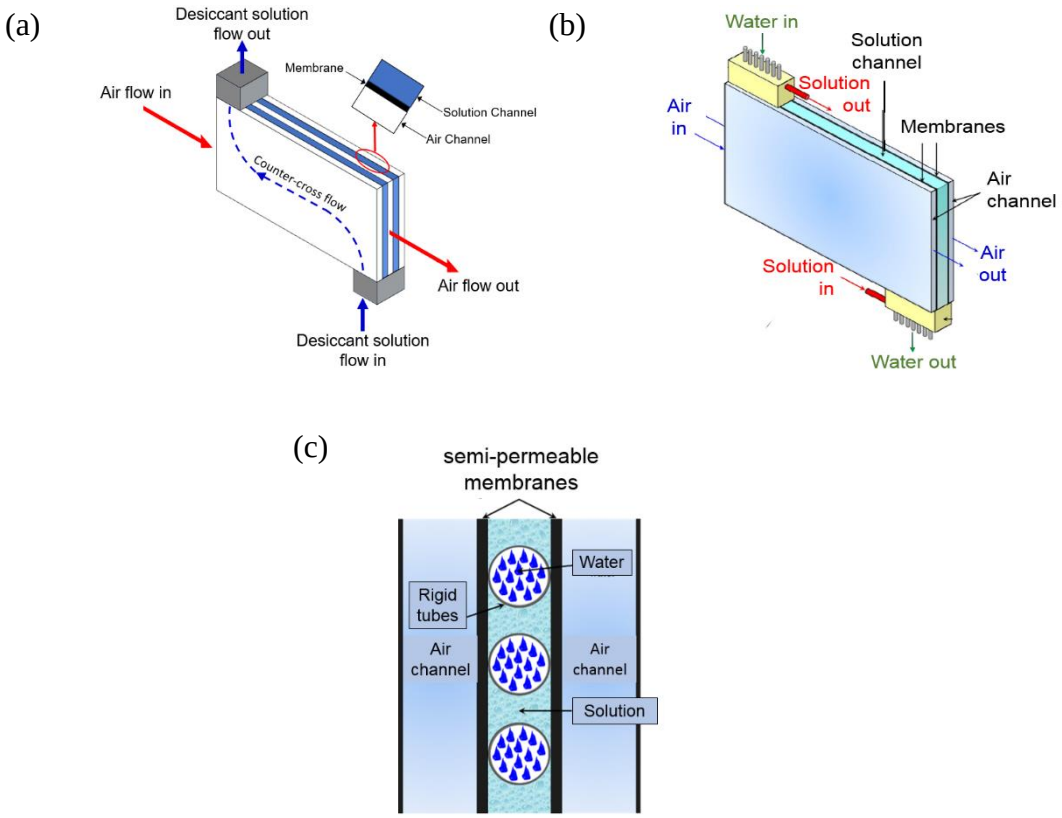

Figure 3.6: Schematic of a (a) 2-fluid LAMEE and (b) 3-fluid LAMEE, and a (c) cross-sectional view of the 3-fluid LAMEE (Courtesy of Abdel-Salam et al. 2016a)

The 3-fluid LAMEE is similar to the 2-fluid LAMEE, however, it contains refrigerant piping within the desiccant solution channels to internally cool the desiccant solution in the dehumidifier and heat the desiccant solution in the regenerator. A refrigerant is piped through the liquid desiccant channel in impermeable titanium piping to heat/cool the desiccant solution along the entire length of the exchanger and, therefore, improve the rates of heat and moisture transfer between the air and desiccant solution.

3.6.2.2 Effectiveness and moisture removal rate

Exchanger performance is characterized by its sensible and latent effectiveness. Sensible effectiveness is the ratio of the actual heat transfer rate between the desiccant solution and the air stream to the maximum possible heat transfer rate between fluid streams. Latent effectiveness is

the ratio of the actual moisture transfer rate between the air and desiccant solution to the maximum possible moisture transfer rate. For a 3-fluid LAMEE in a counter flow configuration, Equation (3.2) is used to determine the sensible effectiveness and Equation (3.3) is used to calculate the latent effectiveness (Abdel-Salam et al. 2017).

$$\varepsilon_{\text{sen}} = \frac{(T_{\text{air,in}} - T_{\text{air,out}})}{(T_{\text{air,in}} - T_{\text{w,in}})} \tag{3.2}$$

$$\varepsilon_{\text{lat}} = \frac{(W_{\text{air,in}} - W_{\text{air,out}})}{(W_{\text{air,in}} - W_{\text{sol@T}_{w,\text{in}},\text{X}_{\text{sol,in}}})} \tag{3.3}$$

where ε is effectiveness, T is temperature (°C), W is humidity ratio (g_v/kg_{da}), X_{sol} is the mass fraction of desiccant in the solution, and $W_{sol@T_{w,in}X_{sol,in}}$ is the equilibrium humidity ratio of the desiccant solution at the inlet refrigerant temperature and inlet mass fraction. Subscripts in and out refer to the inlet and outlet, sen and lat are sensible and latent, sol and w denote the desiccant solution and refrigerant (water), respectively.

The rate at which moisture is removed or released from the air is referred to as the moisture removal rate ($\dot{m}_{rr}$) and is determined using Equation (3.4).

$$\dot{m}_{rr} = \dot{m}_{air}\left(W_{air,in} - W_{air,out}\right) \tag{3.4}$$

where $\dot{m}$ is the mass flow rate (kg/s).

3.6.2.3 Dimensionless parameters

The dimensionless parameters used in this chapter are the same as those presented in Section 2.8.3.

3.6.2.4 The 3-fluid LAMEE model

In Chapter 2, empirical models for the 3-fluid LAMEE were developed using experimental data collected by Abdel-Salam et al. (2016a; 2016b; 2017). These models use empirical correlations (Equations (3.5) to (3.10)) to calculate the sensible and latent effectiveness and outlet desiccant solution temperature for the dehumidifier and regenerator.

Dehumidifier:

$$\varepsilon_{sen} = 0.52 - 0.0797 \cdot T^* - 0.204 \cdot \log(Cr) \tag{3.5}$$

$$\varepsilon_{lat} = 0.37 + 0.0189 \cdot T^* - 0.124 \cdot \log(Cr) \tag{3.6}$$

$$T_{sol,out} = 37.22 - 3.81 \cdot T^* + 7.32 \cdot \log(Cr) \tag{3.7}$$

Regenerator:

$$\varepsilon_{sen} = 0.36 - 0.026 \cdot T^* - 0.83 \cdot Cr + 0.13 \cdot Cr^* \tag{3.8}$$

$$\varepsilon_{lat} = 0.16 - 0.023 \cdot T^* - 0.74 \cdot Cr + 0.12 \cdot Cr^* \tag{3.9}$$

$$T_{sol,out} = 27.4 + 6.26 \cdot T^* - 32.4 \cdot Cr + 4.66 \cdot Cr^* \tag{3.10}$$

The 3-fluid LAMEE model is applicable at outdoor air temperatures above 29°C as highlighted in Chapter 2. The simulations are performed over a week where these conditions are mostly met during occupancy. In addition, the models are each limited to a desiccant solution temperature of 24.5°C and concentration of 32.5%.

3.6.2.5 Performance Parameters

The coefficient of performance (COP) of the M-LDAC system is the ratio of the energy transfer rate (ETR) to the energy consumption rate of the system, and is calculated using Equation (3.11).

$$COP = \frac{Useful\ Energy\ Transfer\ Rate\ (ETR)}{Energy\ Consumption\ Rate\ (ECR)} \tag{3.11}$$

The energy transfer rate is the air cooling and dehumidifying rate of the M-LDAC systems (W) and is calculated using Equation (3.12).

$$ETR = \dot{m}_{air}(h_{air,in} - h_{air,out}) \tag{3.12}$$

where, h denotes enthalpy (J/kg).

The energy consumption rates of the 2-fluid and 3-fluid M-LDAC systems are determined using Equations (3.13) and (3.14), respectively, and is the power required to run the system (W).

$$ECR_{2-fluid} = E_{c,sol} + W_{p,sol} + W_{fan} + E_{h,sol} \cdot 0.3 \tag{3.13}$$

$$ECR_{3-fluid} = E_{c,w} + E_{c,sol} + W_{p,sol} + W_{p,w} + W_{fan} + (E_{h,w} + E_{h,sol}) \cdot 0.3 \tag{3.14}$$

where, W_{fan} and W_{pump} correspond to the electric power (W) consumed by the fan and pump, respectively, E_c denotes the electric power (W) consumed by the chillers, E_h is the thermal power (W) consumed by the heaters, and 0.3 is the assumed equivalent conversion coefficient from thermal power to electrical power.

3.6.2.6 Control of the HVAC systems

The HVAC is controlled to meet the sensible and latent loads of the space. The sensible cooling is controlled by adjusting the water flow rate in the radiant system. The latent cooling (dehumidification) is controlled by controlling the inlet water temperature to the dehumidifier in the 3-fluid M-LDAC system. If more latent cooling is required, the inlet water temperature is decreased to minimum allowable temperature (section 2.10.4). Similarly in the 2-fluid M-LDAC

system, the inlet solution temperature to the dehumidifier is controlled to control the latent cooling in the 2-fluid M-LDAC system to the minimum allowable temperature (Table 3.4). Once the building reaches an air humidity ratio of 11.8 g_v/kg_{da}, the controller raises the inlet water temperature of the dehumidifier in the 3-fluid M-LDAC system or the inlet solution temperature in the 2-fluid M-LDAC system to the maximum allowable temperature (Table 3.4) where an air humidity just below the set value of 12 g_v/kg_{da} can be maintained. It is important to note that the M-LDAC systems are also controlled to avoid heating the supply air to the building and, subsequently, requiring additional cooling from the radiant system. Thus, the controller prevents the inlet water and solution streams from reaching temperatures that require additional radiant cooling. Furthermore, the inlet solution temperature to the regenerator of the 2-fluid M-LDAC system and the inlet water temperature to the regenerator of the 3-fluid M-LDAC system is controlled to ensure the moisture exchanged in the dehumidifier is equal to the moisture exchanged in the regenerator.

3.6.2.7 Operating and design conditions

In the comparison, the 2-fluid and 3-fluid M-LDAC systems are simulated at the operating and design conditions presented in Table 3.4. The design and operating parameters are restricted to the limitations of the 3-fluid LAMEE model presented in Chapter 2.

Table 3.4: Operating and design parameters of the 2-fluid and 3-fluid M-LDAC systems

	Parameter	M-LDAC System	
		2-fluid	3-fluid
Dehumidifier	$T_{air,in}$ (°C)	From weather file	
	$W_{air,in}$ (g_v/kg_{da})	From weather file	
	$T_{sol,in}$ (°C)	1 – 16[a]	24.5
	$T_{w,in}$ (°C)	-	4.46 – 18[a]
	Cr	-	0.025
	Cr*	1.8	1.8
	NTU	1.8	1.8
Regenerator	$T_{air,in}$ (°C)	From weather file	
	$W_{air,in}$ (g_v/kg_{da})	From weather file	
	$T_{sol,in}$ (°C)	70 – 82[b]	40
	$T_{w,in}$ (°C)	-	42 – 60[b]
	Cr	-	0.1
	Cr*	2	2
	NTU	2	2
Desiccant Solution		LiCl	
Desiccant Concentration (%)		45	32.5
Refrigerant		-	Water

[a]Controlled to reach desired humidity of the supply air stream
[b]Controlled to restore solution concentration

3.7 Results

3.7.1 Weekly simulation results

In this section, the results for the base case conditions (default occupant density and infiltration in Table 3.1) are presented. Figure 3.7(a) presents the indoor operative temperatures of the office building equipped with the 2-fluid and 3-fluid M-LDAC HVAC systems as well as the ambient air temperature. For both HVAC systems, the operative temperature is consistently around the set point temperature of 24°C during occupied hours. Each system has similar operative temperatures because they use the same radiant cooling system and controllers to meet the sensible loads. The radiant system is activated an hour before occupancy and cooling performed in three steps, first to 26°C (if the current operative temperature exceeds it), then to 25°C a half hour later and 24°C

during occupancy. At the end of the work day, the systems are turned off which results in a sudden increase in operative temperature at the end of each occupied period.

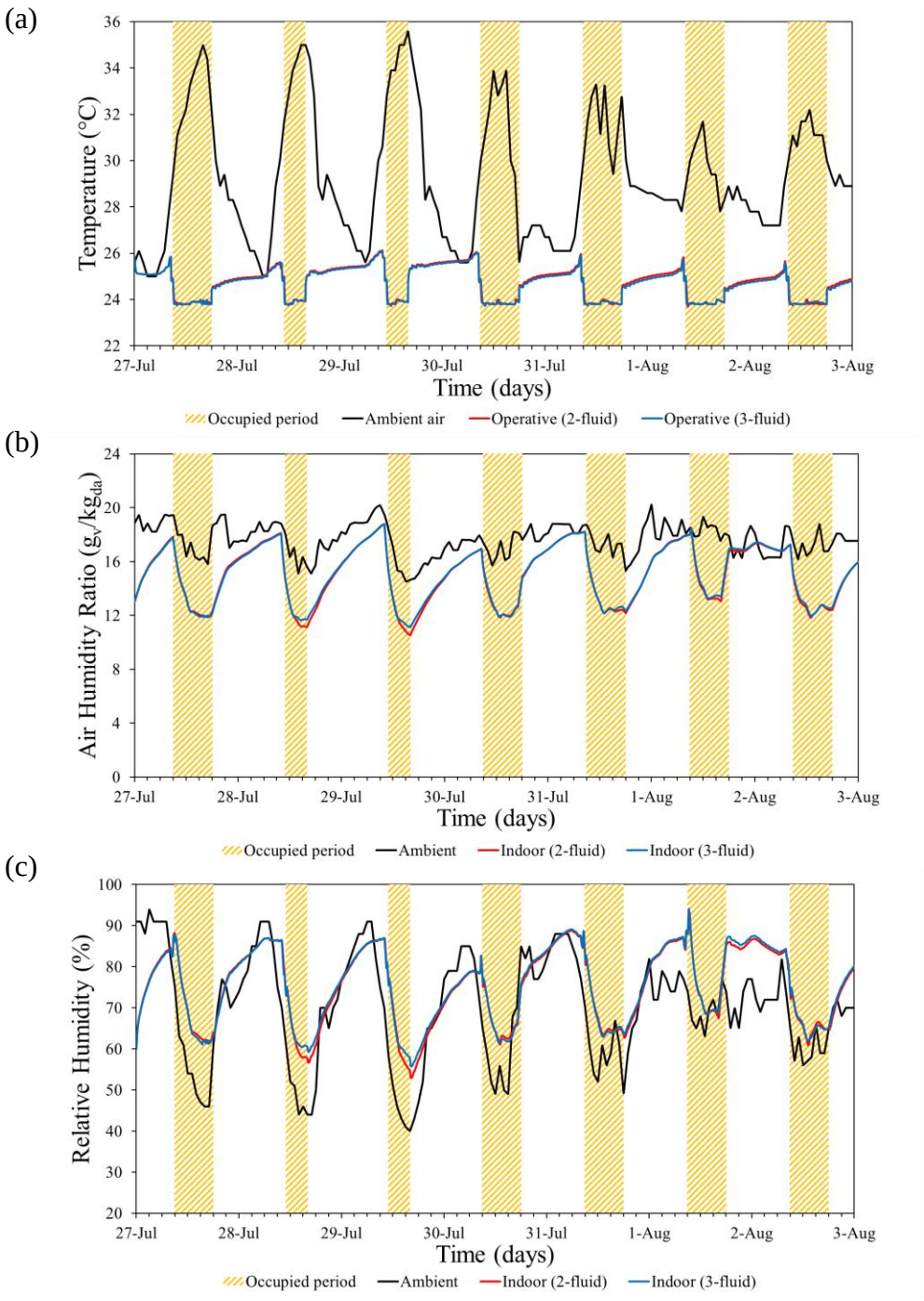

Figure 3.7: (a) the ambient and indoor operative temperatures, (b) the ambient and indoor air humidity ratios, and (c) the ambient and indoor relative humidity provided by the 2-fluid and 3-fluid HVAC systems

Figure 3.7(b) shows the ambient air humidity ratio and the indoor air humidity ratios for both HVAC systems. Similarly, Figure 3.7(c) presents the relative humidity for both systems as well as the relative humidity of the outdoor air. The desired air humidity is reached for both systems during occupied hours with some hours being above 12 g_v/kg_{da} in the morning. The indoor air humidity is nearly the same for both the systems.

Controller use is emphasized in Figure 3.7(b). The M-LDAC systems are only active when the outdoor air conditions are sufficient for the 3-fluid LAMEE model and these conditions are not often met before the occupancy period. For this reason, the beginning of the work day is used to achieve the desirable air humidity of 12 g_v/kg_{da}. Furthermore, once the acceptable air humidity is reached, the controlled input parameters to the 2-fluid and 3-fluid LAMEE are adjusted to maintain this humidity and consume less energy.

Figure 3.8(a) shows the weekly sensible heating provided by each source and the weekly sensible cooling performed by both HVAC systems, which are denoted by their respective M-LDAC system (2-fluid or 3-fluid). The sensible load comes from three main sources: internal gains, infiltration, and solar gains. The internal gains (people, equipment, and lighting) accounts for 77% of the weekly sensible heat gain while infiltration accounts for 7%, and solar gains contributes 16%.

Both HVAC systems meet the sensible load differently. The 2-fluid M-LDAC system provides more sensible cooling than the 3-fluid M-LDAC system. The radiant system is responsible for 85% of the sensible cooling and the 2-fluid M-LDAC system provides 15% of the sensible cooling. In contrast, the radiant system accounts for 92% of the sensible cooling when paired with the 3-fluid M-LDAC system.

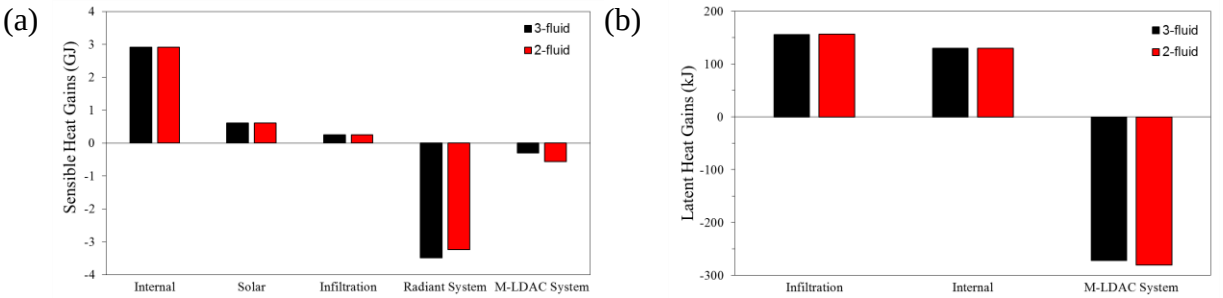

Figure 3.8: (a) Comparison between the amount of sensible heat gain covered by the 2-fluid and 3-fluid systems, and (b) comparison between the amount of latent heat gain covered by 2-fluid and 3-fluid systems

Figure 3.8(b) presents the total latent loads due to infiltration and internal gains as well as the weekly latent heat energy removed by the 2-fluid and 3-fluid M-LDAC systems. For both systems, the sources contribute equal amounts of latent energy and the M-LDAC systems remove similar amounts. The 2-fluid M-LDAC system removed slightly more latent energy because the controller prevents the HVAC systems from supplying air that will require additional radiant cooling. Once the indoor air reaches the set air humidity ratio, the controller reduces the latent cooling provided by the M-LDAC systems by increasing either the inlet water temperature (3-fluid) or solution temperature (2-fluid) of the dehumidifier. If the 2-fluid M-LDAC system maintains the internal air humidity at this set point, the supply air temperature will be above the building set point temperature and heat the building. Therefore, the controller prevents the inlet solution temperature of the dehumidifier from reaching temperatures that will heat the building and, while doing so, the air continues to be dehumidified and cooled. Thus, the 2-fluid M-LDAC system provides more sensible cooling than the 3-fluid M-LDAC system. The 3-fluid M-LDAC system can maintain the set air humidity without heating the building.

Table 3.5 presents the average COP, energy transfer rate, and energy consumption rate of the 2-fluid and 3-fluid M-LDAC systems during occupied hours. The 3-fluid M-LDAC system (COP of 1.03) outperforms the 2-fluid M-LDAC system (COP of 0.63). The COP is also evaluated at an

increased and decreased effectiveness of the 3-fluid LAMEE (not included in Table 3.5) to determine the sensitivity of the COP to uncertainties in the model of the 3-fluid LAMEE. The COP at an increased effectiveness of 10% is 1.05 and the COP at a decreased effectiveness of 10% is 1.01, thus showing an insignificant effect on the results. The COP considers the energy transfer and consumption rates of the M-LDAC systems. The energy consumed by the radiant system is not included in the COP because the COP comparison focuses on the M-LDAC systems. The energy transfer rate of the 2-fluid M-LDAC system is larger than the 3-fluid M-LDAC system because the 2-fluid M-LDAC system performs more sensible cooling.

Table 3.5: Average coefficient of performance (COP), energy transfer rate (ETR), and energy consumption rate (ECR) of the 2-fluid and 3-fluid M-LDAC systems

	M-LDAC system		
Average	3-fluid	2-fluid	Units
COP	1.03	0.63	-
ETR	9.7	11.2	kW
ECR	9.6	17.9	kW

Figure 3.9(a) presents the cumulative energy consumption of the M-LDAC HVAC systems and shows that the 2-fluid M-LDAC HVAC system consumes more energy. Figure 3.9(b) presents the weekly energy consumptions associated with various components of the HVAC system, which includes: solution cooling and heating coils, water heating and cooling coils, pumps and fans, and radiant cooling systems. Solution cooling and heating consumes a significant amount of energy in the 2-fluid M-LDAC system because the solution is cooled to meet the latent demands and then heated for solution regeneration. Therefore, the solution temperature changes considerably as it flows around the M-LDAC system. The 3-fluid M-LDAC system requires less solution cooling and heating energy because the inlet solution temperatures of the dehumidifier and regenerator are fixed and experience less fluctuation. In addition, the water does not require extensive heating or

cooling because it does not experience a large temperature change when passing through the dehumidifier or regenerator. Thus, the 3-fluid M-LDAC system consumes less energy to maintain the water and solution at their respective temperatures.

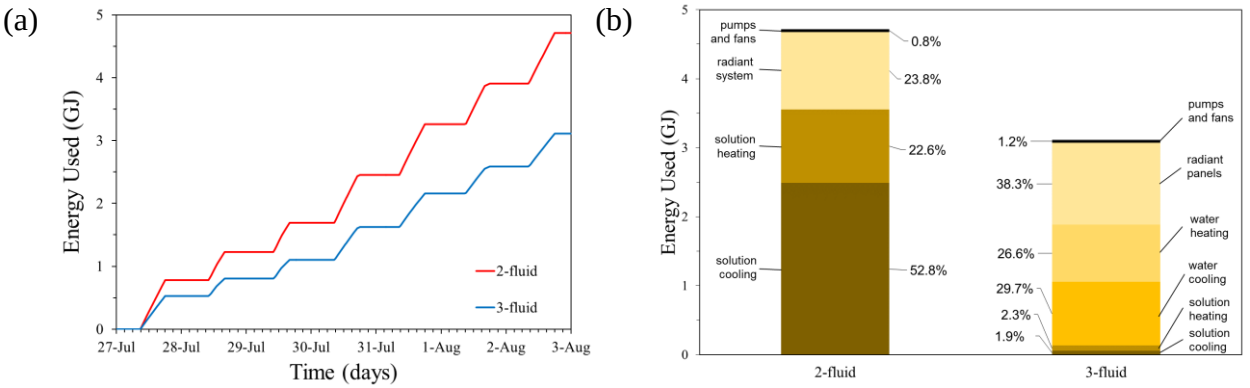

Figure 3.9: Total energy used by the 2-fluid and 3-fluid M-LDAC HVAC systems (a) throughout the week and (b) summarized into contribution by component.

3.7.2 Sensitivity studies

Sensitivity studies are performed on the occupant density and infiltration rates because they are the main sources of latent load. The occupant density (number of people per 100 m^2) is incrementally increased by 5 from the original default occupant density of 5 people/100 m^2. It is important to note that the ventilation rate increases with occupant density since the ventilation rate is coupled with the number of occupants (ASHRAE Standard 62.1 2016). The infiltration rate is studied over increments of 0.2 ACH to study the impact of different building air tightness (i.e., new and old buildings) on the performance of the 2-fluid and 3-fluid systems. Table 3.6 presents the parameters evaluated in this study as well as their reference values and the range of values examined.

Table 3.6: Reference values and range of values of the studied parameters

Parameter	Reference Value	Value range	Units
Number of people per area	5	5, 10, 15, 20, 25	number of people/100 m^2
Air change rate	0.5	0.5, 0.64, 0.79, 0.93, 1.07	ACH
Infiltration	0.2	0.4, 0.6, 0.8, 1.0	ACH

3.7.2.1 Sensitivity study: occupant density

Figure 3.10 presents the ambient and operative temperatures over the week and hottest day for the 2-fluid and 3-fluid M-LDAC HVAC systems under the different occupant densities. The radiant cooling system is able to meet the additional sensible gains introduced by the increasing occupancy. As a result, both HVAC system provide the office space with acceptable and comfortable operative temperatures during occupied hours.

(a)

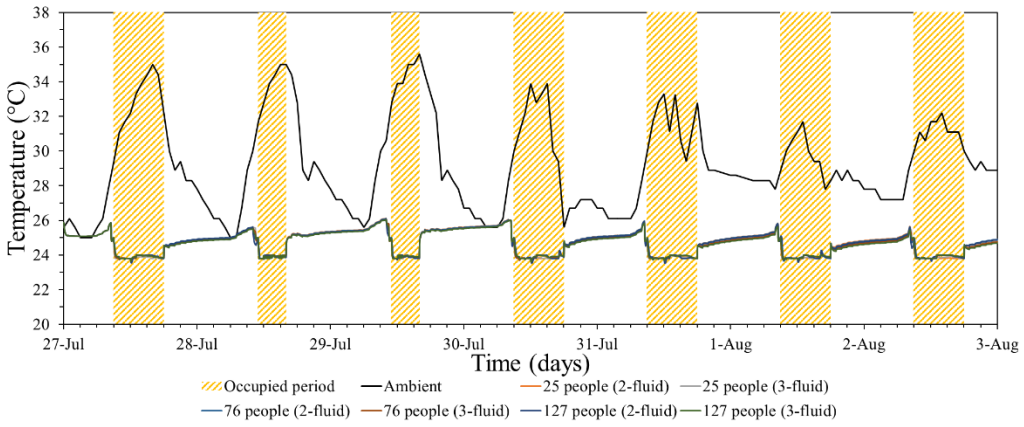

(b)

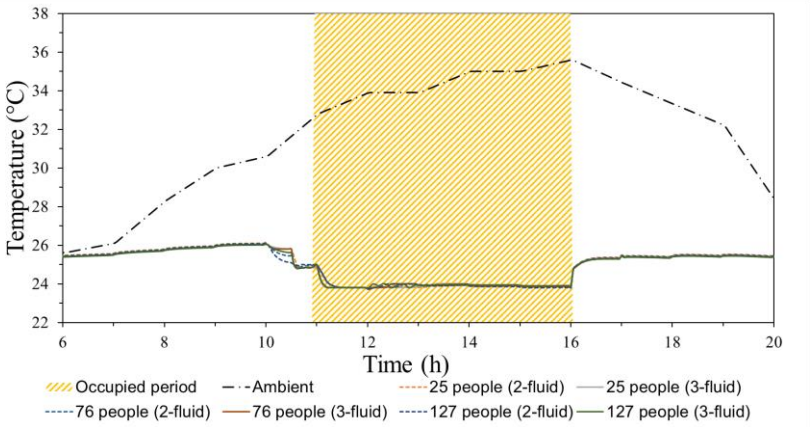

Figure 3.10: Ambient and operative temperatures when using the 2-fluid and 3-fluid M-LDAC systems over (a) a week and (b) the hottest day

In contrast, both M-LDAC systems had difficulties meeting the latent loads introduced at larger occupant densities as illustrated in Figure 3.11 by the indoor air humidity ratios for the week and most humid day. As the number of people increase, the indoor air humidity ratio during occupancy increases because the M-LDAC systems cannot meet these latent loads under these operating conditions. However, the 2-fluid M-LDAC system is slightly closer to the set air humidity ratio compared to the 3-fluid M-LDAC system. This is due to the limitations of the 3-fluid LAMEE model where the minimum inlet water temperature of the dehumidifier in the 3-fluid M-LDAC system is set dependent on the outdoor air temperature (Chapter 2) while the inlet solution

temperature of the dehumidifier in the 2-fluid M-LDAC system can be set to its minimum value (1°C) at any outdoor air temperature allowing for maximum air dehumidifying.

Lastly, the indoor air humidity ratio peaks during the fifth day because the outdoor conditions fail to satisfy the model requirements thereby turning the M-LDAC systems off around 4 pm. The thermal environment become less acceptable as the indoor air humidity ratio departs further from the set value of 12 g_v/kg_{da}. It is important to note that the operating and design parameters of M-LDAC systems are constrained to the 3-fluid LAMEE model limitations.

(a)

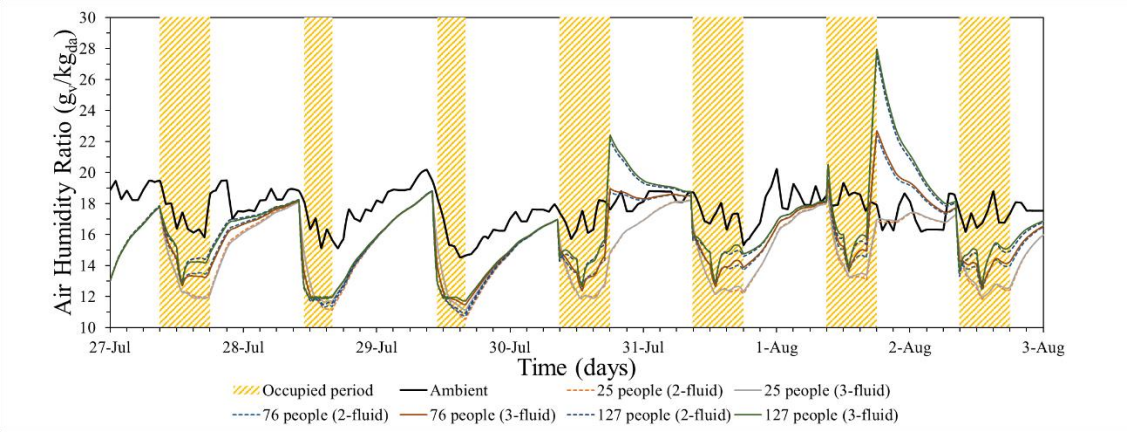

(b)

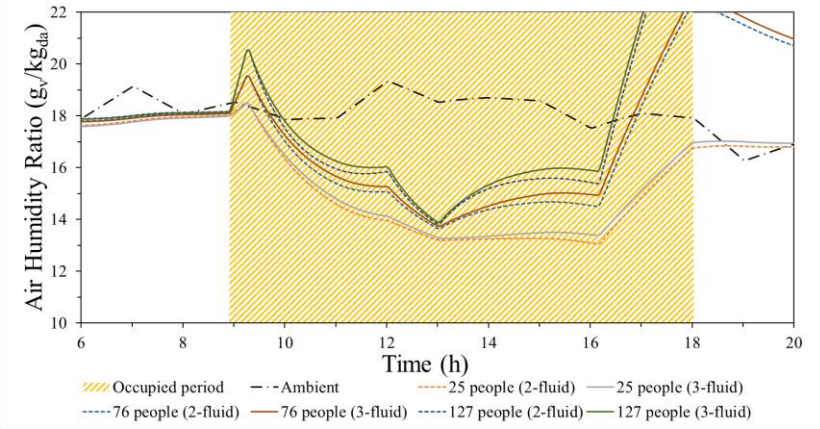

Figure 3.11: The ambient and indoor air humidity ratios (a) throughout the week and (b) on the most humid day of the week for the 2-fluid and 3-fluid M-LDAC HVAC systems

The 3-fluid M-LDAC outperforms the 2-fluid M-LDAC system at all occupant densities. Figure 3.12(a) shows that the weekly average COPs of the M-LDAC systems during occupied hours are relatively unaffected when the number of people is increased since the equipment is sized up to accommodate for the increased ventilation rate. Ventilation rate increases as occupants increase. Since NTU is fixed, the 3-fluid LAMEE is sized up (area increases) to maintain the fixed NTU value at the different ventilation rates. The solution and water flow rates also increase because the operating conditions (Cr and Cr*) are set constant across different occupant densities. The M-LDAC system behaves similarly but at a larger scale which results in a similar ratio between the energy transfer and consumption rates (COP). The weekly average energy transfer rate between the desiccant solution and air stream in the dehumidifier and the average energy consumption rate of the 2-fluid and 3-fluid M-LDAC systems increase as the occupant density is increased as shown by Figure 12 (b) and (c), respectively. The energy transfer rate increases due to the larger ventilation rates at higher occupant densities and the energy consumption rate increases as a result of a rise in air cooling and dehumidifying, solution cooling and heating, fluid distribution (pumps and fans), and water heating and cooling performed at larger air change rates.

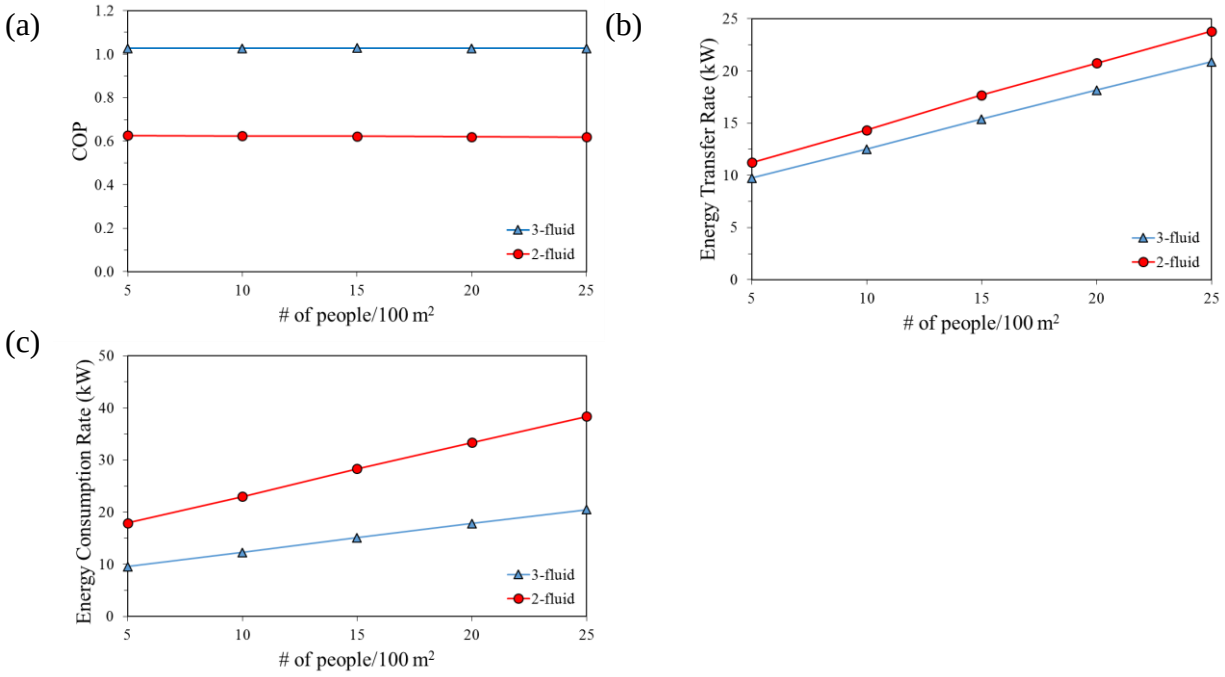

Figure 3.12: The weekly average (a) COPs, (b) energy transfer rate between the desiccant solution and air streams in the dehumidifier, and (c) energy consumption rates of the 2-fluid and 3-fluid M-LDAC systems under different occupant densities

The occupant densities have a large effect on the sensible and latent cooling required by the HVAC systems. Figure 3.13 presents the sensible and latent loads, the sensible cooling performed by the radiant system, and the sensible and latent cooling provided by the 2-fluid and 3-fluid M-LDAC systems at different occupant densities. At the highest occupant density of 25 people/100 m^2, the overall sensible gains (internal, solar, and infiltration gains) increased by 34% and overall latent gains (infiltration and internal gains) increased by 183%.

In order to meet the high sensible loads, the sensible cooling provided by the radiant system increases by 0.91 GJ (26%) when paired with the 3-fluid M-LDAC system and 0.68 GJ (21%) when coupled with the 2-fluid M-LDAC system. The latent cooling provided by the 3-fluid and 2-fluid M-LDAC systems increased by 450 kJ (166%) and 449 kJ (160%), respectively. The latent cooling increases because a higher ventilation rate increases allows for more air to be conditioned through the M-LDAC systems.

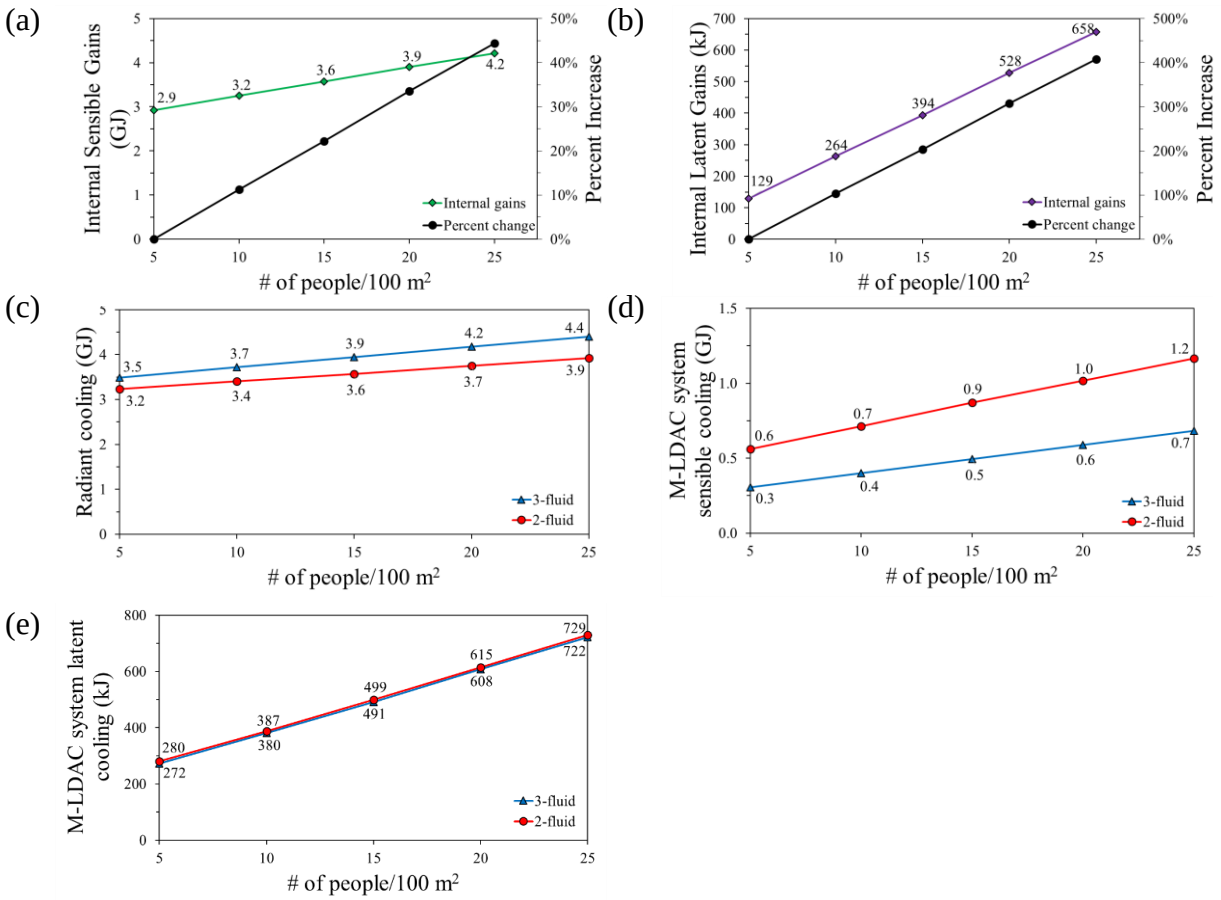

Figure 3.13: The internal (a) sensible and (b) latent gains, (c) the radiant cooling, and the (d) sensible and (e) latent cooling provided by the M-LDAC systems at different occupant densities

Table 3.7 presents the occupant densities used, number of people, air change rates, and the energy consumed by each system component. In addition, this table shows the percent increase in the energy consumption made by each constituent of the HVAC systems compared to the base case of 5 people/100 m^2.

Table 3.7: Energy use of the 2-fluid and 3-fluid M-LDAC HVAC systems under different occupant densities

Occupant density (# people/100 m^2)	Number of people	ACH	2-fluid M-LDAC hybrid HVAC system				
			Solution cooling (GJ)	Solution heating (GJ)	Radiant system (GJ)	Pumps and fans (GJ)	Total Energy (GJ)
5	25	0.50	2.5 *(0%)*	1.1 *(0%)*	1.12 *(0%)*	0.04 *(0%)*	4.7 *(0%)*
10	51	0.64	3.2 *(28%)*	1.4 *(29%)*	1.16 *(3%)*	0.05 *(30%)*	5.8 *(22%)*
15	76	0.79	3.9 *(57%)*	1.7 *(60%)*	1.20 *(7%)*	0.06 *(61%)*	6.9 *(46%)*
20	102	0.93	4.6 *(85%)*	2.0 *(89%)*	1.24 *(10%)*	0.07 *(89%)*	7.9 *(68%)*
25	127	1.07	5.3 *(113%)*	2.3 *(117%)*	1.28 *(14%)*	0.08 *(118%)*	9.0 *(90%)*

Occupant density (# people/100 m^2)	Number of people	ACH	3-fluid M-LDAC hybrid HVAC system						
			Solution cooling (GJ)	Solution heating (GJ)	Radiant system (GJ)	Pumps and fans (GJ)	Water cooling (GJ)	Water heating (GJ)	Total Energy (GJ)
5	25	0.50	0.06 *(0%)*	0.07 *(0%)*	1.19 *(0%)*	0.04 *(0%)*	0.9 *(0%)*	0.8 *(0%)*	3.1 *(0%)*
10	51	0.64	0.08 *(27%)*	0.09 *(27%)*	1.24 *(5%)*	0.05 *(28%)*	1.2 *(28%)*	1.1 *(28%)*	3.7 *(19%)*
15	76	0.79	0.09 *(56%)*	0.11 *(55%)*	1.30 *(9%)*	0.06 *(58%)*	1.5 *(58%)*	1.3 *(58%)*	4.3 *(39%)*
20	102	0.93	0.11 *(84%)*	0.13 *(81%)*	1.35 *(14%)*	0.07 *(85%)*	1.7 *(86%)*	1.5 *(86%)*	4.9 *(58%)*
25	127	1.07	0.13 *(111%)*	0.15 *(107%)*	1.41 *(18%)*	0.08 *(113%)*	2.0 *(115%)*	1.8 *(114%)*	5.5 *(77%)*

Figure 3.14 presents the total energy consumed and percent change in the energy consumption by component of the HVAC systems under different occupant densities. Figure 3.14(b) shows that the energy used by the M-LDAC systems increases by a larger percentage than the energy used by the radiant cooling systems as the occupant density increased. Furthermore, the energy consumed by the components of the 2-fluid and 3-fluid M-LDAC systems increase by approximately the same percentage across occupant densities which is expected since an increase in the air change rate results in a proportional change in the solution and water flow rates due to constant operating conditions (Cr, Cr*).

(a)

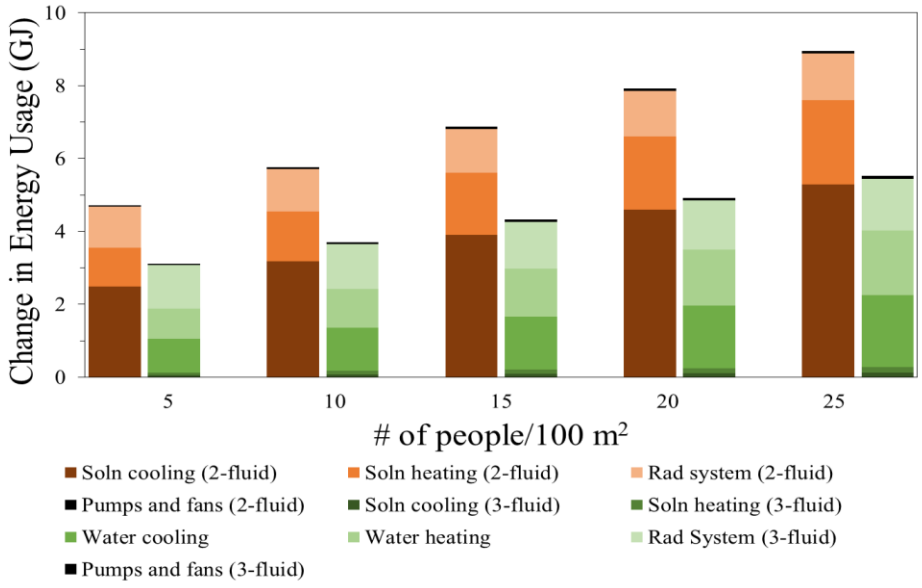

(b)

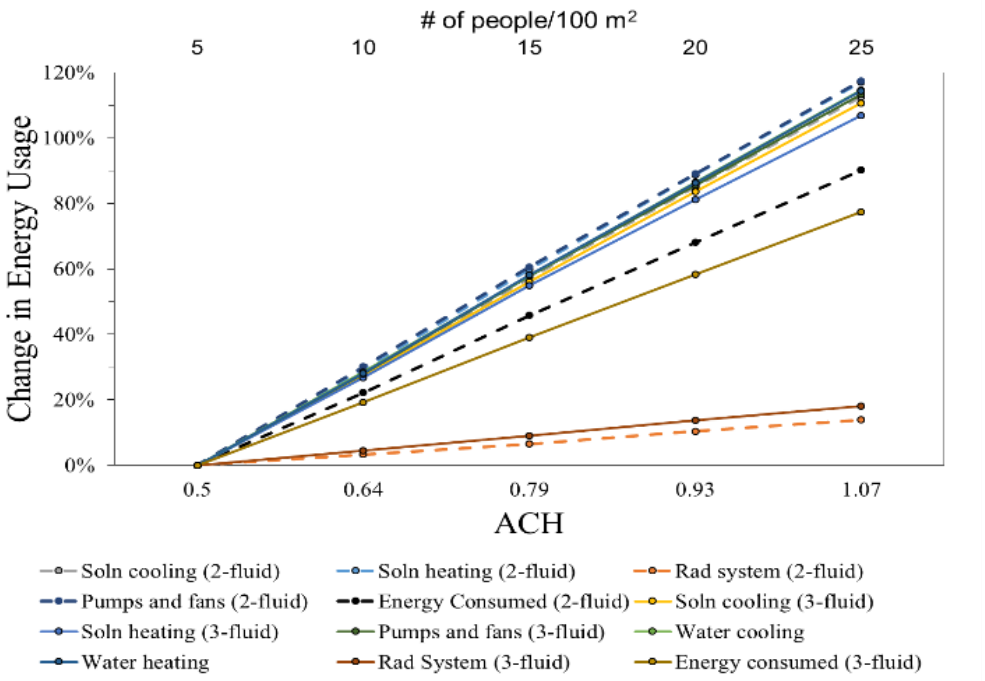

Figure 3.14: Change in energy usage by (a) GJ and (b) percentage for each occupant density

3.7.2.2 Sensitivity study: infiltration

This sensitivity study focuses on the impact the infiltration rate (one of the main sources of latent load) has on the capability of the 2-fluid and 3-fluid M-LDAC HVAC systems to maintain an acceptable thermal environment within the office space. The performance of the HVAC systems

is presented under different building air tightness; newer buildings are tighter than older buildings and experience less infiltration. Therefore, this study will investigate if the building age has influence on the performance of the 2-fluid and 3-fluid systems. Simulations are performed at infiltration rates ranging from 0.2 to 1.0 ACH, where 0.2 ACH signifies a building with a high air tightness while a building with an infiltration rate of 1.0 ACH is considered to have a low air tightness.

Figure 3.15(a) and (b) presents the ambient and indoor operative temperatures during the weekly simulation and hottest day of the week, respectively. The operative temperature is maintained at a temperature of 24°C during occupancy for each infiltration rate and, thereby, demonstrates that the radiant cooling system can account for the additional sensible heat gains introduced by the extra infiltration.

(a)

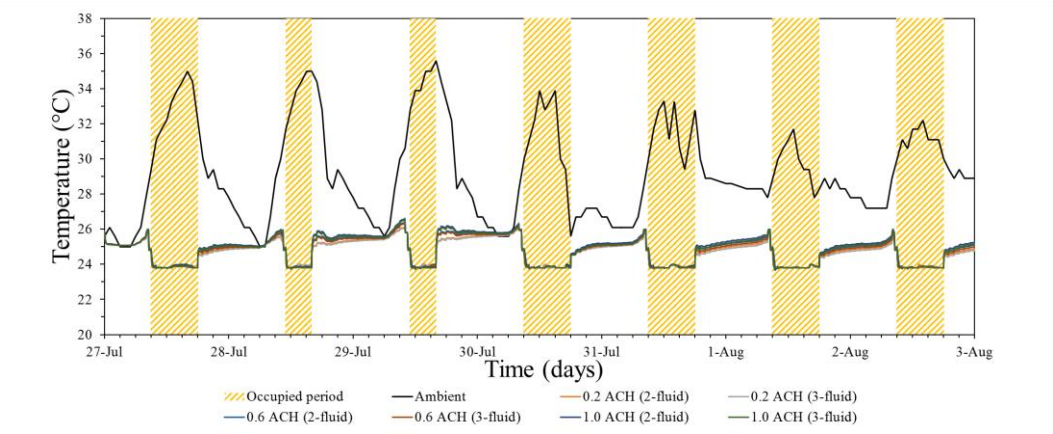

(b)

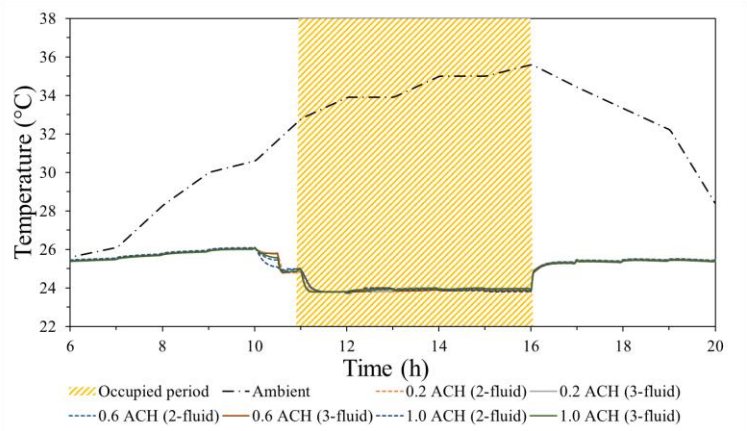

Figure 3.15: The ambient and indoor operative temperatures for the (a) week and (b) hottest day for the 2-fluid and 3-fluid M-LDAC HVAC systems under different infiltration rates.

Figure 3.16(c) and (d) shows the ambient and indoor air humidity ratios for the 2-fluid and 3-fluid M-LDAC systems under different infiltration rates during the week and most humid day of the week. Under the limited operating and design conditions, both M-LDAC systems cannot meet the acceptable indoor air humidity ratio of 12 g_v/kg_{da} at higher infiltration rates.

(a)

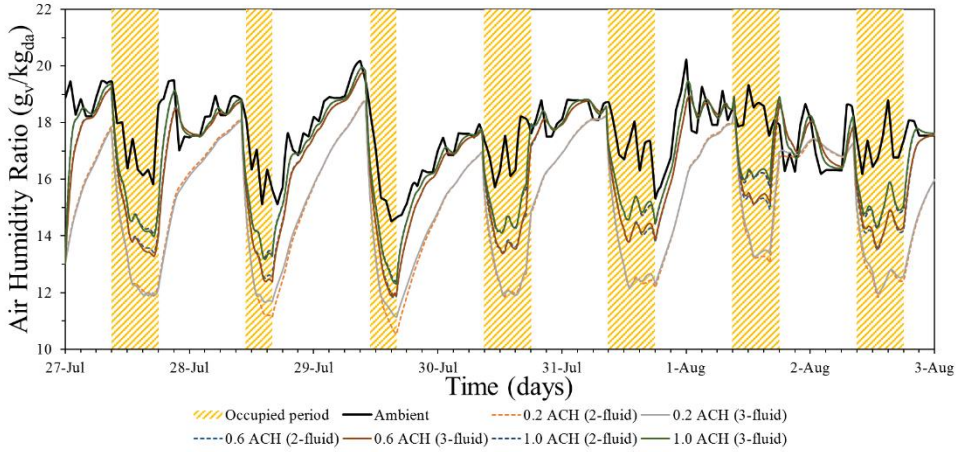

(b)

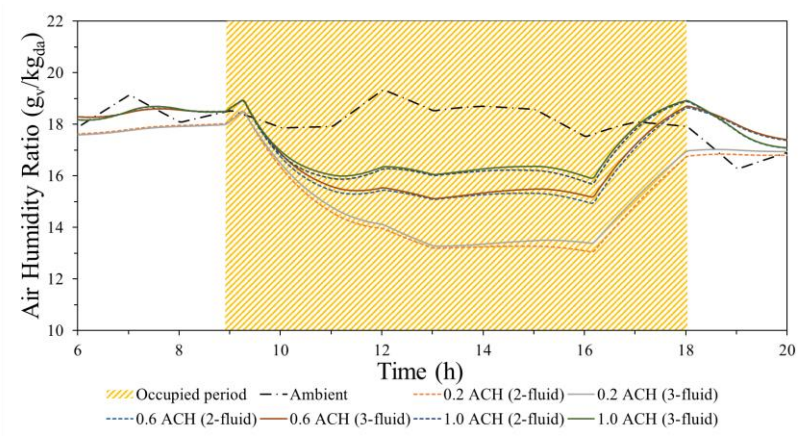

Figure 3.16: The ambient and indoor air humidity ratios for the (a) week and (b) most humid day for the 2-fluid and 3-fluid M-LDAC HVAC systems under different infiltration rates.

Figure 3.17(a) shows the average COP for the 2-fluid and 3-fluid M-LDAC systems under different infiltration rates. The average COPs of the 3-fluid and 2-fluid M-LDAC systems are relatively consistent under the different infiltration rates. The 3-fluid M-LDAC system outperforms the 2-fluid M-LDAC system at all infiltration rates based on energy but not on dehumidification.

In Figure 3.17(b) and (c), the average energy transfer and consumption rates of the 2-fluid and 3-fluid M-LDAC systems are illustrated at each infiltration rate, respectively. At higher infiltrations, the M-LDAC systems fails to provide acceptable indoor humidity conditions and, therefore, run

at the full capacity throughout occupancy; thus, resulting. The M-LDAC systems reaching their maximum energy transfer and consumption rates.

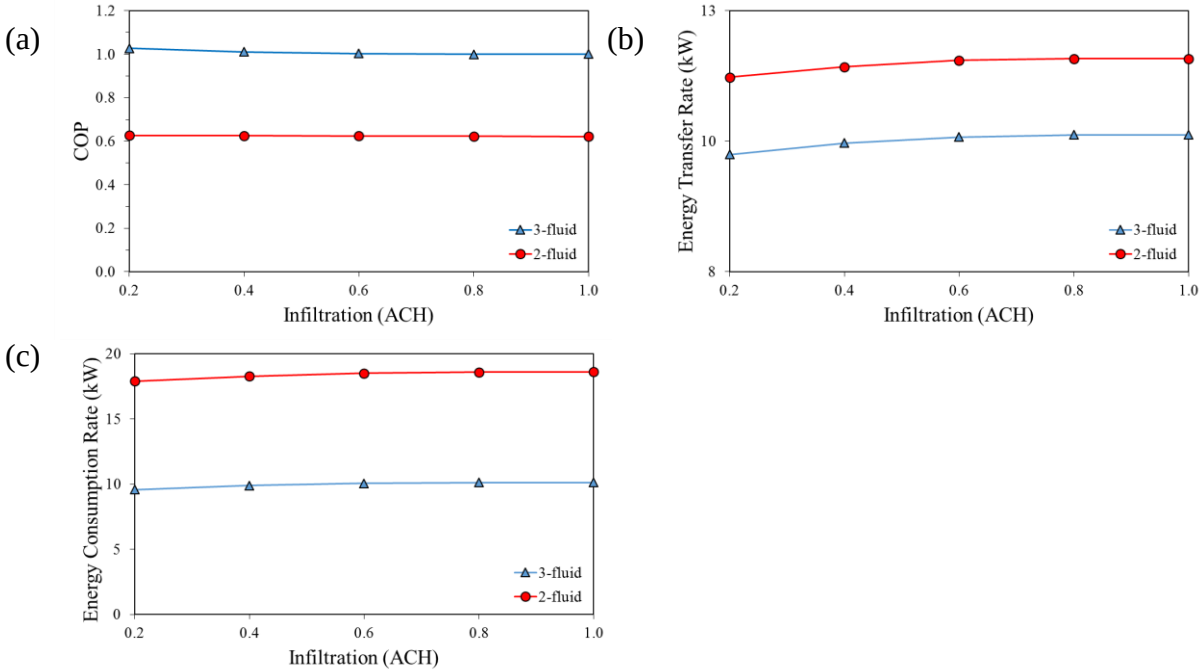

Figure 3.17: The weekly average (a) COPs, (b) energy transfer rates, and (c) energy consumption rates under different infiltration rates.

In a hot-humid climate, an increased infiltration rate to the office space introduces more sensible and latent heat energy and requires more energy by the HVAC systems to account for this increase. The sensible and latent heat energy across the different infiltration rates are shown in Figure 3.18(a) and (b), respectively, where the infiltration sensible gains increase from 0.26 GJ to 1.27 GJ (388%) and the latent energy rises from 159 kJ to 288 kJ (81%). The total sensible and latent load across this range of infiltration rates increases by 27% and 45%, respectively.

Figure 3.18(c), (d), and (e) presents the increase in radiant system cooling and M-LDAC sensible and latent cooling, respectively. For the 2-fluid M-LDAC HVAC system, the radiant cooling increased from 3.23 GJ to 4.17 GJ (29%) whereas, for the 3-fluid M-LDAC HVAC system, the

radiant cooling increased from 3.48 GJ to 4.45 GJ (28%). Furthermore, the latent cooling provided by the 2-fluid M-LDAC system increased from 280 kJ to 394 kJ (41%), whereas, the 3-fluid M-LDAC system increased from 272 kJ to 391 kJ (44%) for latent cooling.

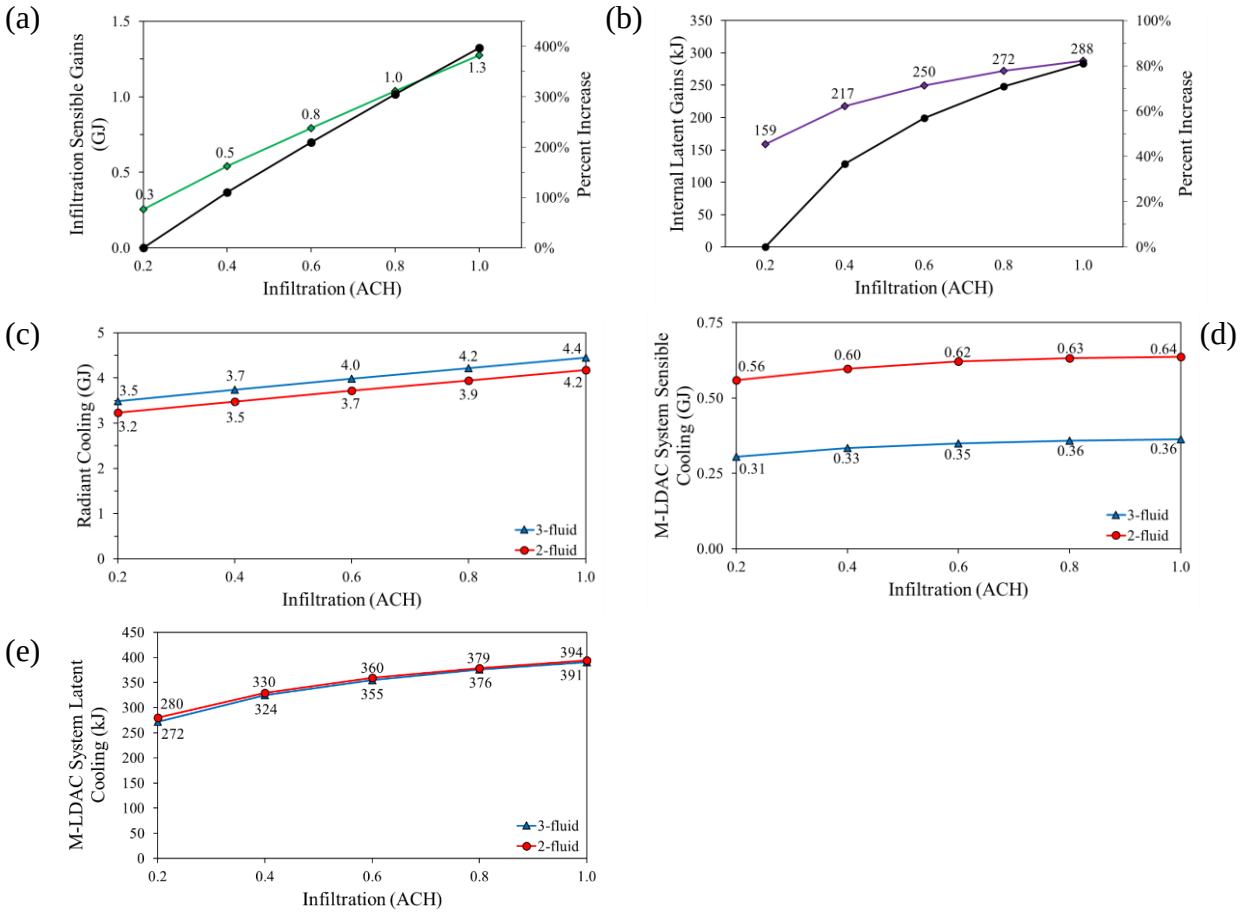

Figure 3.18: The (a) sensible loads, (b) latent loads, (c) radiant cooling, (d) sensible cooling, and (e) latent cooling provided by the M-LDAC systems at different infiltration rates

The energy usage of the 2-fluid and 3-fluid M-LDAC HVAC systems under different infiltration rates is shown in Figure 3.19 in (a) GJ and (b) percentage. The radiant systems experience the largest increase in energy consumption when the infiltration rate is changed from 0.2 to 1.0 ACH as expected since the sensible gains experienced a 400% increase while the latent gains increased

by 80%. The energy consumed by the M-LDAC systems plateau after 0.8 ACH and do not provide much more dehumidifying at 1.0 ACH.

(a)

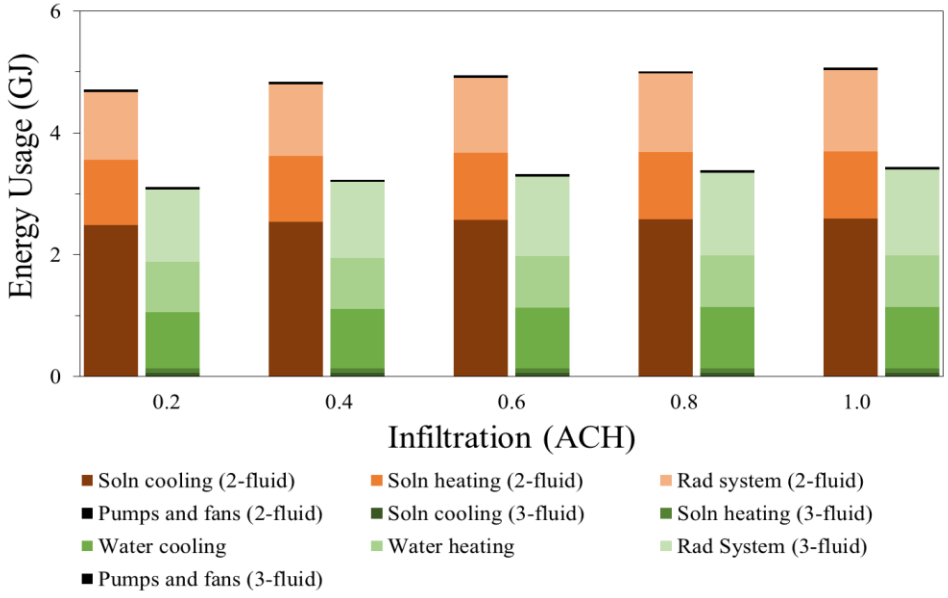

(b)

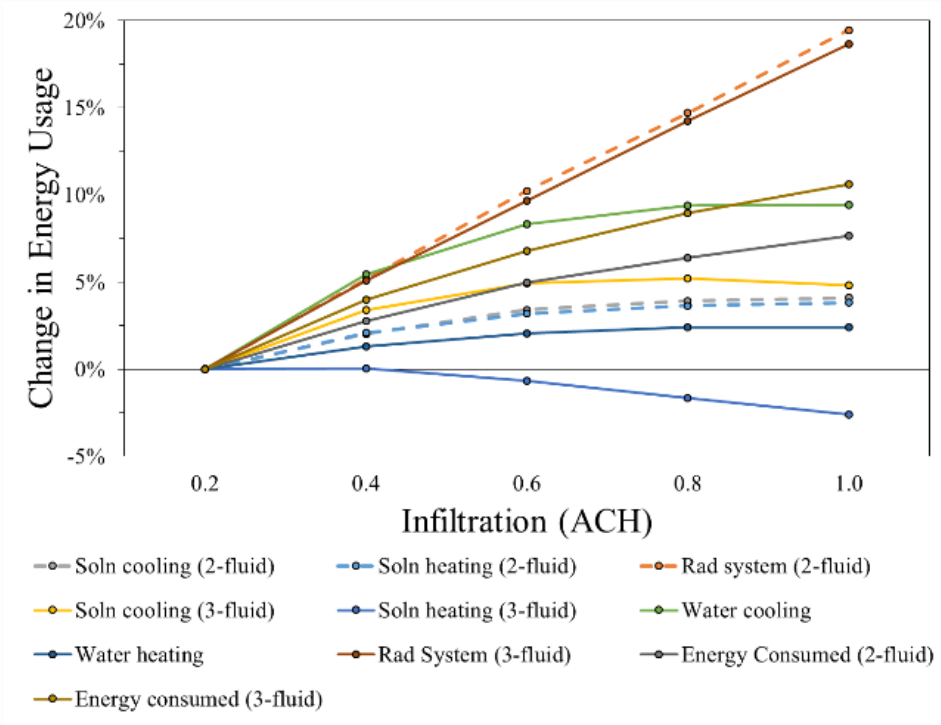

Figure 3.19: Change in energy usage by (a) GJ and (b) percentage for each infiltration rate

Table 3.8 summarizes the energy consumption of the individual parts of the HVAC systems at these infiltration rates as well as their percent increase from the base case scenario.

Table 3.8. Impact of infiltration rates on the energy use of the 2-fluid and 3-fluid M-LDAC HVAC systems

Infiltration Rate (ACH)	2-fluid M-LDAC hybrid HVAC system						
	Solution cooling (GJ)	Solution heating (GJ)	Radiant system (GJ)	Pumps and fans (GJ)	Total Energy (GJ)		
0.2	2.49 *(0%)*	1.07 *(0%)*	1.12 *(0%)*	0.04 *(0%)*	4.71 *(0%)*		
0.4	2.54 *(2%)*	1.09 *(2%)*	1.18 *(5%)*	0.04 *(0%)*	4.84 *(3%)*		
0.6	2.57 *(3%)*	1.10 *(3%)*	1.23 *(10%)*	0.04 *(0%)*	4.94 *(5%)*		
0.8	2.58 *(4%)*	1.10 *(4%)*	1.28 *(15%)*	0.04 *(0%)*	5.01 *(6%)*		
1	2.59 *(4%)*	1.11 *(4%)*	1.34 *(19%)*	0.04 *(0%)*	5.07 *(8%)*		
Infiltration Rate (ACH)	3-fluid M-LDAC hybrid HVAC system						
	Solution cooling (GJ)	Solution heating (GJ)	Radiant system (GJ)	Pumps and fans (GJ)	Water cooling (GJ)	Water heating (GJ)	Total Energy (GJ)
0.2	0.06 *(0%)*	0.07 *(0%)*	1.19 *(0%)*	0.04 *(0%)*	1.92 *(0%)*	3.11 *(0%)*	6.39 *(0%)*
0.4	0.06 *(3%)*	0.07 *(0%)*	1.25 *(5%)*	0.04 *(0%)*	1.98 *(3%)*	3.23 *(4%)*	6.64 *(4%)*
0.6	0.06 *(5%)*	0.07 *(-1%)*	1.31 *(10%)*	0.04 *(0%)*	2.02 *(5%)*	3.32 *(7%)*	6.82 *(7%)*
0.8	0.06 *(5%)*	0.07 *(-2%)*	1.36 *(14%)*	0.04 *(0%)*	2.03 *(6%)*	3.39 *(9%)*	6.95 *(9%)*
1	0.06 *(-5%)*	0.07 *(-3%)*	1.41 *(19%)*	0.04 *(0%)*	2.03 *(6%)*	3.44 *(11%)*	7.05 *(10%)*

3.8 Conclusion

This study simulated the performance of two HVAC systems, composed of either a 2-fluid or 3-fluid membrane liquid desiccant air-conditioning (M-LDAC) system and a radiant cooling panel system. The HVAC systems were investigated under a hot-humid climate and evaluated based on their ability to provide an acceptable indoor thermal environment within an office space. In addition, the performance of the 2-fluid and 3-fluid systems were studied under different occupant densities and infiltration rates to determine how these systems perform under different latent and sensible loads. The radiant system was successful at meeting the sensible loads under all conditions whereas the M-LDAC systems could not meet the higher latent loads.

Results show that under the range of operating and design conditions studied in this chapter, the 3-fluid M-LDAC system consumed less energy than the 2-fluid M-LDAC system to meet the latent loads. In the weekly simulation, the 2-fluid M-LDAC system consumes 50% more energy than the 3-fluid M-LDAC system to meet the latent load. The average COP of the 3-fluid M-LDAC system under the base conditions was 1.03 while the average COP of the 2-fluid M-LDAC system was 0.63. Both systems were able to perform more latent cooling when occupant density increased. However, adequate indoor air humidity was still unattainable. As the infiltration rates increased, the systems reached a maximum amount of latent cooling and the thermal comfort decreased. The applicability of the 3-fluid LAMEE model is very limited for building modeling as it cannot accommodate for a large range of latent loads due to the model limitations.

CHAPTER 4

SUMMARY, CONCLUSIONS, AND RECOMMENDATIONS

4.1 Summary

The main purpose of this thesis was to simulate the performance of a 3-fluid M-LDAC system and compare it with the performance of a 2-fluid M-LDAC system. Prior to this thesis, research on the 3-fluid LAMEE had been limited to experimental measurements under limited test conditions. In order to simulate the 3-fluid M-LDAC system, empirical correlations were developed in this thesis for the 3-fluid LAMEE as a dehumidifier and regenerator based on the previously collected experimental data. The models were verified with experimental data and the extrapolation ranges of the models were determined. Some of the model limitations include: the NTU is limited to 1.8 for the dehumidifier and 2 for the regenerator, Cr^* is limited to 1.8 for the dehumidifier and 2.0 for the regenerator, Cr must be between of 0.01 and 0.42 for the dehumidifier and between 0.04 and 0.63 for the regenerator, the inlet solution temperature of the dehumidifier (24.5°C) and regenerator (42°C) are fixed and the minimum inlet water temperature of the dehumidifier must be above 1°C but depends on the inlet air temperature.

Models of the 3-fluid M-LDAC system (developed in this thesis) and a 2-fluid M-LDAC system (from the literature) were incorporated into the Transient System Simulation (TRNSYS) software and their system performance was evaluated and compared. The 3-fluid M-LDAC system used less energy to dehumidify the air and outperformed the 2-fluid M-LDAC system under most

design conditions with different latent loads. This indicates that the 3-fluid M-LDAC system may be more appropriate for dehumidification applications.

The two M-LDAC systems were then paired with a radiant ceiling cooling panel system and simulated in a hot-humid climate (Miami, Florida). The simulations investigated whether the HVAC systems could provide an adequate thermal environment in an office building. The radiant cooling system covered the sensible load and the M-LDAC systems covered the latent load. The simulations were performed over the warmest week of the year to comply with the model limitations. In addition, two parametric studies (occupant density and infiltration rate) were conducted on the ability of the HVAC system to provide thermal comfort under different latent (and sensible) loads. It was determined that both systems could achieve desirable thermal comfort during occupied hours under the typical occupant densities and infiltration rates; however, the 3-fluid M-LDAC system consumed less energy to meet the latent load than its 2-fluid equivalent. It was shown that both M-LDAC systems failed to meet the latent loads at higher occupant densities and infiltration rates. This inadequacy is more so due to the model limitations opposed to the systems themselves since both systems were constrained by the limitations set by the 3-fluid LAMEE model.

4.2 Conclusions

The 3-fluid LAMEE dehumidifier model is within 8% of the experimental data and the 3-fluid LAMEE regenerator model is within 7% of the experimental data. This thesis concluded that the 3-fluid M-LDAC system is better at removing latent loads than the 2-fluid M-LDAC system. The 2-fluid and 3-fluid M-LDAC systems were simulated under multiple design conditions with different latent loads and the 3-fluid M-LDAC system outperformed the 2-fluid M-LDAC system

under most latent loads conditions. However, the 2-fluid M-LDAC system was more energy efficient at meeting the least demanding latent load. The COP of the 3-fluid M-LDAC system ranged from 0.50 to 1.11 and the COP of the 2-fluid M-LDAC system ranged from 0.45 to 0.68.

The two M-LDAC systems were simulated with an office building and, while both system could provide desirable air humidity under the base conditions, the 3-fluid M-LDAC system was more energy efficient than the 2-fluid M-LDAC system. During the weekly simulation, the 2-fluid M-LDAC system consumed 50% more energy than the 3-fluid M-LDAC system to meet the latent load. The 3-fluid LAMEE is also less susceptible to crystallization fouling as the desiccant solution concentration required to meet the latent loads was 32.5% whereas the desiccant solution concentration in the 2-fluid M-LDAC system was 45%. The sensitivity studies showed that this model is has limited applicability for building modeling as the 3-fluid M-LDAC system could not meet the additional latent loads because the 3-fluid model cannot accommodate for a broad range of operating and design conditions to meet the latent loads due to the model limitations.

4.3 Recommendations for future work

Future work should be done to expand the 3-fluid LAMEE experimental dataset. With a larger dataset, a model that can be used over a broader range of operating conditions and climates can be developed since this model is limited to specific operating parameters and hot-humid conditions. Also, the dataset can be used to verify analytical and CFD models. Empirical correlations can be developed from this new experimental data and substituted for the current models in the system presented in this research. Furthermore, the new dataset can be used to show the behavior of the 3-fluid LAMEE as a dehumidifier and regenerator. To achieve this, experiments should be performed at various inlet air, water, and solution temperatures, air humidity ratios, and operating

and design parameters. Table 4.1 outlines suggested ranges for each of the important control variables in the experiments that can be conducted. The reference values for the inlet air temperature and humidity ratio of the dehumidifier comply with the summer conditions specified in AHRI Standard 1060 (AHRI 2005). The inputs cover a wide spectrum of temperatures, air humidity ratios, and flow rates to provide data for a more universal model of the 3-fluid LAMEE at different operating and design conditions.

Table 4.1: Proposed operating and design conditions for an experimental study to investigate the 3-fluid LAMEE as a dehumidifier and regenerator

	Dehumidifier			Regenerator		
	Reference Value	Range	Increments	Reference Value	Range	Increments
$T_{air,in}$ (°C)	35	24-40	8	24	22-30	4
$W_{air,in}$ (g_v/kg_{da})	16.8	10-22	6	12	8-12	2
$T_{sol,in}$ (°C)	20	10-25	5	40	35-50	5
$T_{w,in}$ (°C)	15	1-25	5	45	35-65	5
Cr	0.1	0.01-0.3	0.1	0.1	0.01-0.3	0.1
Cr*	3	1-7	2	3	1-7	2
NTU	3	1-7	2	3	1-7	2
Concentration	35	30-40	5	35	30-40	5

For the dehumidifier, the experiments should consider a range of inlet air temperatures where they are above or equal to the set point air temperature within a building (usually around 24°C for cooling). The air humidity ratio should be examined at a range from close to the desirable indoor air humidity to very humid conditions. The inlet solution temperature should be set below the air temperature and investigated at several values to evaluate the impact of solution temperature on sensible and latent cooling. Additionally, the inlet water temperature should be tested at a variety of temperatures below the solution temperature as well as at least one between the solution and air temperature. It would be ideal to find a combination of air, solution and water temperatures that

optimizes sensible and latent effectiveness but that may require analytical modeling. Moreover, experiments should be performed at a variety of desiccant concentrations to observe the effects of desiccant concentration on air dehumidifying and mass flow rates should be adjusted to determine the most practical Cr and Cr^* combinations, that is, when there is very little increase in the sensible and latent effectiveness when Cr^* is increased and Cr is decreased.

The regenerator should be examined at multiple inlet conditions to evaluate their effects on performance and effectiveness. The inlet air temperature and humidity ratio range should cover the temperature range of exhaust air. The inlet solution temperature should be warmer than the air temperature and the inlet water temperature should be higher than that of the solution. Furthermore, the effects of concentration, Cr, Cr^*, and NTU have on the 3-fluid LAMEE performance as a regenerator should also be examined.

REFERENCES

Abdel-Salam M.R.H., 2016. Design and performance testing of a novel 3-fluid liquid-to-air membrane energy exchanger. PhD thesis. Department of Mechanical Engineering, University of Saskatchewan, Saskatoon.

Abdel-Salam M.R.H., Besant R.W., Simonson C.J., 2015. Sensitivity of the performance of a flat-plate liquid-to-air membrane energy exchanger (LAMEE) to the air and solution channel widths and flow maldistribution. *International Journal of Heat and Mass Transfer,* **84**,1082-1100.

Abdel-Salam M.R.H., Besant R.W., Simonson C.J., 2016a. Design and testing of a novel 3-fluid liquid-to-air membrane energy exchanger (3-fluid LAMEE). *International Journal of Heat and Mass Transfer,* **92**, 312-329.

Abdel-Salam M.R.H., Besant R.W., and Simonson C.J., 2016b. Performance testing of a novel 3-fluid liquid-to-air membrane energy exchanger (3-fluid LAMEE) under desiccant solution regeneration operating conditions. *International Journal of Heat and Mass Transfer,* **95**, 773-786.

Abdel-Salam, M.R.H., Besant R.W., Simonson C.J., 2017. Performance definitions for three-fluid heat and moisture exchangers. *ASME Journal of Heat Transfer,* **139(2)**, 022003.1-022003-8.

Abdel-Salam M.R.H., Fauchoux M., Ge G., Besant R.W., Simonson C.J., 2014. Expected energy and economic benefits, and environmental impacts for liquid-to-air membrane energy exchangers (LAMEEs) in HVAC systems: a review. *Applied Energy,* **127**, 202-218.

Abdel-Salam M.R.H., Ge G., Besant R.W., Simonson C.J., 2016. Experimental study on effects of phase-change energy and operating parameters on performances of two-fluid and three-fluid liquid-to-air membrane energy exchangers. *ASHRAE Transactions,* **122**, 134-145.

Abdel-Salam M.R.H., Ge G., Fauchoux M., Besant R.W., Simonson C.J., 2014. State-of-the-art in liquid-to-air membrane energy exchangers (LAMEEs): A comprehensive review. *Renewable and Sustainable Energy Reviews,* **39**, 700-728.

Abdel-Salam A.H., Ge G., Simonson C.J., 2013. Performance analysis of a membrane liquid desiccant air-conditioning system. *Energy and Buildings*, **62**, 559-569.

Abdel-Salam A.H., Ge G., Simonson C.J., 2014. Thermo-economic performance of a solar membrane liquid desiccant air conditioning system. *Solar Energy*, **102**, 56-73.

Abdel-Salam A.H., Simonson C.J., 2014. Annual evaluation of energy, environment and economic performances of a membrane liquid desiccant air conditioning system with/without ERV. *Applied Energy,* **116**, 134-148.

Afshin, M., 2010. Selection of the Liquid Desiccant in a Run-Around Membrane Energy Exchanger. MSc. thesis. Department of Mechanical Engineering, University of Saskatchewan, Saskatoon.

Afshin, M., Simonson C.J., Besant R.W., 2010. Crystallization limits of LiCl-Water and MgCl2-Water salt solutions as operating liquid desiccant in the RAMEE system. *ASHRAE Transactions,* **116**, 494-506.

AHRI. 2005. AHRI Standard 1060, Standard for Rating Air-to-Air Exchangers for Energy Recovery Ventilation Equipment. Arlington, VA.

ANSI/ASHRAE Standard 84-2008. 2008. Method of test for air-to-air heat/energy exchangers. *American Society of Heating, Refrigerating, and Air-Conditioning Engineers*, Atlanta.

ASHRAE, 2017. Handbook - Fundamentals (SI). *American Society of Heating, Refrigerating and Air-Conditioning Engineers, Inc.,* Atlanta.

ASHRAE. 2004. 2004 ASHRAE Handbook: Heating, Ventilating, and Air-Conditioning Systems and Equipment. *American Society of Heating, Refrigerating and Air-Conditioning Engineeris, Inc.,* Atlanta.

ASHRAE. 2008. ASHRAE Handbook–HVAC systems and equipment. *American Society of Heating, Refrigerating and Air-Conditioning Engineers, Inc.,* Atlanta.

ASHRAE. 2013. ANSI/ASHRAE Standard 55-2013, Thermal Environmental Conditions for Human Occupancy. *American Society of Heating, Refrigerating and Air-Conditioning Engineers, Inc.*, Atlanta.

ASHRAE. 2013. ANSI/ASHRAE Standard 90.1-2013, Energy Standard for Buildings Except Low-Rise Residential Buildings. *ASHRAE*, Atlanta.

ASHRAE. 2016. ANSI/ASHRAE Standard 62.1-2016, Ventilation for Acceptable Indoor Air Quality. *American Society of Heating, Refrigerating and Air-Conditioning Engineers, Inc.*, Atlanta.

Bergero S., Chiari A., 2001. Experimental and theoretical analysis of air humidification/dehumidification processes using hydrophobic capillary contactors. *Applied Thermal Engineering*, **21(11)**, 1119-1135.

Bergero S., Chiari A., 2010. Performance analysis of a liquid desiccant and membrane contactor hybrid air-conditioning system. *Energy and Buildings*, **42**, 1976-1986.

Bergero S., Chiari A., 2011. On the performances of a hubrid air-conditioning system in different climatic conditions. *Energy*, **36**, 5261-5273.

Beriault D.A., 2011. Run-Around Membrane Energy Exchanger Prototype-4 Design and Laboratory Testing. MSc. Thesis, Department of Mechanical Engineering, University of Saskatchewan. Saskatoon.

Central Air Conditioning Buying Guide: The Coolness Quotient. 2017. Consumer Reports. Retrieved August 5, 2017 (https://www.consumerreports.org/cro/central-air-conditioning/buying-guide).

Chaudhari S.K., Patil K.R., 2002. Thermodynamic Properties of Aqueous Solutions of Lithium Chloride. *Physics and Chemistry of Liquids: An International Journal*, **40(3)**, 317-325.

Chiari A., 2000. Air humidification with membrane contactors: experimental and theoretical results. *International Journal of Ambient Energy*, **21(4)**,187-195.

Chin W.M., Raghavan V.R., 2011. On the adverse influence of higher statistical moments of flow maldistribution on the performance of a heat exchanger. *International Journal of Thermal Sciences*, **50(4)**, 581-591.

Conde-Petit M.R., 2009. Aqueous solutions of lithium and calcium chlorides: Property formulations for use in air conditioning equipment design. M. Conde Engineering, Zurich.

Deru M., Field K., Studer D., Benne K., Griffith B., Torcellini P., Liu B., Halverson M., Winiarski D., Rosenberg M., Yazdanian M., Huang J., Crawley D., 2011. U.S. Department of Energy Commercial Reference Building Models of the National Building Stock. *National Renewable Energy Laboratory*.

efunda. 2017. Thermal Conductivity: Titanium. Retrieved March 26, 2017 (www.efunda.com/materials/elements/TC_Table.cfm?Element_ID=Ti).

El-Dessouky H., Ettouney H., Al-Zeefari A., 2004. Performance analysis of two-stage evaporative coolers. *Chemical Engineering Journal*, **102(3)**, 255-266.

Energy Saver. 2013. Furnaces and Boilers. U.S. Department of Energy. Retrieved August 10, 2017 (https://energy.gov/energysaver/furnaces-and-boilers).

Energy Saver. 2014. Home Cooling. U.S. Department of Energy. Retrieved August 10, 2017 (https://energy.gov/articles/energy-saver-101-infographic-home-cooling).

Ge G., Abdel-Salam A.H., Simonson C.J., 2016. Heat and mass transfer performance comparison between a direct-contact liquid desiccant packed bed and a liquid-to-air membrane energy exchanger for air dehumidification. *Science and Technology for the Built Environment*, **00**, 1-14.

Ge G., Moghaddam D.G., Namvar R., Simonson C.J., Besant R.W., 2013. Analytical model based performance evaluation, sizing and coupling flow optimization of liquid desiccant run-around membrane energy exchanger systems. *Energy and Buildings*, **62**, 248-257.

Ge G., Xiao F., Niu X.F., 2011. Control strategies for a liquid desiccant air-conditioning system. *Energy and Buildings*, **43**, 1499-1507.

Gowri K., Winiarski D., Jarnagin R., 2012. Infiltration Modeling Guidelines for Commercial Building Energy Analysis. Oak Ridge, TN.

Greenspan L., 1977. Equilibrium Relative Humidity Saturated Salt Solutions. *Journal of Research of the National Bureau of Standards - A. Physics and Chemistry,* **1(81A)**, 89-96.

Hemingson, H.B., Simonson, C.J., Besant, R.W., 2011. Steady-state performance of a run-around membrane energy exchanger (RAMEE) for a range of outdoor air conditions. *International Journal of Heat and Mass Transfer,* **54**, 1814-1824.

Hilliard, T., 2012. Stabilization of asymmetric bilateral teleoperation systems with time-varying delays. MASc Thesis, Department of Mechanical Engineering, Dalhousie University. Nova Scotia.

Huang, S.M., Zhang L.Z., 2013. Researches and trends in membrane-based liquid desiccant air dehumidification. *Renewable and Sustainable Energy Reviews,* **28**, 425-440.

International Energy Agency. 2016. Key world energy statistics. Paris.

Isetti C., Magrini A., Nannei E., 1996. The application of vapour-permeable synthetic membranes to the climatic stablization of museum showcases. *Studies in Conservation,* **41(4)**, 229-240.

Isetti C., Nannei E., Magrini A., 1997. On the application of membrane air-liquid contact for dehumidification. *Energy and Buildings,* **25(3)**, 185-193.

Khayet M., 2011. Membranes and theoretical modeling of membrane distillation: A review. *Advances in Colloid and Interface Science,* **164(1-2)**, 56-88.

Kolokotsa D., Rovas D., Kosmatopoulos E., Kalaitzakis K., 2011. A roadmap towards intelligent net zero- and positive-energy buildings. *Solar Energy,* **85**, 3067-3084.

Lalota S., Florentb P., Langc S.K., Berglesc A.E., 1999. Flow maldistribution in heat exchangers. *Applied Thermal Engineering,* **19(8)**, 847-863.

Larson M.D., 2006. The Performance of Membranes in a Newly Proposed Run-Around Heat and Moisture Exchanger. MSc Thesis, Department of Mechanical Engineering, University of Saskatchewan. Saskatoon.

Larson M.D., Simonson C.J., Besant R.W., Gibson P.W., 2007. The elastic and moisture transfer properties of polyethylene and polypropylene membranes for use in liquid-to-air energy exchangers. *Journal of Membrane Science*, **302(1-2)**, 136-149.

Linke W., Seidell A., 1965. Solubilities of Inorganic and Metal Organic Compounds. American Chemical Society. Washington.

Longo G.A., Gasparella A., 2005. Experimental and theoretical analysis of heat and mass transfer in a packed column dehumidifier/regenerator with liquid desiccant. *International Journal of Heat and Mass Transfer*, **48**, 5240-5254.

Lowenstein A., 2008. Review of Liquid Desiccant Technology for HVAC Applications. *HVAC&R Rsearch*, **14(6)**, 819-839.

Mahmud K., 2009. Design and performance testing of counter-cross-flow run-around membrane energy exchanger system. MSc. Thesis, Department of Mechanical Engineering, University of Saskatchewan. Saskatoon.

Mei L., Dai Y.J., 2008. A technical review on use of liquid-desiccant dehumidification for air-conditioning application. *Renewable and Sustainable Energy Reviews*, **12**, 662-689.

Moghaddam D.G., LePoudre P., Besant R.W., Simonson C.J., 2013b. Evaluating the steady-state performance of a small-scale single-panel liquid-to-air membrane energy exchanger (LAMEE) under summer AHRI test conditions. *In: Proceedings of the 11th REHVA world congress & 8th international conference on IAQVEC* Prague congress center, Prague, Czech Republic:16-19.

Moghaddam D.G., LePoudre P, Ge G., Besant R.W., Simonson C.J., 2013a. Small-scale single-panel liquid-to-air membrane energy exchanger (LAMEE) test facility development, commissioning, and evaluating the steady-state performance. *Energy and Buildings*, **66**, 424-436.

Moghaddam D.G., Mahmood G., Ge G., Besant R.W., Simonson C.J., 2013c. Steady-state performance of a prototype (200cfm) liquid-to-air membrane energy exchanger (LAMEE) under summer and winter test conditions. *In: Procedings of the ASME 2013 summer heat transfer conference, Minneapolis, USA; 2013*.

Mohammad A.T., Mat S.B., Sulaiman M.Y., Sopian K., Al-abidi A.A., 2013. Survey of hybrid liquid desiccant air conditioning systems. *Renewable and Sustainable Energy Reviews*, **20**, 186-200.

Mueller A.C., 1987. Effects of some types of maldistribution on the performance of heat exchanger. *Heat Transfer Engineering*, **8(2)**, 75-86.

Namvar R., Ge G., Simonson C.J., Besant R.W., 2013. Transient heat and moisture transfer characteristics of a liquid-to-air membrane energy exchanger (LAMEE) model verifications and extrapolation. *International Journal of Heat and Mass Transfer*, **66**, 757-771.

Namvar R., Pyra D., Ge G., Simonson C.J., Besant R.W., 2012. Transient characteristics of aliquid-to-air membrane energy exchanger (LAMEE) experimental data with correlations. *International Journal of Heat and Mass Transfer*, **55(23-24)**, 6682-6694.

Natural Resources Canada. 2011. Energy Effiiciency Trends in Canada (1990 to 2009). Ottawa.

Natural Resources Canada. 2016. Energy Efficiency Trends in Canada. Ottawa.

Navigant Research. 2015. Energy-Efficient HVAC Systems for Commercial Buildings. *Navigant Consulting Inc.*

Olufade A.O., Simonson C.J., 2017. Detection of crystallization fouling in a liquid-to-air membrane energy exchanger. *Experimental Thermal and Fluid Science*, in press. doi:10.1016/j.expthermflusci.2017.10.017, 2017.

Pérez-Lombard L., Ortiz J., Pout C., 2008. A review on buildings energy consumption information. *Energy and Buildings*, **40**, 394-398.

Rasouli M., 2010. Building energy simulation of a run-around membrane energy exchanger (RAMEE). MSc. Thesis, Department of Mechanical Engineering, University of Saskatchewan. Saskatoon.

Roth K.W., Westphalen D., Dieckmann J., Hamilton S., Goetzler W., 2002. Energy Consumption Characteristics of Commerical Building HVAC Systems Volume III: Energy Savings Potential. Cambridge, MA.

Simonson C.J., Besant R.W., 1999. Energy wheel effectiveness: Part I - development of dimensionless groups. *International Journal of Heat and Mass Transfer*, **42(12)**, 2161-2170.

Spengler J.D., Sexton K., 1983. Indoor air pollution: a public health perspective. *Science*, **221(4605)**, 9-17.

Stephen H., Stephen T., 1963. *Solubilities of Inorganic and Organic Compounds: pt. 1-3. Ternary and multicomponent systems of inorganic substance.* 1st ed. Soviet Union: Pergamon Press.

Stetzenbach L.D., Amman H., Johanning E., King G., Shaughnessy R.J., 2004. Microorganisms, Mold, and Indoor Air Quality. Washington, DC.

Thulukkanam K., 2000. Heat Exchanger Design Handbook. Boca Raton, Florida: CRC Press.

TRNSYS 17, 2017. Transient System Simulation software. University of Wisconsin-Madison. Madison.

U.S. Energy Information Administration. 2011. Air Conditioning in U.S. Homes, by Housing Unit Type, 2009. Washington.

U.S. Energy Information Administration. 2013. Fuel consumption Totals and averages, U.S. homes (2009). Washington.

U.S. Energy Information Administration. 2016. International Energy Outlook. Washington.

Vaisala, 2010. Humidity Conversion Formulas: Calculation formulas for humidity. Vaisala, Helsinki, Finland.

Vali A., 2009. Modeling a run-around heat and moisture exchanger using two counter cross flow exchangers. MSc. Thesis, Department of Mechanical Engineering, University of Saskatchewan. Saskatoon.

Vali A., Simonson C.J., Besant R.W., Mahmood G., 2009. Numerical model and effectiveness correlations for a run-around heat recovery system with combined counter and cross flow exchangers. *International Journal of Heat and Mass Transfer*, **52(25-26)**, 5827-5840.

Vestrelli F., 2006. Study on Membrane Contactors: Performances Analysis, System Simulations and Fields of Application: Tesi Di Dottorato. Genoa, Italy: University of Genoa.

Wickramasinghe S.R., Semmens M.J., Cussler E.L., 1991. Better hollow fiber contactors. *Journal of Membrane Science,* **62(3)**, 371-388.

Wilcox S., Marion W., 2008. User's Manual for TMY3 Data Sets, NREL/TP-581-43156. National Renewable Energy Laboratory. Colorado.

Wilkins C.K., Hosni M.H., 2011. Plug Load Design Factors. *Ashrae Journal*, **53(5)**, 30-34.

Wyon D.P., 2004. The effects of indoor air quality on performance and productivity. *Indoor Air*, **14**, 92-101.

Zhang L.Z., 2010. An analytical solution for heat mass transfer in a hollow fiber membrane based air-to-air heat mass exchanger. *Journal of Membrane Science*, **360(1-2)**, 217-225.

Zhang L.Z., 2011. An Analytical Solution to Heat and Mass Transfer in Hollow Fiber Membrane Contactors for Liquid Desiccant Air Dehumidification. *Journal of Heat Transfer*, **133(9)**, 0921001-0921008.

Zhang L.Z., Huang S.M., 2011. Coupled heat and mass transfer in a counter flow hollow fiber membrane module for air humidification. *International Journal of Heat and Mass Transfer*, **54(5-6)**, 1055-1063.

Zhang L.Z., Huang S.M., Pei L.X., 2012. Conjugate heat and mass transfer in a cross-flow hollow fiber membrane contactor for liquid desiccant air dehumidification. *International Journal of Heat and Mass Transfer*, **55(25-26)**, 8061-8072.

Zhang L.Z., Zhu D.S., Deng X.H., Hua B., 2005. Thermodynamic modeling of a novel air dehumidification system. *Energy and Buildings*, **37**, 279-286.

APPENDIX A

LITHIUM CHLORIDE SOLUTION PROPERTIES

This appendix presents the methods used to calculate LiCl desiccant solution properties.

Enthalpy

Chaudhari and Patil (Chaudhari and Patil 2002) developed a method to calculate the enthalpy of aqueous lithium chloride solution using concentration and temperature. Enthalpy is determined using Equations (A.1) through (A.4).

$$h = A + B \cdot T + C \cdot T^2 \tag{A.1}$$

$$A = -66.2324 + 11.2711 \cdot X - 0.79853 \cdot X^2 + (2.1534 \cdot 10^{-2})X^3 - (1.66352 \cdot 10^{-4})X^4 \tag{A.2}$$

$$B = 4.5751 - 0.146924 \cdot X + (6.307226 \cdot 10^{-3})X^2 - (1.38054 \cdot 10^{-4})X^3 + (1.0669 \cdot 10^{-6})X^4 \tag{A.3}$$

$$C = (-8.09689 \cdot 10^{-4}) + (2.18145 \cdot 10^{-4})X - (1.36194 \cdot 10^{-5})X^2 + (3.20998 \cdot 10^{-7})X^3 - (2.64266 \cdot 10^{-9})X^4 \tag{A.4}$$

where, h is enthalpy (kJ/kg), T is temperature (°C), and X is concentration (%).

Vapor Pressure

Conde-Petit (Conde-Petit 2009) developed a general vapor pressure energy using the mass fraction of the salt in the solution and temperature. Equations (A.5) through (A.12) are used to calculate the vapor pressure of a LiCl desiccant solution.

$$p_{v,s} = p_{ws} \cdot \pi \tag{A.5}$$

$$\pi = \frac{p_{sol}(\xi, T)}{p_{H_2O}(T)} = \pi_{25} \cdot f(\xi, T) \tag{A.6}$$

$$f(\xi, \theta) = A + B\theta \tag{A.7}$$

$$\theta = \frac{T}{T_{c,H_20}} \tag{A.8}$$

$$\xi = \frac{M_{salt}}{M_{sol}} \tag{A.9}$$

$$A = 2 - \left[1 + \left(\frac{\xi}{\pi_0}\right)^{\pi_1}\right]^{\pi_2} \tag{A.10}$$

$$B = \left[1 + \left(\frac{\xi}{\pi_3}\right)^{\pi_4}\right]^{\pi_5} - 1 \tag{A.11}$$

$$\pi_{25} = 1 - \left[1 + \left(\frac{\xi}{\pi_6}\right)^{\pi_7}\right]^{\pi_8} - \pi_9 e^{-\frac{(\xi - 0.1)^2}{0.005}} \tag{A.12}$$

where, $p_{v,s}$ is vapor saturation pressure of the solution (hPA), $p_{w,s}$ is the water vapor saturation pressure (hPA), π is the relative vapor pressure between the desiccant solution and water, T is temperature (K), T_{c,H_2O} is the water critical temperature (K), ξ is the mass fraction between the salt and solution, and A, B, and π_i are coefficients. The following table provides the π_i coefficients, from i=0 to i=9.

The following table provides the π_i coefficients, from i=0 to i=9

Table A.1: The π_i coefficients, from i=0 to i=9, used to calculate vapor pressure

π_i	Value
0	0.28
1	4.3
2	0.6
3	0.21
4	5.1
5	0.49
6	0.362
7	-4.75
8	-0.4
9	0.03

Equilibrium Humidity Ratio

The equilibrium humidity ratio of the desiccant solution is calculated using Equation (A.13).

$$W = \frac{B \cdot p_{v,s}}{p_{tot} - p_{v,s}} \tag{A.13}$$

where, p_{tot} is the total ambient pressure (hPa) and B equals 0.622 kg_w/kg_{da}.

Specific heat capacity

Conde-Petit (Conde-Petit 2009) developed a method of calculating the specific heat capacity of an aqueous lithium chloride solution, Equations (A.14) through (A.18).

$$c_{p,sol}(T,\xi) = c_{p,H_2O}(T) \cdot \left(1 - f_1(\xi) \cdot f_2(T)\right) \tag{A.14}$$

$$c_{p,H_2O}(\theta,\xi) = A + B\theta^{0.02} + C\theta^{0.04} + D\theta^{0.06} + E\theta^{1.8} + F\theta^{8} \tag{A.15}$$

$$\theta = \frac{T}{228} - 1 \tag{A.16}$$

$$f_1(\xi) = A\xi + B\xi^2 + C\xi^3 \quad \text{for } \xi \leq 0.31 \tag{A.15}$$

$$f_1(\xi) = D + E\xi \quad \text{for } \xi > 0.31 \tag{A.15}$$

$$f_2(\theta) = F\theta^{0.02} + G\theta^{0.04} + H\theta^{0.06} \tag{A.15}$$

where, T is temperature (K), $c_{p,sol}$ is the specific heat capacity of the solution (kJ/(kg·K)), c_{p,H_2O} is the specific heat capacity of water (kJ/(kg·K)), and coefficients A through F are provided in the following table.

Table A.2: Coefficients used to determine the specific heat capacity of LiCl

Coefficient	Value
A	1.4398
B	-1.24317
C	-0.1207
D	0.12825
E	0.62934
F	58.5225
G	-105.6343
H	47.7948

Water vapor saturation pressure

Water vapor saturation pressure is calculated using Equations (A.16) and (A.17) (Vaisala 2010)**.**

$$\ln\left(\frac{p_{w,s}}{p_c}\right) = \frac{T_c}{T}\left(C_1\theta + C_2\theta^{1.5} + C_3\theta^3 + C_4\theta^{3.5} + C_5\theta^4 + C_6\theta^{7.5}\right) \tag{A.16}$$

$$\theta = 1 - \frac{T}{T_c} \tag{A.17}$$

where, $p_{w,s}$ is the saturation water pressure (hPa), T is temperature (K), T_c is the water critical temperature (647.096 K), p_c is the water critical pressure (220 640 hPa), and coefficients C_1 to C_6 are provided below.

$C_1 = -7.85951783$

$C_2 = 1.84408259$

$C_3 = -11.7866497$

$C_4 = 22.6807411$

$C_5 = -15.9618719$

$C_6 = 1.80122502$

APPENDIX B

EXPERIMENTAL DATA AND MODEL COMPARISON

This appendix presents the experimental data used to develop the empirical correlations. Furthermore, the model outputs are presented along with a percent difference comparison between the experimental data and the model outputs.

Dehumidifier Experimental Data and Model Results

Table B.1: Experimental and Model results for the 3-fluid LAMEE as a dehumidifier

Case		$T_{air,in}$ (°C)	$T_{air,out}$ (°C)			$T_{sol,in}$ (°C)	$T_{sol,out}$ (°C)			$T_{w,in}$ (°C)	$T_{w,out}$ (°C)			$W_{air,in}$ (g_v/kg_{da})	$W_{air,out}$ (g_v/kg_{da})		
	Tw,in/ Cr	Exp/ Model	Exp	Model	% Diff	Exp/ Model	Exp	Model	% Diff	Exp/ Model	Exp	Model	% Diff	Exp/ Model	Exp	Model	% Diff
Inlet Water Temperature ($T_{w,in}$)	24.6	35.2	28.9	29.3	1.4%	25.3	30.3	28.8	4.9%	24.6	26.3	26.2	0.3%	17.2	12.5	12.4	1.1%
	20.6	35.3	27.7	27.5	0.6%	24.8	27.2	27.6	1.3%	20.6	23.9	23.3	2.4%	17.4	11.6	11.7	0.4%
	15.1	35.0	25.4	25.4	0.0%	24.8	25.4	25.5	0.4%	15.1	20.5	18.9	8.1%	17.5	10.9	10.9	0.4%
	10.1	35.0	23.9	24.2	1.0%	25.2	23.7	23.3	1.8%	10.1	16.2	15.0	7.3%	17.0	10.0	9.9	0.3%
Inlet water mass flow rate (Cr)	0.055	35.1	26	25	0.5%	24.2	23.1	22.9	0.8%	20.6	21.8	21.5	1.1%	17.9	11.0	10.9	0.7%
	0.11	35.3	26	27	0.1%	24.5	24.5	25.1	2.3%	20.8	22.6	22.3	1.4%	17.9	11.3	11.4	1.5%
	0.26	35.3	28	28	0.6%	24.8	27.2	27.6	1.3%	20.6	23.9	23.1	3.4%	17.4	11.6	11.7	0.4%
	0.42	34.9	28	28	1.1%	24.5	28.7	29.3	1.9%	20.7	24.5	23.7	3.3%	18.1	12.4	12.4	0.4%

Regenerator Experimental Data and Model Results

Table B.2: Experimental and model results for the 3-fluid LAMEE as a regenerator

Case	Inlet water temperature (°C)		Cr		Cr*		Sensible Effectiveness			Latent Effectiveness		
	Exp.	Model	Exp.	Model	Exp.	Model	Exp.	Model	Difference	Exp.	Model	Difference
Solution Mass Flow Rate (Cr*)	42.29	42.29	0.26	0.26	2	2.0	36%	37%	0.43%	17.63%	17%	0.37%
	43.09	43.09	0.45	0.45	3.4	3.4	40%	39%	1.38%	15.47%	20%	4.31%
	43.37	43.37	0.63	0.63	4.8	4.8	41%	42%	0.71%	24.66%	23%	2.14%
Water Mass Flow Rate (Cr)	57.11	57.11	0.27	0.26	2	2.0	33%	33%	0.23%	14.90%	14%	0.70%
	58.38	58.38	0.14	0.14	2	2.0	44%	43%	0.53%	22.96%	23%	0.37%
	55.31	55.31	0.04	0.04	2	2.0	52%	52%	0.40%	31.00%	31%	0.14%
Inlet Water Temperature (Tw,in)	42.29	42.29	0.27	0.26	2	2.0	36%	37%	0.43%	17.63%	17%	0.37%
	49.93	49.93	0.27	0.26	2	2.0	35%	35%	0.06%	16.45%	16%	0.72%
	57.11	57.11	0.27	0.26	2	2.0	33%	33%	0.23%	14.90%	14%	0.70%
	65.70	65.70	0.27	0.26	2	2.0	31%	31%	0.19%	10.97%	12%	1.06%

Case	Inlet Water Temperature (°C)	Cr	Cr*	$T_{air,in}$ (°C)	$T_{air,out}$ (°C)			$T_{sol,in}$ (°C)	$T_{sol,out}$ (°C)			$T_{w,in}$ (°C)	$T_{w,out}$ (°C)			$W_{air,in}$ (g_v/kg_{da})	$W_{air,out}$ (g_v/kg_{da})		
					Exp	Model	% Diff	Exp	Exp	Model	% Diff		Exp	Model	% Diff		Exp	Model	% Diff
Solution Mass Flow Rate (Cr*)	42.29	0.26	2	29.56	34.18	34.23	0.17%	40.04	35.97	35.78	0.51%	42.29	39.97	42.21	5.46%	12.93	14.75	14.72	0.24%
	43.09	0.45	3.4	30.17	35.40	35.22	0.51%	39.96	37.03	36.98	0.15%	43.09	40.83	43.15	5.53%	15.03	16.48	16.88	2.41%
	43.37	0.63	4.8	30.01	35.49	35.59	0.27%	40.05	37.55	37.58	0.08%	43.37	41.23	43.34	5.00%	13.20	16.04	15.80	1.52%
Water Mass Flow Rate (Cr)	57.11	0.27	2	29.85	38.84	38.90	0.16%	40.52	43.64	44.17	1.21%	57.11	50.99	53.07	3.99%	12.38	18.37	18.08	1.56%
	58.38	0.14	2	30.10	42.54	42.39	0.36%	40.39	51.60	49.59	3.98%	58.38	52.44	54.60	4.04%	12.82	22.79	22.95	0.73%
	55.31	0.04	2	29.95	43.01	43.11	0.24%	39.85	50.34	51.53	2.35%	55.31	53.21	54.08	1.63%	13.21	23.91	23.86	0.20%
Inlet Water Temperature (Tw,in)	42.29	0.27	2	29.56	34.18	34.23	0.17%	40.04	35.97	35.78	0.51%	42.29	39.97	42.21	5.46%	12.93	14.75	14.72	0.24%
	49.93	0.27	2	29.69	36.78	36.76	0.03%	40.43	39.62	39.98	0.90%	49.93	45.00	47.95	6.35%	13.14	16.84	16.68	0.96%
	57.11	0.27	2	29.85	38.84	38.90	0.16%	40.52	43.64	44.17	1.21%	57.11	50.99	53.07	3.99%	12.38	18.37	18.08	1.56%
	65.70	0.27	2	29.95	40.86	40.94	0.18%	40.16	50.08	50.10	0.05%	65.70	55.08	58.85	6.61%	13.22	20.87	21.61	3.48%

APPENDIX C

3-FLUID LAMEE MODEL EXTRAPOLATION

This appendix presents the extrapolation of the 3-fluid LAMEE model. The figures in this section show that the model follows physical trends outside the experimental dataset. Important note: although the experimental data is included in the figures presented in this section, this appendix is not meant for validation. The outputs disagree from the experimental data because the exact same inputs are not used.

Figure D.1(a), (b), and (c) show the outlet air temperature, air humidity ratio, and solution temperature, respectively, across a range of inlet air and water temperatures for the 3-fluid LAMEE dehumidifier model. In Figure D.1(a), as the inlet air temperature decreases from 40°C, the outlet air temperature decreases. However, for each inlet water temperature, there is a point where the outlet air temperature begins to deviate from the expected trend. These points help define the range of acceptable inlet water temperatures across different inlet air temperatures and it is important to avoid them when using the model. Figure D.1(b) shows that the outlet air humidity ratio is much more forgiving since it does not depart drastically from the observed trend until the inlet air temperature decreases to 28°C. On the other hand, in Figure D.1(c), the outlet solution temperature shows deviation from the trend at higher inlet air temperatures. Outlet water temperature is omitted since it is determined through an energy balance and, therefore, it can be assumed that when one fluid shows deviation, the water will also deviate.

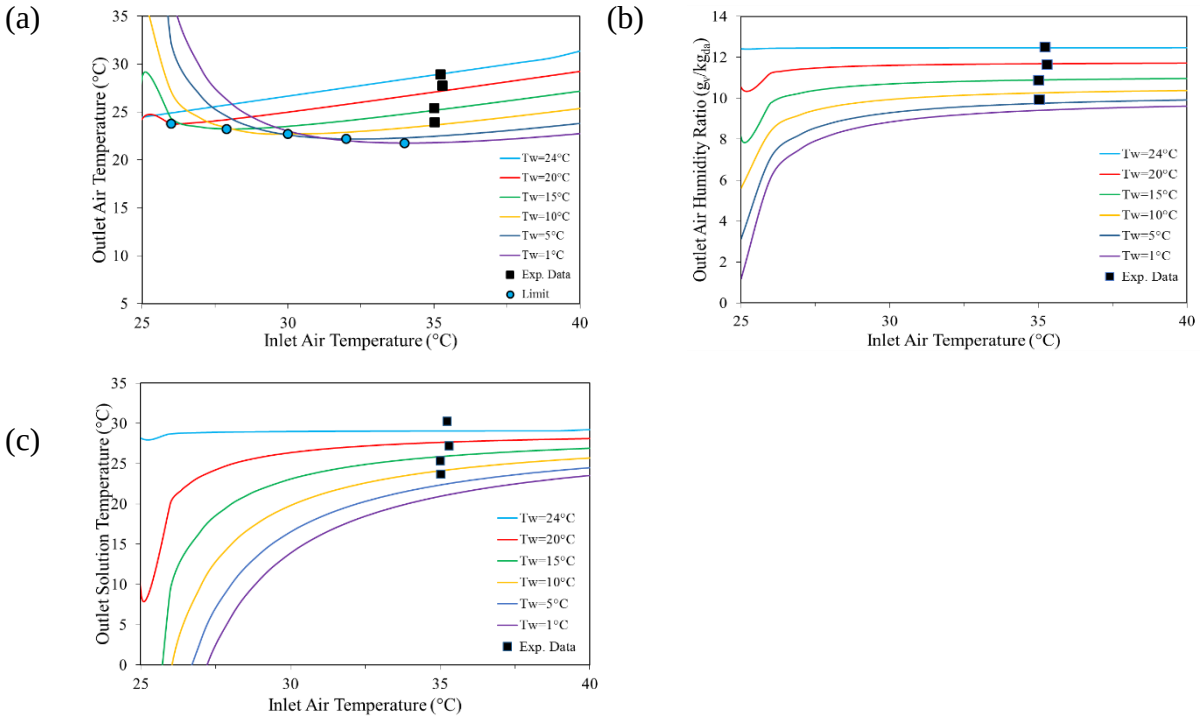

Figure C.1: 3-fluid LAMEE dehumidifier model behavior for (a) outlet air temperature, (b) outlet air humidity ratio, and (c) outlet solution temperature at different inlet water and air temperatures ($T_{sol,in} = 24.5°C$, $W_{air,in} = 17.6 \frac{g_v}{kg_{da}}$, $Cr^* = 1.8$, $Cr = 0.26$)

A similar analysis was performed to investigate model sensitivity across different Cr values and inlet air temperatures. Figure D.2(a), (b), and (c) show the effects of changing Cr has on outlet air temperature, air humidity ratio, and solution temperature, respectively. Compared to inlet water temperature, the model is slightly more stable with different Cr values. As can be seen, the outlet air temperature, air humidity ratio, and solution temperature deviate from their trends at lower inlet air temperatures than when varying the inlet water temperature. Thus, although consideration must be used when using Cr values outside of the experimental range, it is not detrimental to the model since the model abides by the appropriate inlet water temperatures. Figure D.2(d) was used to determine the minimum allowable air temperature (29°C). This was done by setting all the input parameters to deliver maximum dehumidification and 29°C is when the outlet air temperature deviates from the expected trend.

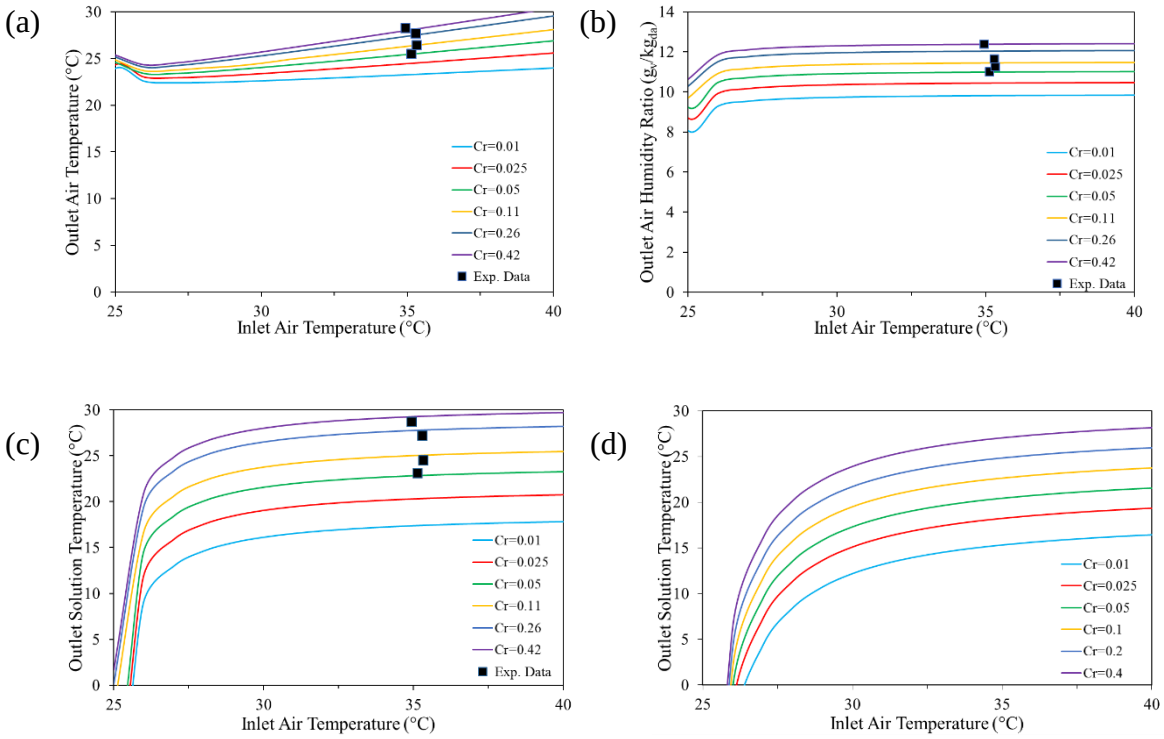

Figure C.2: 3-fluid LAMEE dehumidifier model behavior for (a) outlet air temperature, (b) outlet air humidity ratio, (c) outlet desiccant solution temperature at different inlet air temperatures and Cr values ($T_{sol,in} = 24.5°C$, $W_{air,in} = 18 \frac{g_v}{kg_{da}}$, $Cr^* = 1.8$, $T_{w,in} = 20.7°C$) and (d) outlet desiccant solution temperature at different inlet air temperatures and Cr values ($T_{sol,in} = 24.5°C$, $W_{air,in} = 18 \frac{g_v}{kg_{da}}$, $Cr^* = 1.8$, $T_{w,in} = 20.7°C$

Figure D.3(a), (b), and (c) show the outlet air temperature, air humidity ratio, and desiccant solution temperature across different inlet water and air temperatures for the regenerator 3-fluid LAMEE model. Whereas, Figure D.3(d), (e), and (f) show the outlet air temperature, air humidity ratio, and desiccant solution temperature across different inlet air temperatures and Cr values. The regenerator models are much more agreeable across varying inlet water and air temperatures than the dehumidifier models. An inlet air temperature range of 20°C-30°C and air humidity ratio of 12 g_v/kg_{da} are considered because the regenerator is likely to take building exhaust air which falls within these ranges. Figure D.4 shows that across different inlet air and water temperatures and Cr values, the outlet conditions follow similar trends and do not deviate.

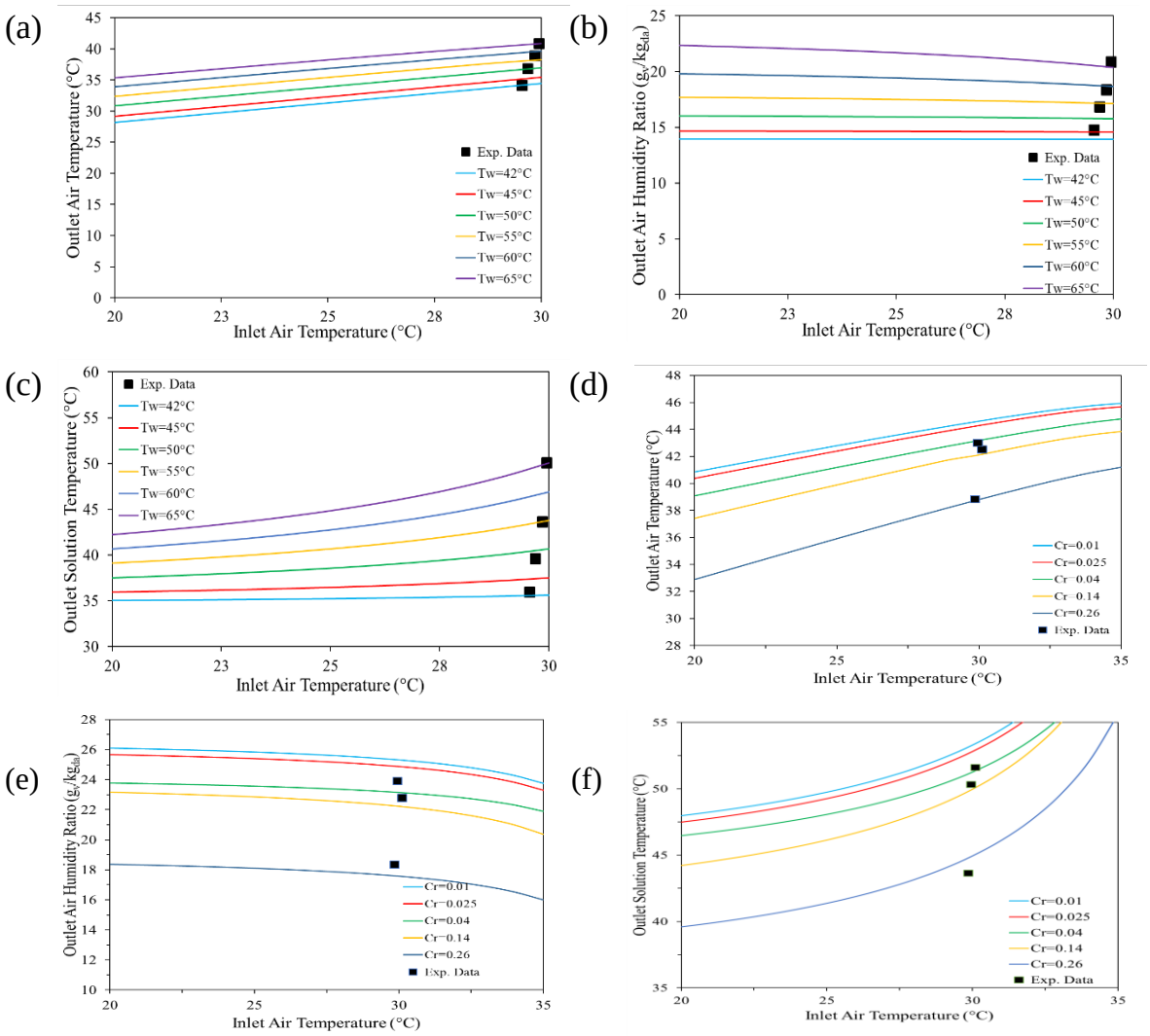

Figure C.3: 3-fluid LAMEE regenerator model behavior for (a) outlet air temperature, (b) outlet air humidity ratio, and (c) outlet desiccant solution temperature at different inlet water and air temperatures ($T_{sol,in} = 40°C$, $W_{air,in} = 12.0 \frac{g_v}{kg_{da}}$, $Cr^* = 2$, $Cr = 0.27$), and (a) outlet air temperature, (b) outlet air humidity ratio, and (c) outlet desiccant solution temperature at different inlet air temperatures and Cr values ($T_{sol,in} = 40°C$, $W_{air,in} = 12.0 \frac{g_v}{kg_{da}}$, $Cr^* = 2$, $T_{w,in} = 57°C$)

The outlet air humidity ratios of the dehumidifier and regenerator models were also evaluated across a range inlet water temperature, inlet air humidity ratios, and Cr values. Figure 8(a) and (b) display the outlet air humidity ratio for the dehumidifier 3-fluid LAMEE across different inlet

water temperatures and Cr values, respectively. Similarly, for the regenerator models, Figure 9(b) and (c) show the outlet air humidity ratio across varying inlet water temperatures and Cr values. There is no obvious departure from the linear trends which reassures the abilities of the models to extrapolate beyond test air humidity ratios.

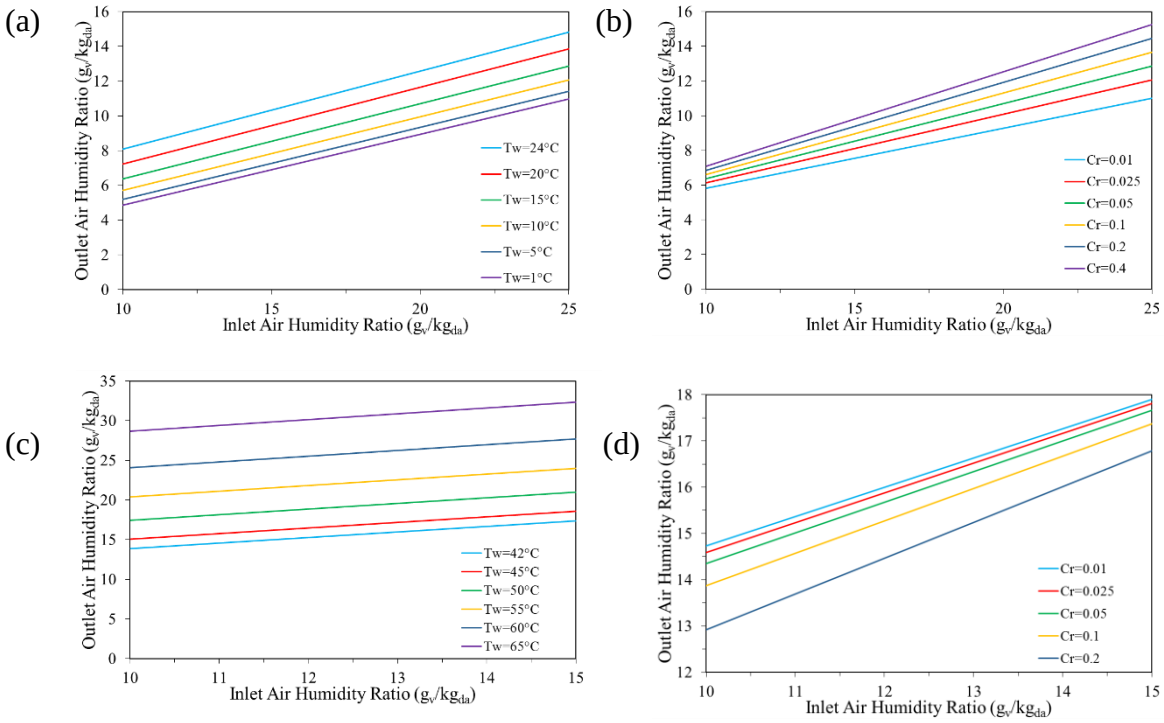

Figure C.4: Outlet air humidity ratio at different (a) inlet water temperatures and (b) Cr values for the dehumidifier, and the outlet air humidity ratio at different (c) inlet water temperatures and (d) Cr values for the regenerator across different inlet air humidity ratios